The Influence of the Overworld and the Middleworld on the Annular Modes

Maria Teresa Maçarico Morins

Supervisor / First reviewer
Dr. A. J. van Delden

Second reviewer
Prof. Dr. Henk A. Dijkstra

Institute for Marine and Atmospheric research Utrecht

(IMAU)

Utrecht University

ABSTRACT

The possible connections between the Middleworld, the Overworld and the annular modes (AMs) are examined by applying principal component analysis (PCA) to zonal means of monthly means of potential vorticity (PV) on the 600 K and 350 K isentropic surfaces from ERA-Interim, covering the full period from 1979 to 2013. The 600 K isentropic surface lies in the Overworld where all the isentropes lie above the tropopause, whilst the 350 K belongs to the Middleworld which englobes the tropical upper troposphere and the lowermost stratosphere.

Principal component analysis results show that PV on the 600 K isentrope represents fairly well stratospheric variability in the tropics and extratropics, with the first three eigenvectors being associated with respectively, the Quasi-biennial Oscillation (QBO), the stratospheric Northern annular mode (NAM) and the stratospheric Southern annular mode (SAM). The leading eigenvector represents PV anomalies in the tropical stratosphere that are clearly associated with the QBO. In the westward (eastward) phase of the QBO PV is below (above) average in the tropics of both hemispheres. Further analysis shows that the westward (eastward) QBO is also associated with dilution (concentration) of potential vorticity substance (PVS), hence a decrease (increase) of PV within the tropics. These changes in PVS are probably associated with the secondary meridional circulation (SMC) induced by the QBO. The second eigenvector is a clear representation of the stratospheric NAM where positive (negative) PV anomalies at midlatitudes and negative (positive) ones at polar latitudes represent the negative (positive) phase of the stratospheric NAM, thus a weak (strong) stratospheric polar vortex. The same reasoning applies to the SH with respect to the SAM, which is represented by the third eigenvector.

Potential vorticity on the 350 K results show that the first three eigenvectors represent respectively variability in the tropical upper troposphere and variability in the lowermost stratosphere in both hemispheres. In the tropics, according to the leading eigenvector, PV transport on the 350 K depends mainly on the strength of the Hadley circulation (HC), which is measured by the cross isentropic flow, the associated strength of the subtropical jet and the phases of the SOI. Above average PV is observed in the upper troposphere at times when the subtropical jet is weak, due to a weak Hadley cell, and during La Niña events. Conversely, below average PV in the tropics is strongly associated with a strong subtropical jet, hence a stronger Hadley cell, and El Niño events during which enhanced diabatic heating is clearly captured by the cross isentropic flow. The annular

modes (AMs) are not directly captured by this eigenvector although a link may exist through the strength of the subtropical jet, since the latter is strongly correlated with the NAM and SAM at respectively 750 and 150 hPa.

In the lowermost stratosphere in the SH (second eigenvector) the interpretation of the results is not straightforward. The principal component associated with the second eigenvector clearly shows variations in the lowermost stratosphere in the winter. However, the mechanisms responsible for the PV transport into and out of the southern polar latitudes were unclear.

In the Northern Hemisphere (third eigenvector), the picture is similar to the one in the Southern Hemisphere. However, in the Northern Hemisphere analysis more conclusions were able to be drawn. According to the results, stratosphere-troposphere coupling is only seen in cases of strong stratospheric polar vortex events which are directly associated with cross isentropic flow anomalies specifically on the 475 K isentropic surface and at 76.5°N.

Principal component analysis was further applied to climate indices that were calculated using the method of Li and Wang (2003). Although these climate indices were only evaluated for the Northern Hemisphere, the resultant principal components show strong correlations with the ones found in the previous analysis mainly with respect to the NAM, and tropical variability. These results reinforce the obtained conclusions associated with the principal component analysis applied to the atmospheric variables for the full domain on the above mentioned isentropic surfaces of Overworld and the Middleworld.

ACKNOWLEDGMENTS

First I would like to express my sincere gratitude to my supervisor, Dr. A. J. van Delden, for giving me the opportunity to work on such a fantastic topic. His guidance, knowledge and patience, whilst allowing me the room to work on my own way, were not only crucial for the completion of this project, but also an experience that I will carry for life. I also would like to thank Prof. Dr. Henk A. Dijkstra for his important contribution and criticism with respect to the statistics of the results.

Many thanks to my friends Kyriacos Chrysostomou, Remko Klaver and Stravos Fostiropoulos, to who I am grateful, not only for all the help and support, but also for the good laughs during this master.

To my dear parents, Aurora and Filipe, a very special thank for all the support, motivation and most important, for believing in me. Finally, to my beloved husband, Rutger Vos, thank you for being there at every single step during my journey in Utrecht University. Your infinite patience, understanding and help allowed me to fight for my goals and, what was a simple dream a few years ago is now a reality. For all the reasons, this thesis is dedicated to you.

TABLE OF CONTENTS

LIST OF FIGURES.....vi
LIST OF TABLES.....xii
LIST OF ABBREVIATIONS.....xiii
1. INTRODUCTION.....1
2. THEORETICAL BACKGROUND.....3
2.1 Atmospheric structure and circulation.....3
2.2 Annular modes.....7
2.3 The Southern Oscillation Index (SOI).....11
2.4 The Hadley circulation (HC).....13
2.5 The Brewer Dobson Circulation (BDC).....13
2.6 The quasi-biennial oscillation (QBO).....14
2.7 Potential vorticity (PV).....16
3. METHODOLOGY.....19
3.1 Data.....19
3.2 Principal Component Analysis (PCA).....20
4. RESULTS AND DISCUSSION.....22
4.1 Isentropic surfaces.....22
4.2 Potential vorticity on the 600 K isentropic surface (PV600K).....27
4.3 Potential Vorticity on the 350 K isentropic surface (PV350K).....39
4.4 PCA applied to Climate Indices.....63
4.4.1 Climate indices - Overview.....64
4.4.1.1 PV600I.....64
4.4.1.2 PV350I.....65
4.4.1.3 U350I and U600I.....65
4.4.1.4 CrIs350I, CrIs600I and CrIs600IBD.....66
4.4.2 Climate indices - PCA results.....67
5. CONCLUSIONS.....82
6. REFERENCES.....85
7. APPENDIX.....90

7.1 Definition of the NAM indices at, 1000, 975, 750, 600, 500, 350, 250, 200, 150, 100, 50, 30, 20 and 10 hPa:.....90

7.2 Maximum in anticorrelation for the NH and for the SH respectively from 10.5°N to 90°N and from 10.5°S to 90°S for each of the isentropic surfaces at 265 K, 275 K, 285 K, 300 K, 315 K, 330 K, 350 K, 370 K, 395 K, 430 K, 475 K, 530 K, 600 K, 700K and 850 K. 90

LIST OF FIGURES

Figure 2.1.1 Vertical thermal structure of the Earth's atmosphere up to 120 km. Source: Mohanakumar (2008)**. 5**

Figure 2.1.2 Schematic view of the atmosphere as a function of latitude and height. Source: Hoskins (1991)**. 6**

Figure 2.1.3 Schematic view of the atmosphere highlighting the transporting paths into and out of the lowermost stratosphere. Source: Dessler et al. 1995**. 6**

Figure 2.1.4 The zonal average, monthly average zonal wind (red contours, labeled in ms^{-1}), potential vorticity, PV (green contours, labeled in PVU; interval is 50 PVU for absolute values greater than 50) and pressure (black dashed contours, labeled in hPa) as a function of potential temperature and latitude according to the COSPAR International Reference Atmosphere (CIRA) for January and July. Source: van Delden (2012)**. 7**

Figure 2.2.1 Correlation between zonal mean monthly mean SLP anomalies in the NH (1958-2000). Source: J. Li and J. X. L. Wang, (2003). **.....10**

Figure 2.4.1 Top panel: zonal mean, annual mean diabatic heating as a function of pressure and latitude (for the period 1979-2001). Lower panel: annual average, zonal average streamlines in the vertical plane perpendicular to the equator. Source: van Delden (2012)**. 12**

Figure 2.5.1 Schematic of the Brewer Dobson circulation (BDC) in the stratosphere. Source: Flury et al., 2013**. 14**

Figure 2.6.1 A composite plot of the QBO according to the easterly-westerly transition at 20 hPa. Source: Baldwin et al. (2001)**. 15**

Figure 2.6.2 Schematic of the secondary meridional circulation (SMC) of the QBO. Source: Flury et al., (2013)**. 16**

Figure 2.7.2 Schematic latitudinal distributions of PV (Q) on an isentropic surface in the stratosphere, before (thin curve) and after (thick curve) a large-amplitude planetary wave breaking event centered at midlatitudes. Source: McIntyre (1981)**.....19**

Figure 4.1.1 Maximum in anticorrelation for the NH from 10.5°N to 90°N for each of the isentropic surfaces at 265 K, 275 K, 285 K, 300 K, 315K, 330 K, 350 K, 370 K, 395 K, 430 K, 475 K, 530 K, 600 K, 700K and 850 K, displayed as a function of height and correlation coefficient**.....25**

Figure 4.1.2 Maximum in anticorrelation for the NH from 10.5°N to 90°N for each of the isentropic surfaces at 265 K, 275 K, 285 K, 300 K, 315K, 330 K, 350 K, 370 K, 395 K, 430 K, 475 K, 530 K, 600 K, 700K and 850 K, displayed as a function of height and latitude. Figure due to van Delden, A. J**... .....25**

Figure 4.1.3 Climatology of zonal mean monthly mean PV (in PVU) on the 600 K isentropic surface for January until December for the period 1979 – 2013.**. 26**

Figure 4.1.4 Climatology of zonal mean zonal wind (U in ms^{-1}) on the 600 K isentrope for January until December for the period 1979–2013. **.....26**

Figure 4.1.5 Climatology of PV (in PVU) on the 350 K isentropic surface for January until December for the period 1979 – 2013.**. 27**

Figure 4.1.6 Climatology of zonal mean zonal wind (U in ms^{-1}) on the 600 K isentrope for January until December for the period 1979 – 2013. Two years are plotted for clarity. Contour interval is 2.5 ms^{-1}. **.....27**
Figure 4.2.1 Cross-correlation matrix of PV at 600 K. The upper triangle shows correlations of PV anomalies including the seasonal cycle (anomalies with respect to the mean) and the lower triangle shows correlations with seasonal cycle filtered out (anomalies with respect to the climatology) for the period of time 1979-2013**. 34**
Figure 4.2.2 Leading eigenvector (EOF1PV600K, black solid line) from PCA applied to the PV anomaly filed (with seasonal cycle filtered out and normalized) on the 600 K isentropic surface. The explained variance is shown between parentheses. EOF1PV600K is displayed in terms of the correlation coefficient resultant from the regression of the above mentioned PV field upon the standardized first principal component (PC1PV600K). Also shown is the regression between the same PV anomaly field upon the standardized QBO time series at 30 mb**. 35**
Figure 4.2.3 Second eigenvector (EOF2PV600K, red line) and third eigenvector (EOF3PV600K, black line) from PCA applied to the PV anomaly field (with seasonal cycle filtered out and normalized) on the 600 K isentropic surface. The explained variance is shown between parentheses. EOF2PV600K and EOF3PV600K are displayed in terms of the correlation coefficient resultant from the regression of the above mentioned PV field upon, respectively, the second and third standardized principal components (PC2PV600K and PC3PV600K)**. 35**
Figure 4.2.4 First principal component (PC1PV600K) and the QBO time series defined at 30 mb. The correlation coefficient between the two time series is r = -0.85 at lag 0. Positive (negative) values of the QBO are representative of eastward (westward) winds**. 36**
Figure 4.2.5 Cross correlation between the standardized PC1PV600K and the PVS (contours) anomaly field (with seasonal cycle filtered out and normalized) on the 600 K isentropic surface, as well as the QBO time series at 30 mb and the above mentioned PVS anomaly field (colors). Negative lags (in months) means that the PVS leads PC1PV600K and the QBO. Lag in months**. 36**
Figure 4.2.6 Correlation between the NAM indices defined at several geopotential heights using the method of Li and Wang (2003), which is explained in section 2.2, and the PV anomaly field (with seasonal cycle filtered out and normalized) on the 600 K isentropic surface**. 37**
Figure 4.2.7 Time series of the NAM index defined at 20 hPa (NAMI_20) using the method of Li and Wang (2003) and the second principal component (PC2PV600K) from PCA applied to the PV anomaly filed (with seasonal cycle filtered out and normalized) on the 600 K isentropic surface. Dates associated with negative values of PC2PV600K correspond to SSWs**. 37**
Figure 4.2.8 Scatterplot of the NAM index calculated at 20 hPa (NAMI_20) and the second principal component (PC2PV600K) from PCA applied to the PV anomaly filed (with seasonal cycle filtered out and normalized) on the 600 K isentropic surface**. 38**
Figure 4.2.9 Same as in figure 4.2.6 but with the SAM indices calculated with the zonal mean zonal wind at 60°S**. 38**
Figure 4.2.10 Time series of the zonal mean zonal wind at 60°S and at 20 hPa (U_20, solid red line) and the third principal component (PC3PV600K, solid black line) from PCA applied to the PV anomaly field (with seasonal cycle filtered out and normalized) on the 600K isentropic surface. The SSW of September 2002 in the SH is captured by both time series**.....38**

Figure 4.2.11 Scatterplot of the zonal mean zonal wind at 60°S at 20 hPa (U_20) and the third principal component (PC3PV600K) from PCA applied to the PV anomaly field (with seasonal cycle filtered out and normalized) on the 600 K isentropic surface. **.....39**
Figure 4.3.1 Cross-correlation matrix of PV at 350 K. The upper triangle shows correlations of PV anomalies including the seasonal cycle and the lower triangle shows correlations with seasonal cycle filtered out by subtracting the PV data from the climatology (monthly means with respect to the 1979-2013 time period)**.....50**
Figure 4.3.2 Leading eigenvector (EOF1PV350K) from PCA applied to the PV anomaly field (with seasonal cycle filtered out and normalized) on the 350 K isentropic surface. The explained variance is shown between parentheses. EOF1PV350K is displayed in terms of the correlation coefficient resultant from the regression of the above mentioned PV field upon the standardized first principal component (PC1PV350K)**. 51**
Figure 4.3.3 Time series of the first principal component (PC1PV350K) from PCA applied to the PV anomaly filed (with seasonal cycle filtered out and normalized) on the 350 K isentropic surface**. 51**
Figure 4.3.4 Leading eigenvector (EOF1CrIs350K) from PCA applied to the cross isentropic flow (CrIs) anomaly filed (with seasonal cycle filtered out and normalized) on the 350 K isentropic surface. The explained variance is shown between parentheses. EOF1CrIs350K is displayed in terms of the correlation coefficient resultant from the regression of the above mentioned CrIs flow field upon the standardized first principal component (PC1CrIs350K). The explained variance is shown between parentheses**. 52**
Figure 4.3.5 Time series of the first principal component (PC1PV350K, black line) from PCA applied to the PV anomaly field (with seasonal cycle filtered out and normalized) on the 350 K isentropic surface and the first principal component (PC1CrIs350K, red line) from PCA applied to the CrIs flow anomaly field (with seasonal cycle filtered out and normalized) on the 350 K isentropic surface. The correlation between the two time series is r= -0.43 at lag 0. Note that the time domain is now from 1980 until 2013 since this is the period of time available for the cross isentropic flow**. 52**
Figure 4.3.6 Leading eigenvector (EOF1PrecpT) from PCA applied to the tropical precipitation anomaly filed (between 30°N and 30°S with seasonal cycle filtered out and normalized). The explained variance is shown between parentheses. EOF1PrecptT is displayed in terms of the correlation coefficient resultant from the regression of the above mentioned tropical precipitation field upon the standardized first principal component (PC1PrecpT). The explained variance is shown between parentheses**. 52**
Figure 4.3.7 Time series of the first principal component (PC1PV350K, red line) from PCA applied to the PV anomaly field (with seasonal cycle filtered out and normalized) on the 350 K isentropic surface and the first principal component (PC1PrecpT) from PCA applied to the tropical precipitation flow anomaly field (with seasonal cycle filtered out and normalized). The correlation between the two time series is r=-0.57 at lag 0**. 53**
Figure 4.3.8 Time series of the first principal component (PC1PV350K, red line) from PCA applied to the PV anomaly field (with seasonal cycle filtered out and normalized) on the 350 K isentropic surface, time series of the first principal component (PC1PrecpT, black line) from PCA applied

to the tropical precipitation flow anomaly field (with seasonal cycle filtered out and normalized) and the SOI (blue line). 53
Figure 4.3.9 Scatterplot of PC1PrecpT and PC1CrIs350K (red dots) and PC1PrecpT and the SOI (blue dots); the associated correlation coefficients are in red and blue respectively. 54
Figure 4.3.10 Second eigenvector (EOF2U350K) from PCA applied to the zonal wind (U) anomaly filed (with seasonal cycle filtered out and normalized) on the 350 K isentropic surface. The explained variance is shown between parentheses. EOF1U350K is displayed in terms of the correlation coefficient resultant from the regression of the above mentioned U field upon the standardized second principal component (PC2U350K). The explained variance is shown between parentheses. 54
Figure 4.3.11 Time series of the first principal component (PC1PV350K) from PCA applied to the PV anomaly field (with seasonal cycle filtered out and normalized) on the 350 K isentropic surface and the second principal component (PC2U350K) from PCA applied to the U anomaly field (with seasonal cycle filtered out and normalized) on the 350 K isentropic surface. The correlation between the two time series is r=-0.68 at lag 0. 55
Figure 4.3.12 Top ten maxima and minima of PC2U350K (PC2U350Kmin corresponds to a strong subtropical jet; PC2U350Kmax corresponds to a weak subtropical jet) and the SOI (SOImin corresponds to El Niño events; SOImax corresponds to La Niña events) associated with PC1PV350K (grey line). 55
Figure 4.3.13 Top ten maxima and minima of the NAM index defined at 750 hPa (respectively NAMI750min and NAMI750max), the SAM index defined at 150 hPa(SAMI150min and SAMI150max) and the SOI (SOImin corresponds to El Niño events; SOImax corresponds to La Niña events) associated with PC2U350K (grey line). 55
Figure 4.3.14 Correlation matrix between PC2U350K and the NAM indices defined at several geopotential heights using the method of Li and Wang (2003). Negative lags (in months) means that the NAM leads PC2U350K. 56
Figure 4.3.15 Same as in figure 4.3.14 but with the SAM indices instead of the NAM 56
Figure 4.3.16 Top ten maxima and minima of the NAM index defined at 750 hPa (respectively NAMI750min and NAMI750max), the SAM index defined at 150 hPa(SAMI150min and SAMI150max) and the SOI (SOImin corresponds to El Niño events; SOImax corresponds to La Niña events) associated with PC2U350K (grey line). 56
Figure 4.3.17 Second eigenvector (EOF2PV350K, black line) from PCA applied to the PV anomaly filed (with seasonal cycle filtered out and normalized) on the 350 K isentropic surface and EOF3PV600K (section 4.1, figure 4.2.3). EOF1PV350K is displayed in terms of the correlation coefficient resultant from the regression of the above mentioned PV field on the 350 K isentrope upon the standardized second principal component (PC2PV350K). The explained variance is shown between parentheses. 57
Figure 4.3.18 Time series of the second principal component (PC2PV350K) from PCA applied to the PV anomaly field (with seasonal cycle filtered out and further normalized) on the 350 K isentropic surface. 57

Figure 4.3.19 Cross correlation between PC2PV350K and the cross isentropic flow on the 600K (CrIs600K) isentropic surface. Negative lags (in months) means that the cross isentropic flow leads. Lag in months. **58**
Figure 4.3.20 Second eigenvector of PV350K for full domain, from 90°N to 90°S (EOF2PV350K) and the leading eigenvector of PV350K for the domain 10.5°S to 90°S (EOF1PV350KSH) from PCA applied to the PV anomaly filed (with seasonal cycle filtered out and normalized) on the 350 K isentropic surface. The explained variance is shown between parentheses..... **58**
Figure 4.3.21 Time series of the PC2PV350K (red dotted line) and the time series of PC1PV350SH from PCA applied to the SH. The latter is only shown for comparison. **59**
Figure 4.3.22 Third eigenvector (EOF3PV350K) from PCA applied to the PV anomaly filed (with seasonal cycle filtered out and normalized) on the 350 K isentropic surface. The explained variance is shown between parentheses. EOF3PV350K is displayed in terms of the correlation coefficient resultant from the regression of the above mentioned U field upon the standardized second principal component (PC3PV350K). The explained variance is shown between parentheses..... **59**
Figure 4.3.23 Time series of the third principal component (PC3PV350K) from PCA applied to the PV anomaly field (with seasonal cycle filtered out and further normalized) on the 350 K isentropic surface. **59**
Figure 4.3.24 Cross correlation between PC3PV350K and the NAM indices defined at different pressure levels. Negative (positive) lag means NAM leads (lags). Lag in months. **60**
Figure 4.3.25 Top ten maxima and minima values of the NAM indices (at lag -1 when the NAM leads) defined at 50 hPa (NAMI_50), 30 hPa (NAMI_30) and 20 hPa (NAMI_20) associated with PC3PV350K (grey line). **60**
Figure 4.3.26 Top ten maxima and minima values of the NAM indices (at lag 0) defined at 150 hPa (NAMI_150) and at the surface (NAMI) associated with PC3PV350K (grey line)..... **60**
Figure 4.3.27 Correlation coefficient between PC3PV350 and the NAM indices (defined at different pressure levels) at lag -1 (solid line) and at lag 0 (dotted line) with height. **61**
Figure 4.3.28 Top ten maxima and minima values of the cross isentropic flow on the 350 K isentrope at 69°N (CrIs350(69°N)min and max at lag 0) and on the 475 K isentrope at 76.5°N (CrIs475(76.5°N)min and max at lag -1 when CrIs475K leads by one month) associated PC3PV350K (grey line). **61**
Figure 4.4.1 Time series of the PV600K index (PV600I) which is defined as the difference between the PV anomaly field (with seasonal cycle filtered out and normalized) on the 600 K isentropic surface at 73.5°N and 48.75°N (PV350I=PV(73.5°N)–PV(48.75°N)..... **72**
Figure 4.4.2 Correlation between the PV index at 600K (PV600I) and the NAM index defined at 20 hPa (NAMII_20, black circles, r = 0.93) and with PC2 of PV600K (PC2PV600K, red circles, r = 0.95). **72**
Figure 4.4.3 Time series of the PV350K index (PV350I) which is defined as the difference between the PV anomaly field (with seasonal cycle filtered out and normalized) on the 350 K isentropic surface at 34.5°N and 15°N (PV350I=PV350(34°N) – PV350(15°N) and PC1PV350K (section 4.3). The correlation coefficient between the two time series is -0.83 at lag 0. ..... **72**

Figure 4.4.4 Time series of the zonal wind index on the 350K isentrope (U350I) which is defined as the difference between the zonal wind (U) anomaly field (with seasonal cycle filtered out and normalized) on the 350 K isentropic surface at 32.5°N and 51°N N (U350I=U350(32.5°N)-U350(51°N))**. 73**

Figure 4.4.5 Time series of the zonal wind index on the 600K isentrope (U600I) which is defined as the difference between the zonal wind (U) anomaly field (with seasonal cycle filtered out and normalized) on the 600 K isentropic surface at 56.25°N and 27.75°N (U600I=U600(56.25°N)-U600(27.75°N))**.....73**

Figure 4.4.6 Time series of the CrIs350K index (CrIs350I) which is defined as the difference between the cross isentropic flow (CrIs) anomaly (with seasonal cycle filtered out and normalized) on the 350 K isentropic surface at 0° and 13.5°N (CrIs350I=CrIs350(0°) – CrIs350(13.5°N), black line) and PC1CrIs350K (red line, section 4.3, figures 4.3.9 and 4.3.10). The correlation between the two time series is 0.71 at lag 0**.....74**

Figure 4.4.7 Time series of the CrIs600K index (CrIs600I) which is defined as the difference between the cross isentropic flow (CrIs) anomaly (with seasonal cycle filtered out and normalized) on the 600 K isentropic surface at 22.5°N and 1.5°N. Also plotted is the time series of the QBO at 50 mb. The maximum correlation between the two time series is -0.73 where the QBO leads by 4 months. At lag 0 the correlation coefficient is r=-0.35**. 74**

Figure 4.4.8 Time series of the CrIs600K index (CrIs600I) which is defined as the difference between the cross isentropic flow (CrIs) anomaly (with seasonal cycle filtered out and normalized) on the 600K isentropic surface at 22.5°N and 1.5°N. Also plotted is the time series of the principal component of PV on the 600K isentrope (PC1PV600K, see section 4.2). The correlation between the two time series is -0.7 where the CrIs600I leads by 4 months. At lag zero the correlation coefficient is r=-0.39**. 75**

Figure 4.4.9 Cross correlation between the first principal component resulting from the PCA applied to the climate indices (PC1CI) and the NAM indices defined at 15 different pressure levels. Negative (positive) lag means NAM leads (lags). Lag in months**. 75**

Figure 4.4.10 Top ten maxima and minima values of the NAM indices (at lag 0) defined at the surface (NAMI) and at 150 hPa (NAMI_150) as well as the zonal wind index on the 350 K isentropic surface(U350I) associated with the first principal component resulting from PCA applied to the climate indices (PC1CI, grey line). See also figure 4.4.11 for completeness**.....76**

Figure 4.4.11 Top ten maxima and minima values of the cross isentropic flow on the 475 K isentropic surface (CrIs475K at lag 0) associated with the first principal component resulting from PCA applied to the climate indices (PC1CI, grey line)**. 76**

Figure 4.4.12 Regression of PC2CI (black solid line), the SOI, the cross isentropic flow index on the 350K (CrIs350I), tropical precipitation as found in section 4.2 (PC1PrecpT) the PV index on the 350K isentrope (PV350I) upon the PV anomaly (with respect to the climatology and further divided by the standard deviation) field on the 350 K isentropic surface**.....76**

Figure 4.4.13 Top ten maxima and minima values of the SOI, the PV index on the 350K isentrope (PV350I) and the zonal wind index on the 350K isentrope (U350I) associated with the second principal component resulting from PCA applied to the climate indices (PC2CI, grey line)**.....77**

Figure 4.4.14 Top ten maxima and minima values of the first principal component of tropical precipitation (PC1PrecpT found in section 4.2) and the cross isentropic flow index on the 350K isentrope (CrIs350I) associated with the second principal component resulting from PCA applied to the climate indices (PC2CI, grey line)**.....77**

Figure 4.4.15 Top ten maxima and minima values of the NAM index defined at the surface (NAMI), the zonal wind index on the 350K isentropic surface (U350I) and the first principal component of tropical precipitation (PC1PrecpT found in section 4.2) associated with the third principal component resulting from PCA applied to the climate indices (PC3CI, grey line)**. 78**

Figure 4.4.16 Top ten maxima and minima values of the SOI, the cross isentropic flow index on the 350K isentropic surface (CrIs350I) , the cross isentropic flow index on the 600K isentropic surface (CrIs600I) associated with the third principal component resulting from PCA applied to the climate indices (PC3CI, grey line)**.....78**

Figure 4.4.17 Cross correlation between the third principal component resulting from the PCA applied to the climate indices (PC1CI) and the NAM indices defined at 15 different pressure levels. Negative (positive) lag means NAM leads (lags). Lag in months**.....79**

Figure 4.4.18 Regression of the cross isentropic flow anomalies (with seasonal cycle filtered out and normalized) on the 600 K isentropic surface upon the forth standardized principal components (PC4CI)**. 79**

Figure 4.4.19 Cross correlation between the forth principal component resulting from the PCA applied to the climate indices (PC4CI) and the PV anomaly field (with seasonal cycle filtered out and normalized) on the 600 K isentropic surface. Negative (positive) lag means PC4CI leads (lags). Lag in months**. 80**

LIST OF TABLES

Table 1 Correlation coefficients (r) at lag zero between the principal components of PV, cross isentropic flow and the zonal wind on the 350 K isentropic surface (respectively PC1PV350K, PC1CrIs350K and PC2U350K), tropical precipitation (PC1PrecpT), SOI and the AMs (NAM and SAM) **62**

Table 2 Short description of the positive and negative values of the principal components (PCs) resultant from PCA applied to PV, cross isentropic flow and zonal wind on the 350 K and 600 K isentropic surfaces as well as the PCs resultant from PCA applied to climate indices for the NH.. ..... **62**

Table 3 Definition of the climate indices for potential vorticity and cross isentropic on the 600K (respectively PV600I and CrIs600I) and potential vorticity, zonal wind and cross isentropic flow on the 350K (respectively PV350I, U350I and CrIs350I) as well as the NAM index (NAMI). **80**

Table 4 Correlations between the climate indices. **80**

Table 5 First four eigenvectors (total of 75.5% of the total variance) resulting from PCA applied to the climate indices: NAM index at the surface (NAMI), NAM index at 150 hPa (NAMI_150), NAM index at 20 hPa (NAMI_20), the Southern Oscillation Index (SOI), PV index on the 350K (PV350I) and on the 600K (PV600I) isentropic surfaces, the cross isentropic flow index on the 350K (CrIs350I) and on the 600K isentropic surfaces, including the equator (CrIs600I) and excluding the equator (CrIs600IBD). In total the four eigenvectors represent 75.5% of the total variance. **81**

Table 6 Correlation between the time series associated with the first four eigenvectors (PC1CI, PC2CI, PC3CI and PC4CI respectively) with each of the indices previously defined..... **81**

LIST OF ABBREVIATIONS

AM(s): Annular mode(s)

BDC: Brewer-Dobson circulation

ENSO: El Niño-Southern Oscillation

Gph: Geopotential height

HC: Hadley circulation

ITCZ: Intertropical convergence zone

MSLP: Mean sea level pressure

NAM: Northern annular mode

NH: Northern Hemisphere

PC(s): Principal component(s)

PCA: Principal component analysis

PV: Potential vorticity

PVS: Potential vorticity substance

QBO: Quasi-biennial oscillation

RW: Rossby waves

RWB: Rossby wave breaking

SAM: Southern annular mode

SH: Southern Hemisphere

SLP: Sea level pressure

SMC: Secondary meridional circulation

SOI: Southern oscillation index

SSW: Sudden stratospheric warming

1 INTRODUCTION

This thesis project is concerned with the possible links between PV distribution in the Overworld and in the Middleworld, and main modes of climate variability with particular attention to the annular modes (AMs). For that end, two specific isentropic surfaces are chosen, the 600 K which lies in the Overworld and the 350 K which belongs to the Middleworld.

In the Overworld all the isentropes are above the tropopause, hence they lie in the stratosphere. Therefore, the analysis of the PV distribution in this region of the atmosphere may provide further insight about stratospheric variability, such as the quasi-biennial oscillation (QBO) in the tropics, the Brewer Dobson Circulation (BDC) as well as the stratospheric Northern Annular Mode (NAM) and the Southern Annular Mode (SAM) in the extratropics.

The isentropic surfaces of the Middleworld, on the other hand, cut the tropopause at about 40° latitude. This implies that the isentropes of the Middleworld do not lie entirely in the stratosphere nor in the troposphere, rather they englobe both regions of the atmosphere. Therefore, the study of the PV distribution on these isentropic surfaces might shed light on variability in the tropical upper troposphere, which is dominated by the Hadley circulation (HC) and the El Niño Southern Oscillation (ENSO), as well as extratropical variability which in turn is dominated by the annular modes (AMs).

Nowadays is well accepted that deep understanding of atmospheric dynamics can be gained by evaluating potential vorticity (PV) on isentropic surfaces, which in the absence of diabatic processes and friction is materially conserved. This conservation principle leads to the fact that PV can be considered as an active tracer, in the sense that the evolution of PV on an isentropic surface provides information about the motion of air masses, i.e., features in PV are carried away with the air motion along an isentrope. Furthermore, the invertibility principle states that, with appropriate boundary conditions and assuming some kind of balance, all other dynamical fields such as wind and temperature can be obtained from the PV distribution (Hoskins et al. 1985). Also, since PV gradients are the restoring mechanism for Rossby waves (RW), the analysis of the PV distribution is a good indicator of wave activity.

Potential vorticity on isentropic surfaces has been mostly used for the analysis of stratospheric variability, particularly the polar vortices (e.g. Rongcai and Cai, 2006; Waugh and Polvani, 2010) and associated sudden stratospheric warmings (SSW) (McIntyre, 1981), which are a result of Rossby

wave breaking (RWB). Since the strongest PV gradients are seen in locations of strong eastward winds, and because PV is materially conserved during a period of time of several days, the structure and temporal evolution of the polar vortices is clearly seen on maps of isentropic PV (Waugh and Polvani, 2010).

The stratosphere-troposphere coupling has also been analyzed by means of the PV distribution. Hartmann et al., (2000) and Ambaum and Hoskins (2002) showed that strong stratospheric polar vortex as measured by the positive stratospheric Northern Annular Mode (NAM) is associated with the positive phase of the tropospheric NAM. This connection is due to the fact that in the positive phase of the tropospheric NAM, Rossby waves of tropospheric origin tend to propagate upward and equatorward which implies less wave activity directed to the stratospheric polar vortex. Since PV can be irreversibly mixed along isentropic surfaces by Rossby wave breaking (RWB), weak wave activity in the polar stratosphere will be associated with strong PV gradients, hence a less disturbed polar vortex. Therefore, the conservation properties of PV on isentropic surfaces provide a powerful tool for the analysis of the complex interactions and mechanisms associated with stratospheric as well as tropospheric variability and the possible coupling between the two.

In the troposphere, the tropics are regions of strong diabatic anomalies associated mainly with the El Niño Southern Oscillation (ENSO), the Hadley circulation (HC) and associated Intertropical Convergence Zone (ITCZ). Diabatic processes in the stratosphere are mainly associated with the Brewer Dobson circulation (BDC) which in turn is directly affected by the Quasi-biennial Oscillation (QBO) (e.g. Flury et al. 2013). In these regions where strong diabatic heating or cooling occurs, PV is materially changed due to cross isentropic flow which is able to transport mass across isentropes but not potential vorticity substance (PVS). PVS can only be concentrated or dilute by a decrease or increase of mass within a layer bounded by two isentropic surfaces and therefore PV values increase or decrease within that layer. The fact that PV can only change in the presence of cross isentropic flow makes it particular useful for the study of modes of variability where diabatic processes play a significant role.

This thesis is organized as follows. In section 2 an overview of the structure and circulation of the atmosphere is given (section 2.1), and a literature review is made of the annular modes (section 2.2), the southern oscillation index (section 2.3), the Brewer-Dobson circulation (section 2.4) and isentropic potential vorticity (section 2.5). In section 3 the methodology is described which englobes the data treatment (section 3.1) and a short overview of principal component analysis

(section 3.2). Section 4 shows the results and discussion. The reason for analyzing PV on the 600 K and 350 K isentropic surfaces is given in section 4.1. PCA results of PV on the 600 K are given in section 4.2 and the same is repeated for PV on the 350 K with the results presented in section 4.3. Climate indices were further computed using the method of Li and Wang (2003) for the zonal mean PV, the zonal mean zonal wind and the cross isentropic flow on both the 600 K and 350K isentropic surfaces as well as geopotential height for the calculation of the annular modes indices. PCA was then applied to the climate indices described above and the results are shown in section 4.4. A brief summary is given at the end of each section. Finally the conclusions are presented in section 5.

2 THEORETICAL BACKGROUND

2.1 Atmospheric structure and circulation

The atmosphere is conventionally divided into layers according to changes in temperature with height (**figure 2.1.1**). The two atmospheric layers that are of most importance, due to their role on climate variability and atmospheric dynamics, are the troposphere and the stratosphere. The troposphere extends from the surface to about 10 km altitude and contains about 75% of the total mass of the atmosphere. This is that part of the atmosphere where, what is commonly referred to as “weather” occurs, and is characterized by low values of static stability and strong vertical motions. The region between 10 km and 50 km altitude is called the stratosphere. In contrast to the troposphere, there is an increase of temperature with height due to absorption of solar ultraviolet radiation by ozone. Therefore static stability is large and fast vertical motions are thus suppressed.

The circulation of the stratosphere varies strongly with height, latitude and longitude. However, the strongest variations are in height and latitude (Haynes, 2005). Zonal means (average around a latitude circle) are thus an appropriate approach for the analysis of stratospheric variability. Although the tropospheric circulation varies somewhat more in longitude, in general the zonal mean approach can also be applied to this region. The reason being that in most of the atmosphere the winds are mainly zonal and transport in the zonal direction is fast enough so that the analysis of the atmospheric circulation is in general fairly well described in the meridional plane (Plumb et al., 1987). Therefore, the temporal evolution of a particular atmospheric variable will depend more strongly on latitude than on longitude.

The troposphere and the stratosphere are separated by the tropopause. The tropopause is commonly defined in two different ways. The thermal tropopause, used for the tropics, is defined by the World Meteorological Organization (WMO) as the lowest level at which the lapse rate decreases to 2 K/km or less, provided that the average lapse rate between this level and all higher levels within 2 km does not exceed 2 K/km. The dynamical tropopause, used for the extratropics, is defined as the isentropic surface where PV has a value of about 2 PVU (1 PVU=10^{-6} m^2 K s^{-1} kg^{-1}), where PVU stands for potential vorticity unit. Following the latter approach, the atmosphere can be subdivided into three different regions: the Overworld, the Middleworld and the Underworld (Hoskins, 1991) (**figure 2.1.2**). In the Overworld, the isentropic surfaces lie entirely above the tropopause (near the 380 K isentrope), hence in the stratosphere. That part of the atmosphere where isentropic surfaces cut the tropopause is called the Middleworld (between approximately the 310 K and 380 K isentropes). This is a very interesting part of the atmosphere since it encompasses air from the stratosphere and troposphere. Poleward of about 40° latitude, the isentropes of the Middleworld lie in the stratosphere (the so called lowermost stratosphere) whereas equatorward of 40° latitude the isentropic surfaces lie in the upper troposphere. **Figure 2.1.3** shows a schematic view of the atmosphere in which the transport pathways into and out of the lowermost stratosphere are clearly indicated. Air can reach the stratospheric part of the Middleworld by three paths: path A is associated with the downward branch of the BDC which leads to diabatic descent from the Overworld into the lowermost stratosphere, path B represents diabatic ascent from the troposphere at midlatitudes and path C indicates along isentropic transport from the upper troposphere across the tropopause into the lowermost stratosphere and is sometimes referred to as transport through the 'tropopause gap' (Dessler et al. 1995). The Middleworld is therefore particularly suitable for the study of the stratosphere-troposphere as well as the troposphere-stratosphere exchange. Finally, the Underworld is defined as that part of the atmosphere where all the isentropic surfaces lie below the tropopause, thus in the troposphere, and cut the Earth's surface.

Figure 2.1.4 shows the monthly mean zonal mean zonal wind, PV and pressure as a function of potential temperature and latitude for January and July. The zonal wind shows a clear seasonal cycle, with stronger eastward winds in the winter hemisphere in the stratosphere, especially in the SH. During the winter season, the polar cap does not receive solar radiation but still emits longwave radiation out to space. This leads to a cooling of the polar cap and an enhanced horizontal

temperature gradient between the poles and the tropics, which by thermal wind balance should be accompanied by a band of strong eastward winds. This strong jet of the stratospheric winter hemisphere is located above the 450 K isentrope, at about 65° latitude and is called the stratospheric polar night jet. The stratospheric winter polar vortex is therefore a cyclonic system centered over the pole and is characterized not only by a strong eastward jet but also by very high values of PV. In summer, the polar vortex vanishes and the zonal wind reverses direction becoming weakly westward due to the combine effects of planetary wave drag and diabatic processes (van Delden, 2012). However, the characteristic summer wind reversal can also occur during mid- winter in the NH, a phenomenon known as sudden stratospheric warmings (SSW). SSWs are a result of upward propagating planetary waves, which originate in the troposphere, that are able to reach the stratosphere and break there, mixing momentum and heat. The result is an increase of the stratospheric temperature over the polar cap, and a reversal of the zonal wind.

At lower levels, near the 350 K isentrope (approximately 200 hPa) at 30° latitude a second eastward jet is clearly visible from **figure 2.1.4**. This is the so called subtropical jet. The subtropical jet does not reverse direction in any season and the seasonal cycle is characterized by strong eastward winds centered at approximately 30° latitude during winter especially in the NH, and weak eastward winds centered near 45° latitude, during summer.

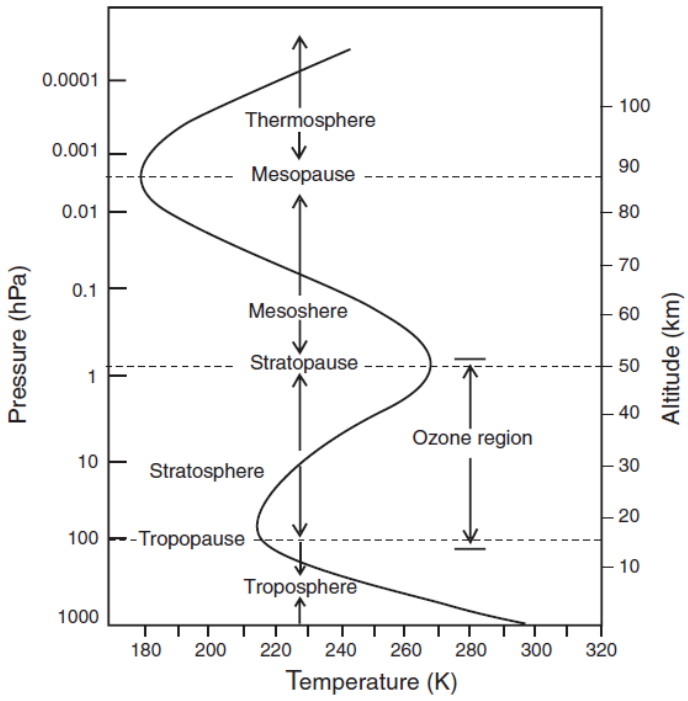

Figure 2.1.1 Vertical thermal structure of the Earth's atmosphere up to 120 km. Source: Mohanakumar (2008).

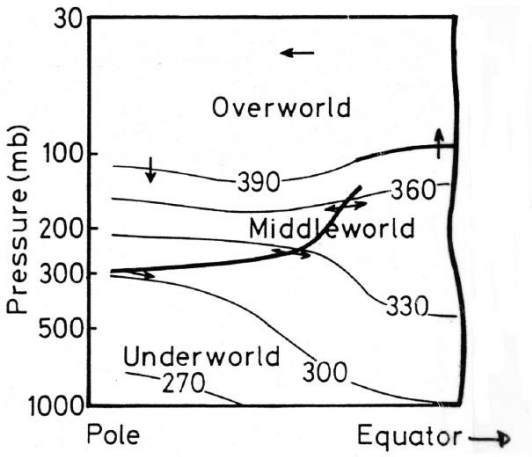

Figure 2.1.2 Schematic view of the atmosphere as a function of latitude (pole-equator) and height (surface-30 hPa). The dynamical tropopause is marked by a thick line and isentropes every 30 K from 270-390 K by thin lines. The arrows indicate some adiabatic (horizontal arrows) and diabatic cross isentropic (vertical arrows) transport. Source: Hoskins (1991).

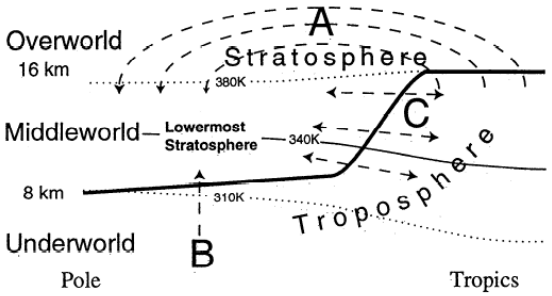

Figure 2.1.3 Schematic view of the atmosphere highlighting the transporting paths into and out of the lowermost stratosphere. The thick line corresponds to the tropopause. The lowermost stratosphere lies between the tropopause and approximately the 380 K isentropic surface. Dashed lines represent the Overworld-Middleworld and Middleworld-Underworld boundaries. The letters A, B and C shows pathways by which air may enter or leave the lowermost stratosphere. Path A represents descent from the Overworld, path B represents transport of air from the troposphere to the lowermost stratosphere and path C indicates along isentrope transport from the upper troposphere. Source: Dessler et al. 1995.

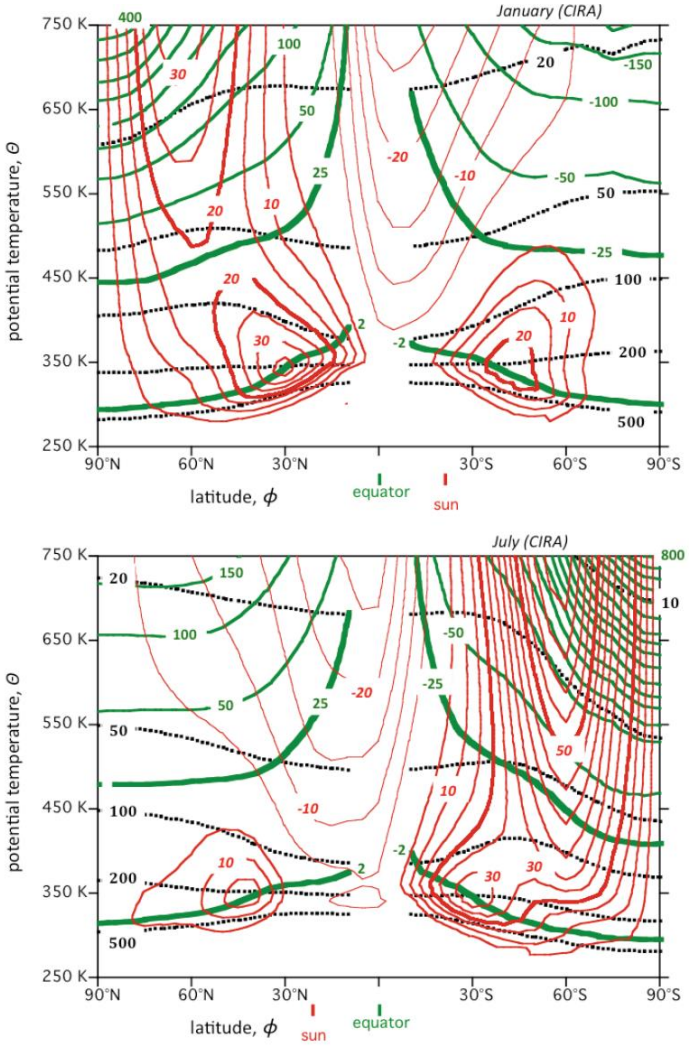

Figure 2.1.4 The zonal average, monthly average zonal wind (red contours, labeled in ms^{-1}), potential vorticity, PV (green contours, labeled in PVU; interval is 50 PVU for absolute values greater than 50) and pressure (black dashed contours, labeled in hPa) as a function of potential temperature and latitude according to the COSPAR International Reference Atmosphere (CIRA) for January and July. The monthly average overhead position of the Sun is indicated in red below each figure. Source: van Delden (2012).

2.2 Annular modes

The annular modes (AMs) are atmospheric teleconnections, which are defined as significant simultaneous temporal correlations between distinct, widely separated spatial points (Wallace and Gutzler, 1980). These atmospheric teleconnections, as measured mainly by pressure, geopotential height or winds, as well as PV, are thus representatives of climate variability.

The exact terminology of the AMs is still today somewhat unclear. In the Northern Hemisphere (NH), the main mode of variability has been defined as the North Atlantic Oscillation (NAO), the

Artic Oscillation (AO) or Northern Annular Mode (NAM), while in the Southern Hemisphere (SH) one finds the Antarctic Oscillation (AAO) or Southern Annular mode (SAM). The AMs are analyzed with the aid of indices which provides the temporal evolution of their strength.

The NAO index was first defined by Felix Exner (1913) and later on by Walker and Bliss (1932) who used simultaneous linear combination of time series of surface air pressure measured at 4 different stations and surface air temperature at other five. Several years later, the NAO index was simplified by Rogers (1984) by using only sea level pressure (SLP) anomalies between Ponta Delgada, Azores (Portugal) and Akureyri in Iceland whilst Hurrel (1995) used SLP between Lisbon (Portugal) and Stykkisholmur (Iceland). The NAO index defined by Rogers and Hurrel are still in use today, and they represent in general, a seesaw of pressure between the subtropics and high latitudes. When the NAO index is positive (positive phase of the NAO), the subtropical high pressure system (which is a permanent feature in the subtropics) is stronger than average and at the same time, the Icelandic low pressure system (which is also a permanent feature near Iceland) is lower than average. The consequences of this increase in pressure gradient are stronger tropospheric winds in the Atlantic region, and a northward shift of the storm track. In this scenario, the northern Europe will experience above average precipitation and temperature associated with the arrival of low latitude warm air masses. The opposite is true for the negative phase of the NAO.

The AO or the NAM differs from the NAO only with respect to the location of the low pressure system which in this case is located over the Arctic. Thompson et al. (2003) defined the AO/NAM index as the principal component associated with the leading eigenvector that explains most of the variability of the hemispheric geopotential height fields poleward of 20°N and concluded that, while the NAO is a regional phenomenon, the NAM is a hemispheric one and therefore the NAO could be interpreted as a regional manifestation of the NAM. Wallace (2000) on the other hand, had already pointed out that the difference between the NAO and the NAM lies simply in their respective definitions. This was later on supported by Feldstein and Franzke (2006), which not only found, from a mathematical perspective using standard statistic techniques, that the NAM and the NAO are drawn from the same population, therefore they are statistically indistinguishable, but also that these modes of variability are not a mathematical artifact as already pointed out in some studies. Throughout this thesis we share the same ideas of Wallace (2000), hence the NAM (SAM) index will represent the main mode of climate variability in the northern (southern) hemisphere.

Although the most common way to define the AMs indices is by EOF analysis, other approaches can be equally valid. Li and Wang (2003) used cross correlation maps of zonal mean SLP anomalies in the NH and showed that there is a strong negative correlation in SLP between the subtropics and higher latitudes with two homogeneous zones centered at 35°N and 65°N (**figure 2.2.1**). The maximum in anticorrelation in zonal mean SLP within these zones, the annular belts of action, are then a representation of the strength of the subtropical high and the subpolar low. Therefore, Li and Wang (2003) defined the NAM index (ZI) as the difference in normalized zonal mean monthly mean SLP ($\widehat{\mathrm{P}}$) between the center of maximum anticorrelation at 35°N and 65°N,

$$\mathrm{ZI} = \widehat{\mathrm{P}}_{35°\mathrm{N}} - \widehat{\mathrm{P}}_{65°\mathrm{N}} \qquad \textbf{2.2.1}$$

Like this, the positive NAM index is associated with a stronger than average subtropical high and a lower than average subpolar low, with the opposite for the negative phase, in agreement with observations and theory.

Li and Wang defined the NAM index using mean SLP, however the AMs can also be defined throughout the troposphere and stratosphere at different pressure levels. In fact, several studies pointed out that the role of the AMs in the stratosphere is distinct from that in the troposphere (e.g. Kushner, 2010). In the stratosphere, the NAM and the SAM are manifested as the strength of the polar vortex, with positive (negative) phase of NAM/SAM representing a strong (weak) polar vortex. In the troposphere, the NAM is manifested by latitudinal changes, in terms of zonal mean zonal wind, of the midlatitude (eddy-driven) jet (Witman, Charlton and Polvani, 2004, Lorenz and Hartmann, 2002; Eichelberger and Hartmann 2007). In its positive phase, the NAM consist of a stronger midlatitude jet, hence a weaker subtropical jet and vice-versa. On the other hand, the positive phase of the tropospheric SAM consists of a poleward shift of the tropospheric jet (Kushner, 2010). According to Kushner (2010), these differences between the tropospheric NAM and SAM arise from the difference in the spatial structure of the tropospheric jets in both hemispheres.

Recent studies, however, suggest a direct relationship between the strength of the polar vortex, hence the stratospheric NAM, and the tropospheric NAM (e.g. Ambaum and Hoskins, 2002, Baldwin and Dunkerton, 1999). Baldwin and Dunkerton (1999) showed that typically the NAM anomalies first appear in the stratosphere and then propagate downward with a period of few weeks. As already proved by Hartmann et al. (2000) and later on by Ambaum and Hoskins (2002), the positive phase of the surface NAM (NAM index defined using SLP or geopotential height at the surface) is

associated with upward propagating Rossby waves which tend to be refracted equatorward. Like this, less wave activity is found at polar latitudes in the stratosphere which leads to a stronger (less perturbed) stratospheric polar vortex. They further showed that a strong positive NAM at the surface leads a strong stratospheric polar vortex with a lag of a few days. In contrast with the findings of Ambaum and Hoskins, Black and McDaniel (2009) found that the NAM in the middle stratosphere and the tropospheric NAM are poorly correlated. In spite of a continuous research on the subject, the dynamics behind the coupling between the stratosphere and troposphere in terms of the AMs is not yet fully understood.

Although the dynamics of the NAM in the troposphere and especially in the stratosphere in the extratropics seems to be relatively well understood, less attention has been given to the role of the tropics. According to Thompson and Wallace (2000) the positive phase of the AMs are also associated with high temperature anomalies near the equator at 100 hPa (due to a weaker BDC) and westward surface winds anomalies that extend deep into the subtropics. Thompson and Lorenz (2004) on the other hand, found that the link between the tropospheric AMs and the tropical circulation was evident only for the NAM during the winter NH months and during the El Niño, the negative phase of the Southern Oscillation index (SOI).

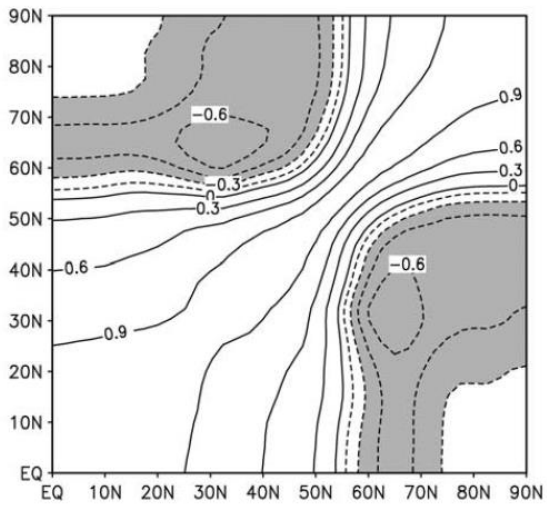

Figure 2.2.1 Correlation between zonal mean monthly mean SLP anomalies in the NH (1958-2000). The contour interval is 0.3 for positive values and 0.1 for negative values. Note the map is symmetric about the diagonal. Source: J. Li and J. X. L. Wang, 2003: A modified zonal index and its physical sense.

2.3 The Southern Oscillation Index (SOI)

El Niño and La Niña are terms commonly used to describe an ocean-atmosphere interaction in the Pacific. During the El Niño phase the sea surface temperatures (SST) in the east equatorial Pacific are anomalously high, whilst during La Niña the SSTs are lower than normal. In the atmosphere, the change in pressure between the east and west tropical Pacific, associated with the El Niño and La Niña is referred to as the Southern Oscillation (SO). The El Niño and the SO are two phenomena of one oscillation with an irregular period of several years known as ENSO (El Niño Southern Oscillation). The ENSO is measured by the Southern Oscillation index (SOI) which is defined by the difference in normalized SLP between Tahiti and Darwin. The negative (positive) phase of the SOI, which is associated with below (above) average SLP over Tahiti and above (below) SLP in Darwin, corresponds to the El Niño (La Niña) events. During the El Niño, excess of heat in the oceans due to the warmer sea surface, is redistributed within the tropical Pacific and it is released to the atmosphere mainly by evaporation leading to an anomalous warming of the tropical troposphere by diabatic heating associated with tropical precipitation (Trenberth et al., 2002). The El Niño and associated enhanced tropical diabatic heating has profound implications for the atmospheric circulation on a global scale. This is seen not only in terms of precipitation patterns, with above average precipitation at the equator and midlatitudes and below average in the subtropics (Seager et al., 2003), but also in its effects on the intensity of the Hadley circulation.

2.4 The Hadley cell (HC)

The HC (**figure 2.4.1**), which lies between 30°N and 30°S, is one of the three meridional circulations that exist within the troposphere, being the other two the Ferrel cell at midlatitudes and the Polar cell at polar latitudes. While the Ferrel cell is an indirect circulation, i.e., cold air rises on the poleward side and warm air sinks on the equatorward side, the Polar cell is a direct circulation, with warm air rising on the equatorward side and cold air sinking on the poleward side. The HC is also thermally driven (direct circulation) with air ascending in the tropics, transported poleward in the upper troposphere (altitude of about 15 km), descending in the subtropics with a return equatorward flow at the surface. The descending branch of the HC, which is responsible for the formation of the subtropical high pressure belt (subtropical anticyclones) such as the Azores high in the NH, is stronger during winter. The winter HC is characterized by an upward branch in the summer hemisphere and a downward branch in the winter hemisphere. The two branches of the

HC are separated by a narrow region near the equator characterized by strong latent heat release associated with convective cloud systems, known as the Intertropical convergence zone (ITCZ). The ITCZ is a result of the convergence of the trade winds of both hemispheres which constitutes the surface branches of the HC, and the strong latent heating observed in this region associated with precipitation drives the HC (van Delden, 2012). Therefore, when an El Niño causes enhanced diabatic heating in the tropics, it is expected a strengthening of the HC. In fact some studies results showed that the ENSO as well as the AMs can impact the strength and extent of the HC. For example, Oort and Yienger (1996) showed that during El Niño events the subtropical jets (at 200 hPa) tend to increase in both hemispheres, while they tend to be weaker during La Niña events. They further suggest that the strength of the subtropical jets could be a good indicator of the HC intensity, since they are located in the vicinity of the HC's downward branches. In a more recent paper, Nguyen et al. (2012) showed that, the HC tends to contract and intensify during the El Niño's, with the opposite behavior during the La Niña's. According to their results, while the intensity of the HC is mainly influenced by the ENSO, the extent and width of the HC is associated with the AMs due to a displacement of the eddy driven jet. Changes in the intensity of the HC have therefore a direct effect not only in the atmospheric circulation due to the high altitude diabatic heating, but also in climate variability in the tropics and subtropics through its downward branch.

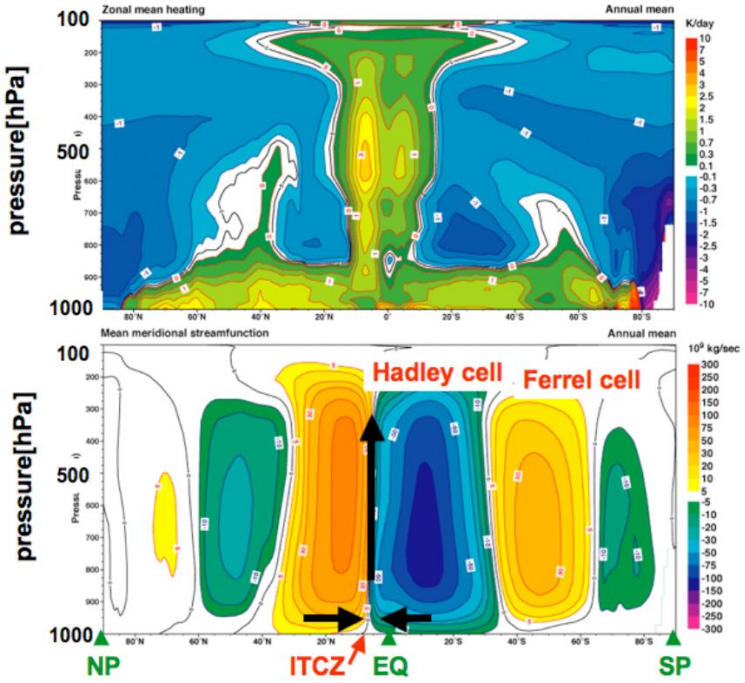

Figure 2.4.1 Top panel: zonal mean, annual mean diabatic heating as a function of pressure and latitude (for the period 1979-2001). Lower panel: annual average, zonal average streamlines in the vertical plane perpendicular to the equator. Arrows indicate direction of

flow. Flow converges near the equator at the ITCZ. The Hadley cell and Ferrel cell on the SH are indicated. Source: van Delden (2012).

2.5 The Brewer Dobson Circulation (BDC)

In the stratosphere, the BDC is a large scale, wave driven circulation first hypothesized by Dobson (1929) and later on by Brewer (1949). **Figure 2.5.1** shows the schematic of this circulation. In general, the BDC consists of air crossing the tropical tropopause to the stratosphere in the tropical pipe, followed by a poleward drift where it is redistributed from the tropics to the higher latitude regions where it sinks. The poleward air flow is due to planetary Rossby waves that are generated in the extratropical troposphere which are able to propagate upwards if the background winds are eastward and below a certain critical value. When these waves reach the stratosphere, they eventually break and dissipate transferring westward momentum to the mean flow, resulting in a tendency for the air to move poleward due to an eventual balance between the wave induced force and the Coriolis acceleration (Holton et al., 1995). The resulting descent of air is a consequence of mass continuity: upwelling in the tropics followed by poleward motion must be balanced by downwelling at higher latitudes and a return flow towards lower latitudes.

The BDC is characterized by two branches which depend on the altitude and the latitude of the descent. The shallow branch, which lies in the lowermost stratosphere, is characterized by rising air in the tropics and sinking in the subtropics/midlatitudes, while the deep branch reaches the mid/upper stratosphere and descends into the surf zone and the polar vortex in mid and high latitudes. The type of waves that drive these two branches differs. The shallow branch, which is characterized by a two cell circulation, is driven by synoptic and planetary waves that break in the lower stratosphere. The deep branch on the other hand, is characterized by a single cell circulation towards the winter hemisphere dominated by planetary waves which are able to reach the mid to upper stratosphere and eventually break there (Plumb, 2002). Therefore, the upper branch is stronger in the NH than in the SH due to stronger wave activity in the former.

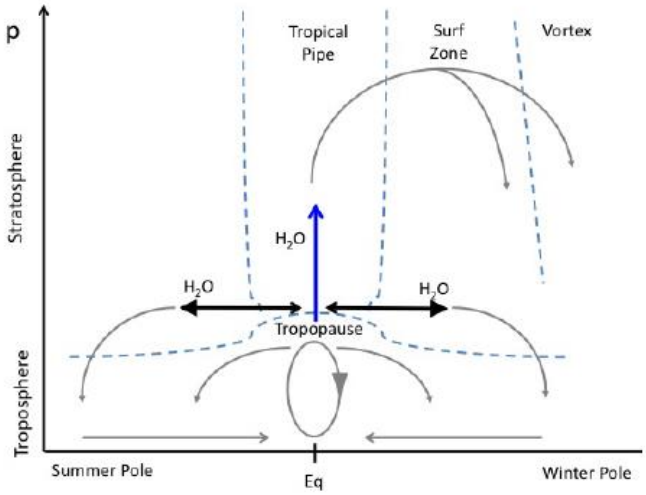

Figure 2.5.1 Schematic of the Brewer Dobson circulation (BDC) in the stratosphere. Thick black arrows represent poleward transport and mixing of air in the lowermost stratosphere. The ellipse centered at the equator and the two associated branches (light gray) represent the Hadley circulation. Just above the tropopause the thin light gray arrows represent the shallow branch of the BDC, while higher up they represent the deep branch. Source: Flury et al., 2013.

2.6 The quasi-biennial oscillation (QBO)

Also in the stratosphere but confined to the tropics, the QBO is the main mode of variability. The QBO can be seen between approximately 1 hPa and 70 hPa (475K) and is characterized by downward propagation of alternating eastward and westward wind regimes with an average period of about 28 months (Baldwin et al., 2001) (**figure 2.6.1**). The mechanism behind the QBO involves the interaction of different atmospheric waves with the background flow, such as equatorial kelvin waves, which could account for the eastward phase of the QBO (Wallace and Kousky, 1968; Holton and Lindzen, 1972) and Rossby-gravity waves which could account for the westward QBO phase (Lindzen and Holton, 1968). Although the QBO's driving mechanism involving Kelvin and gravity Rossby waves is still accepted, more recent studies showed that only these two were not sufficient to produce, in models, the observed period of oscillation of the QBO (Dunkerton, 1997). Until today, a complete understanding about the exact mechanism by which the QBO arises is not fully understood.

There is increasingly evidence that the QBO modulates the transport of chemical species in the atmosphere. Approaches to study stratospheric transport associated with QBO include parcel trajectories using chemistry-climate models (Punge et al., 2009), ozone (e.g. Hamilton et al., 1988), stratospheric water vapor (Flury et al., 2013) among others. It is also by now accepted that the QBO

induces a secondary meridional circulation (SMC) mainly in the tropics and subtropics (e.g. Baldwin et al., 2001) which is superimposed upon the BDC, therefore affecting not only the meridional transport to the extratropics but also the stratospheric tropical upwelling. **Figure 2.6.2** shows the schematic of the SMC of the QBO. Due to its relative long period and equatorial symmetry (e.g. Baldwin et al. 2001), the atmosphere in the equatorial region can be considered in thermal wind balance (which implies that above average temperature anomalies are associated with the westerly vertical shear while below average temperature anomalies are associated with the easterly vertical shear). For thermal wind balance to be maintained, the westerly vertical shear (eastward shear) should be accompanied by adiabatic heating (downwelling). Conversely, adiabatic cooling (upwelling) should occur in the easterly shear vertical zone (westward shear). The air subsidence in the westerly shear zone will decelerate the upward branch of the BDC weakening it, while in the easterly shear zone enhanced upwelling will result in a stronger BDC (Flury et al., 2013). Therefore, eastward winds (positive QBO) are associated with reduced upwelling below the altitude of the maximum eastward winds and a weaker BDC, whilst westward winds (negative QBO) are associated with enhanced upwelling below the westward wind maximum, hence a stronger BDC. At the location of maximum eastward (westward) winds, the maximum of horizontal convergence (divergence) occurs.

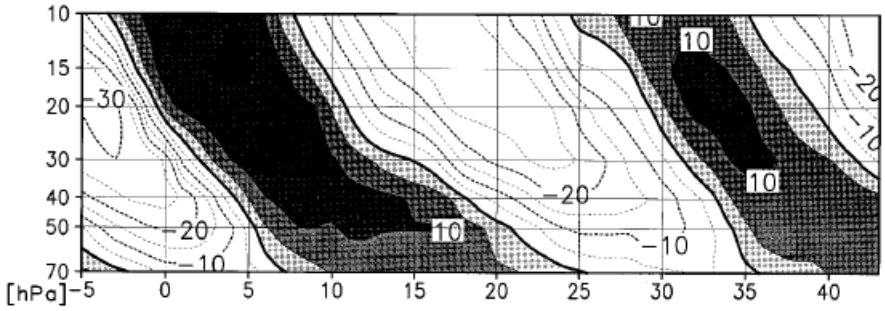

Figure 2.6.1 A composite plot of the QBO according to the easterly-westerly transition at 20 hPa. Westerlies are shaded. The contour interval is 5 ms^{-1}. Source: Baldwin et al. (2001).

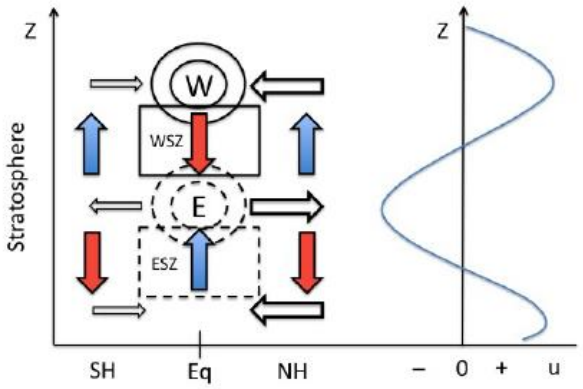

Figure 2.6.2 Schematic of the secondary meridional circulation (SMC) of the QBO on the left and the zonal wind at the equator on the right. The letters W and E stand for respectively westerly (eastward winds) and easterly (westward winds). Red (blue) arrows represent vertical motion and associated warm (cold) temperature anomalies. In the easterly shear zone (ESZ), which is associated with cold temperature anomalies, just below the easterlies maximum (E) upwelling is enhanced. At the altitude of maximum easterlies air diverges poleward increasing the strength of the BDC. At the altitude of the maximum westerlies (W) air converges towards the equator and descends in the westerly shear zone (WSZ) which is associated with warm temperature anomalies. In this case, the descending air slows down the upward branch of the BDC, hence its strength. Source: Flury et al., (2013).

2.7 Potential vorticity (PV)

During adiabatic processes an air parcel does not exchange heat with its environment. Adiabatic heating, which for instance occurs in the downward branch of the BDC, is associated with local warming due to compression of air, while adiabatic cooling in the upward branch of the BDC is associated with local cooling due to expansion of air.

Potential temperature (θ), is the temperature an air parcel would have if it would be brought adiabatically to a reference pressure and is described by the Poison's equation

$$\theta = T\left(\frac{P_0}{p}\right)^{R/C_p}, \qquad \textbf{2.7.1}$$

where T is temperature, p pressure, R the dry-air gas constant and C_p is the specific heat of air at constant pressure. For adiabatic conditions, potential temperature is conserved and so is entropy. Since entropy is proportional to the natural logarithm of potential temperature, lines of constant θ are called isentropes or lines of constant entropy. Isentropic surfaces behave like material surfaces, thus air parcels are thermodynamically bounded to a particular isentrope in the absence of diabatic processes (Moore, 1989). Furthermore, in a stable atmosphere, potential temperature increases

with height, hence in isentropic coordinates potential temperature is simply a vertical coordinate and the motion of the atmosphere is then two dimensional (Moore, 1989).

Planetary (Rossby) waves are perhaps the main cause of atmospheric large scale variability in the extratropics. These waves were first identified by Rossby (1939). Rossby waves can only propagate upward in weak eastward flows and owe their existence to strong latitudinal gradients of PV, which is defined as

$$\mathrm{PV} = -\frac{1}{\mathrm{g}}(\zeta_\theta + \mathrm{f})\frac{\partial \mathrm{p}}{\partial \theta} = \frac{(\zeta_\theta + \mathrm{f})}{\sigma}, \qquad \textbf{2.7.2}$$

where g is the acceleration due to gravity, ζ_θ is the relative vorticity on an isentropic surface, $f = 2\Omega \sin\phi$ is the planetary vorticity (or Coriolis parameter) with $\Omega = 7{,}292 \times 10^{-5} s^{-1}$ the angular frequency of the Earth's rotation and ϕ is latitude. The isentropic density is defined as $\sigma = -\frac{1}{g}\frac{\partial p}{\partial \theta}$ and is equivalent to mass per unit area in a layer of thickness equal to one degree of potential temperature (van Delden, 2012).

PV is conserved under adiabatic and frictionless conditions, thus PV contours on isentropic surfaces also behave like material surfaces. Under these conditions, Rossby waves can be viewed as reversible undulations of PV contours, provided that the wave amplitude is relatively small. However, for sufficient large amplitudes, material contours are strongly deformed and eventually break leading to irreversible horizontal mixing of PV which is commonly referred to as Rossby Wave Breaking (RWB). The concept of RWB was first applied in studies of the stratospheric polar vortex dynamics. McIntyre and Palmer (1984) showed that wave breaking is characterized by high PV air (at polar latitudes) being stripped out of the vortex and mixed with the surrounding low PV air (at lower latitudes). This can be seen in **figure 2.7.2** which shows a schematic latitudinal distribution of PV (Q in the figure) in the stratosphere before and after a RWB event. Before the Rossby wave breaks (thin line), PV values decrease from the pole toward the equator where it attains a minimum. After the breaking event (curvy thicker line), PV values decrease at higher latitudes and increase at lower ones. These two regions of PV anomalies of opposite sign are separated by a mixing region, the so called 'surf zone'. The concept of a surf zone surrounding the stratospheric polar vortex was first proposed by McIntyre and Palmer (1983, 1984) who suggested that, in analogy with the breaking of ocean waves, the breaking of RW in this region would lead to weak meridional PV gradients due to strong irreversible mixing of PV along isentropic surfaces. Therefore

in the stratosphere, the poleward edge of the surf zone marks the edge of the polar vortex which is characterized by sharp PV gradients.

As explained above, for adiabatic and frictionless processes PV is a conserved quantity that can be transported horizontally, i.e., along isentropes. However, in the presence of diabatic heating or cooling, thus vertical motion, PV is materially changed.

In isentropic coordinates, the vertical velocity is simply $d\theta/dt$ and, since potential temperature increases with increasing height, diabatic heating (cooling) is understood as upward (downward) motion (Moore, 1989). This implies that, for instance, air that belongs to the Overworld can only reach the troposphere if it descends across isentropic surfaces and air from the Underworld can only reach the stratosphere if it rises across isentropes. Therefore vertical velocities, which occur in the presence of diabatic processes, are understood as cross isentropic flow. Since in these conditions PV is no longer conserved, one way to analyze the effect of the cross isentropic flow on the PV distribution is to interpret it as the mixing ration of a conserved quantity called potential vorticity substance (PVS),

$$PV = \frac{PVS}{\sigma} \qquad \textbf{2.7.3}$$

Using this approach, PV can be viewed as the 'amount' per unit mass of a substance called PVS (van Delden, 2012). According to the impermeability theorem (Haynes and McIntyre, 1990), PVS cannot be transported across isentropic surfaces, i.e., isentropes are impermeable to PVS. However, according to equation 2.7.4 (van Delden, 2014), where I_d is the cross isentropic mass flux, mass can be transported across isentropes, therefore isentropes are permeable to mass.

$$I_d = \frac{d\theta}{dt}\sigma \qquad \textbf{2.7.4}$$

This implies that cross isentropic flow $\left(\frac{d\theta}{dt}\right)$ is able to transport mass (σ) but not PVS. Because PVS cannot be created or destroyed in layer bounded by two isentropic surfaces which do not intersect the ground (Haynes and McIntyre, 1990), the effect of an increase (decrease) of mass in the layer will lead to a dilution (concentration) of PVS, hence a decrease (increase) of PV values in that layer. In other words, if there is more mass entering a layer than leaving it, PVS will be diluted and PV values will decrease. Conversely, if there is more mass leaving a layer than entering, PVS will be concentrated and PV values will increase. Therefore, PVS can be diluted or concentrated when mass

leaks diabatically into (convergence) or out (divergence) of a layer bounded by two isentropic surfaces resulting in a decrease (increase) of PV values within the layer.

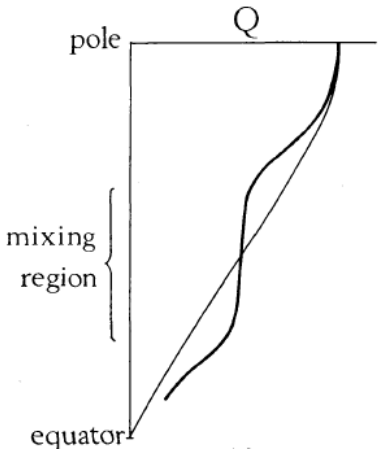

Figure 2.7.2 Schematic latitudinal distributions of PV (Q) on an isentropic surface in the stratosphere, before (thin curve) and after (thick curve) a large-amplitude planetary wave breaking event centered at midlatitudes. Source: McIntyre (1981).

3 METHODOLOGY

3.1 Data

The primary data used in this project are zonal means of monthly means of potential vorticity (PV) and the horizontal component of the wind (U) on the 350 K and 600 K isentropic surfaces, mean sea level pressure (MSLP), geopotential height (gph) at 1000, 925, 875, 750, 600, 500, 350, 250, 200, 150, 100, 50, 30, 20 and 10 hPa and total precipitation from ERA-Interim reanalysis in a grid of 0.75°×0.75° for the period 1979 – 2013. The zonal mean monthly mean cross isentropic flow (CrIs) also on the 350K and 600K isentrope was kindly provided by Remko Klaver (IMAU, Utrecht University) for the period of time 1980 – 2013 on a 1.5°×1.5° grid.

All the data were centralized by subtracting the climatological mean (monthly means) for the period in consideration, that is, with respect to PV, U, SLP and gph, monthly means with respect to the 1979-2013 period and for the cross isentropic flow, monthly means for the 1980-2013 period. The data were further normalized by division by its standard deviation. In this way all data sets have the seasonal cycle filtered out, a mean of zero and a variance of one.

Furthermore, trends were also calculated for all data sets following the method of Santer et al., (2000). Only very weak trends were found for PV and the cross isentropic flow on the 350 K isentropic surface and no trends for the rest of the data sets. The results of the analysis using PV

and the cross isentropic flow detrended and not detrended did not vary in any significant way. Nevertheless, the detrended PV and cross isentropic flow on the 350 K were the ones used throughout this project.

The Southern Oscillation Index (SOI) and the Quasi-Biennial Oscillation index (QBO) at 30 and 50 mb were obtained from the National Oceanic & Atmospheric Administration, NOAA, (http://www.esrl.noaa.gov/psd/data/climateindices/list/). The QBO index is defined by the zonal mean zonal winds at Singapore, therefore its sign is in agreement with the conventional sign of the winds, i.e., the negative QBO represents westward winds while the positive QBO represents eastward winds.

3.2 Principal Component Analysis (PCA)

Principal component analysis (PCA) has been extensively used to analyze variability in meteorological data, as the ones used in this study. PCA arose first as Empirical Orthogonal Function (EOF) analysis when Lorenz (1956) attempted to improve the so called statistical weather forecasting, and although the terminology is due to Lorenz, the method has been already applied by Obukhov in 1947. Nowadays PCA and EOF analysis are, from a mathematical point of view and for most of the researchers, indistinguishable. The result of applying PCA to a data field is a set of orthogonal spatial patterns, the eigenvectors or EOFs, and associated (and uncorrelated) time series, or principal components (PCs). Today, PCA (or EOF analysis) is mainly used to reduce a climate data set with a large amount of variables into a data set that contains much fewer new variables which are linear combinations of the original ones (Wilks, 2011), as well as individual modes of variability (teleconnections) such as the Annular Modes (AM), or even to compare observations and reanalysis to climate model simulations (A. Hannachi et al., 2007).

In this project, PCA is applied in the following manner (H. Björnsson and S. A. Venegas). A matrix of normalized anomalies (with respect to the climatology), X, of time versus latitude $(n \times m)$ is constructed for each of the meteorological fields. In case of PCA applied to the full domain of the fields (90°N to 90°S) with a period of time 1979-2013 and grid 0.75°×0.75° (case of PV and U), the matrix X will be equal to (420×241), while $X = (408 \times 121)$ for the cross isentropic flow since the time period is from 1980 to 2013 and the grid 1.5°×1.5°. The cross-correlation matrix (normalized covariance matrix), C, is obtained from $C = X^T X$. The eigenvalues and eigenvectors

are then found by solving $CR = R\Lambda$, where Λ is a diagonal matrix containing the eigenvalues λ_i and the r_i column vectors of R are the eigenvectors of C corresponding to the eigenvalues λ_i. The eigenvalues and associated eigenvectors are order from the highest explained variance to the lowest one and the principal components (PCs) associated with the eigenvectors (EOFs) are found by projection of X onto the j-th EOF according to $\overrightarrow{PC_j} = X \times EOF_j$.
By definition the resulting PCs are uncorrelated and centralized (mean equal to zero), thus they are further divided by their standard deviation in order to have a variance of one.

In order to visualize the resulting eigenvectors (EOFs), regressions are made of the respective time series (PCs) on the meteorological field anomalies (with respect to the climatology) which are of importance for the interpretation of the eigenvectors. The method is the one used by Baldwin et al. (2009) in which a spatial pattern $\boldsymbol{e}$ can be obtained by "projecting the data onto the time series" using the following formula,

$$\boldsymbol{e} = \frac{\boldsymbol{X^T y}}{\boldsymbol{y^T y}} \qquad \textbf{3.2.1}$$

Like this, if we wish to visualize, for instance the spatial pattern of the NAM, we could choose $\boldsymbol{X}$ to be the mean sea level pressure data in the northern hemisphere and $\boldsymbol{y}$ the NAM index. Furthermore, according to Baldwin and Thompson (2009), the above formula can be used generally to obtain a spatial pattern from any dataset and time series that have the same time length. In case the data matrix $\boldsymbol{X}$ is centralized (in this study always with respect to the climatology)**,** the resulting spatial pattern will have units of the climate data matrix used (with the time series $\boldsymbol{y}$ **also** standardized), if $\boldsymbol{X}$ is standardized (anomalies with respect to the climatology divided by their standard deviation), the resulting spatial pattern will be presented in terms of correlation coefficients which in this case are just equal to the regression coefficients (again with the time series $\boldsymbol{y}$ **also** standardized). Therefore throughout this project, rather than displaying the eigenvectors (EOFs) with their actual amplitude, they will be displayed in terms of correlations between the associated standardized PCs (or any other time series) and the standardized data field being used according to equation 3.2.1. The original EOFs spatial pattern is unchanged but by plotting correlations instead for the amplitudes of the EOFs (which are not easy to interpret in terms of useful quantities), one has more information about the local variance represented by a particular eigenvector (H. Björnsson and S. A. Venegas).

4 RESULTS AND DISCUSSION

In the next sections PCA will be applied to the full domain (90°N until 90°S) of potential vorticity on the 600 K (PV600K) and 350 K (PV350K) isentropic surfaces with the main goal of finding patterns of climate variability associated with PV distribution.

4.1 Isentropic surfaces

As already mentioned in the Introduction, the goal of this thesis is to find the possible links between the Overworld, the Middleworld and main modes of climate variability by analyzing PV on isentropic surfaces. The idea is to choose a specific isentrope that lies in the Overworld, hence representative of the stratosphere, and another that lies in the Middleworld which in principle could provide the connection between the upper troposphere in the tropics and the lowermost stratosphere in the extratropics, hence tropical and extratropical variability. For that end, the method of Li and Wang (2003) will be used and the approach is what follows. One starts by calculating a cross correlation matrix (normalized covariance matrix) of zonal mean monthly mean PV on the 265 K, 275 K, 285 K, 300 K, 310 K, 330 K, 350 K, 370 K, 395 K, 430 K, 475 K, 530 K, 600 K, 700K and 850 K isentropic surfaces (an example of such cross correlation matrix for PV on the 600 K isentrope is shown in section 4, **figure 4.2.1**), for the full domain, i.e. from 90°N to 90°S and full period from 1979 until 2013. Although in the next sections PCA is applied to the full domain of the PV field, the domain used for the choice of the isentropic surfaces is between 10.5°N and 90°N.

The cross correlation matrices are calculated with PV anomalies with respect to their mean and with respect to the climatology and further standardized by division by their standard deviation. Only the latter are of use in this project being the former only shown for comparison. The cross correlation matrices will therefore provide information about the simultaneous correlation of PV anomalies associated with two particular latitudes bands. Here, only the maximum of anticorrelation is of interest and that is because, in analogy to the NAM index defined by Li and Wang (2003), a negative PV anomaly at higher latitudes and a simultaneous positive one at lower latitudes must be associated with PV transport from higher to lower latitudes.

Figure 4.1.1 shows the correlation coefficients resultant from the cross correlation matrices applied to the isentropic surfaces mentioned above and the maximum in anticorrelation (note that in the figure the correlation coefficients are in absolute value) for each of those isentropes. **Figure 4.1.2** shows the latitudes associated with the maximum anticorrelation for the same isentropic surfaces.

In the Overworld, PV on the 600 K isentropic surface has a strong negative correlation of r = -0.82 between 48°N and 73.5°N, while in the Middleworld, on the 350 K isentrope the maximum in anticorrelation is r = -0.57 between 15°N and 34.5°N. Therefore PV on the 600 K isentrope should provide mainly variability between middle and high latitudes in the stratosphere, while PV on the 350 K should be representative of the NH variability between the tropics and subtropics in the upper troposphere. The PV variability on these two isentropic surfaces at the specified latitudes will be further explored in section 4.4.

Figure 4.1.3 shows the climatology of PV and **figure 4.1.4** the zonal mean zonal wind, both on the 600 K isentrope. In the NH, PV values increase sharply poleward of approximately 60°N between November and December, where a maximum value of 160 PVU at polar latitudes is attained between December and January. This is the period of time where the zonal mean zonal winds attain a maximum of about 30 ms^{-1} near 60°N. In February PV values start to decrease and between May and August, meridional PV gradients are absent and the zonal winds are weakly westward.
In the SH (where PV is by definition negative due to the Coriolis parameter), PV values are higher than in the NH and increase fast from about April to June. The maximum of PV occurs during the end of June until the end of August with PV values above 200 PVU (in absolute value). The zonal mean zonal wind again appears with its maximum of approximately 70 ms^{-1} between approximately 55°S and 65°S coinciding with the edge of the PV maximum at the same period of time. These eastward jets seen in the stratosphere in the winter hemisphere on the 600 K isentrope are in good agreement with the observed stratospheric polar night jet (section 2.1). Between 30°N and 30°S, the PV field appears to be rather constant throughout the year.

As it will be shown in the next sections, the ring of high PV values seen at polar latitudes in the winter hemisphere is a clear representation of the stratospheric polar vortex in both hemispheres: a strong undisturbed polar vortex is associated with sharp PV gradients, maximum values of PV right at the pole and strong cyclonic (eastward winds) flow. Furthermore, it is also clear from **figure 4.1.3** the differences in the PV distribution as well as the zonal wind strength between the NH and the SH. PV and associated zonal winds in the SH are much higher/stronger than in the NH. The reason is simply the fact that wave activity is much less in the SH than in the NH (mainly due to differences in topography between the two hemispheres), thus the PV field is less disturbed leading to a stronger and long-lived polar vortex in the SH than in the NH where wave activity is intense and the vortex is more prone to perturbations.

Figure 4.1.5 shows the climatology of PV and **figure 4.1.6** the zonal mean zonal wind, both on the 350 K isentrope. In both hemispheres the maximum in eastward wind in centered at 30° latitude in the winter hemisphere, with a maximum of about 46 ms^{-1} during January and February in the NH and 42 ms^{-1} from June until August in the SH. This is the location of the subtropical jet which is a permanent feature on the 350 K isentrope (section 2.1). In the NH, the tropospheric jet appears to be dominated by the subtropical jet, while in the SH, the jet appears as a subtropical and extratropical part consistent with theory (Kushner, 2010).

The values of PV between 18°N and approximately 18°S are nearly zero and the PV field doesn't show any kind of variation throughout the year. In the NH, from January to April, PV values increase sharply from less than 1 PVU at 18°N to about 6 PVU near 40°N. This period of time coincides with the strong NH subtropical jet. During the NH summer months (June-September), PV values are below 1 PVU further poleward (in comparison with the winter months) and a sharp increase in PV values occurs from approximately 25°N to 50°N where PV attains a value of 6 PVU. A maximum of PV of nearly 10 PVU is also seen at polar latitudes in August. This feature is not seen in winter months. The poleward shift of the latitudinal PV gradients during summer in the NH coincides with a weak subtropical jet and strong westward winds near the equator.

In the same way as for the NH, a poleward shift of the sharp increase of the latitudinal PV gradient is also seen during the period of time when the subtropical jet is weak in the SH. However, the high PV values found at polar latitudes do not seem to coincide with the weak subtropical jet. Rather, these rings of high PV appear at the same time as a second maximum of the eastward winds between August and October which is located between approximately 45°S and 60°S, in the extratropical part of the tropospheric jet.

At this point is important to recall that poleward of approximately 40° latitude, the air enclosed by the 350 K isentropic surface belongs to the stratosphere. Therefore the high polar PV values seen in both hemispheres as well as the extratropical secondary maximum in eastward winds of the winter SH lie in the stratospheric part of the Middleworld, the so called lowermost stratosphere.

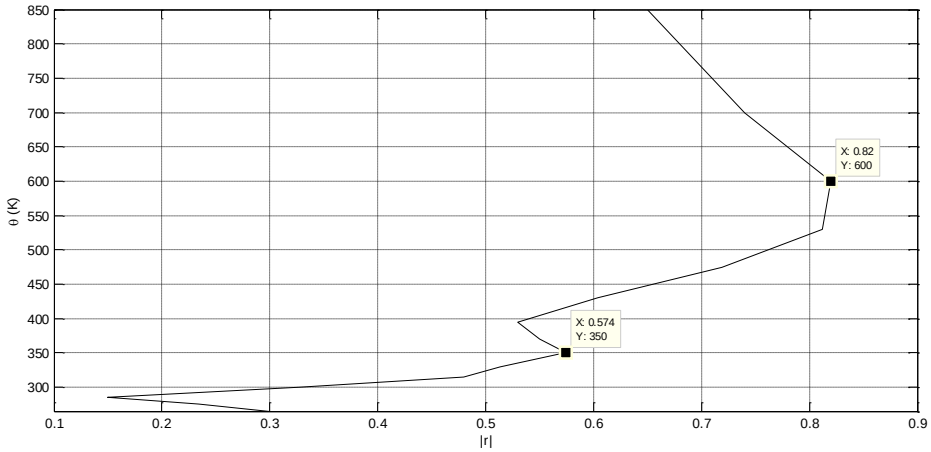

Figure 4.1.1 Maximum in anticorrelation for the NH from 10.5°N to 90°N for each of the isentropic surfaces at 265 K, 275 K, 285 K, 300 K, 315K, 330 K, 350 K, 370 K, 395 K, 430 K, 475 K, 530 K, 600 K, 700K and 850 K, displayed as a function of height and correlation coefficient (in absolute value, |r|.

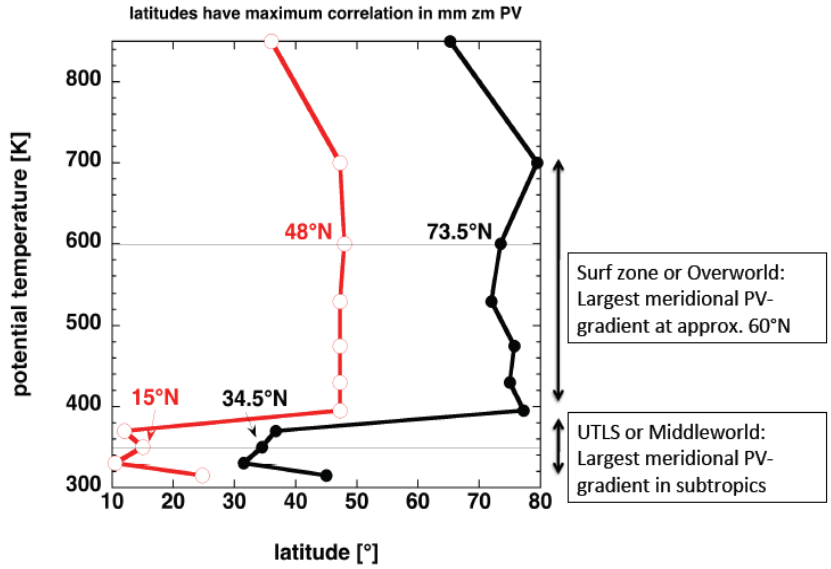

Figure 4.1.2 Maximum in anticorrelation for the NH from 10.5°N to 90°N for each of the isentropic surfaces at 265 K, 275 K, 285 K, 300 K, 315K, 330 K, 350 K, 370 K, 395 K, 430 K, 475 K, 530 K, 600 K, 700K and 850 K, displayed as a function of height and latitude. Figure due to van Delden, A. J..

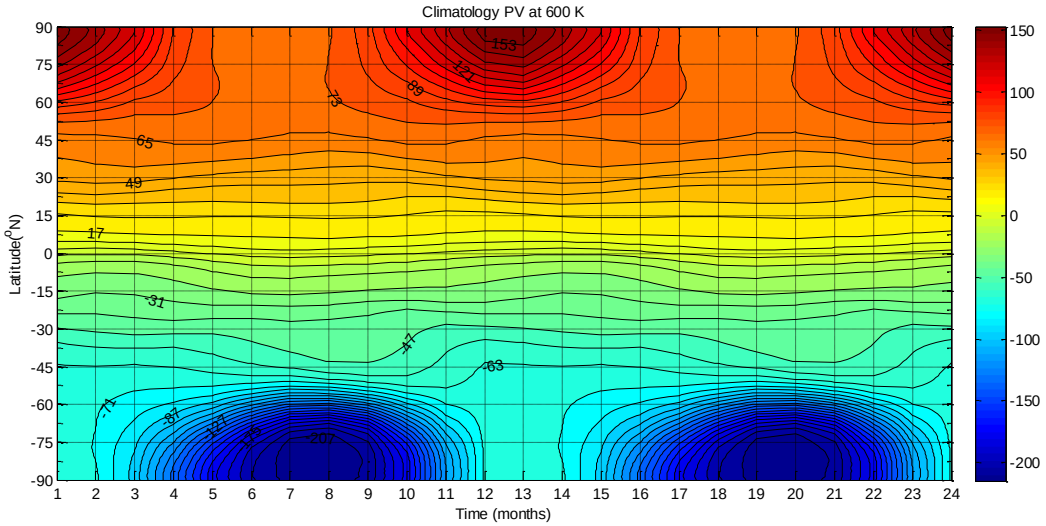

Figure 4.1.3 Climatology of zonal mean monthly mean PV (in PVU) on the 600 K isentropic surface for January until December for the period 1979 – 2013. Two years are plotted for clarity. Contour interval is 8 PVU.

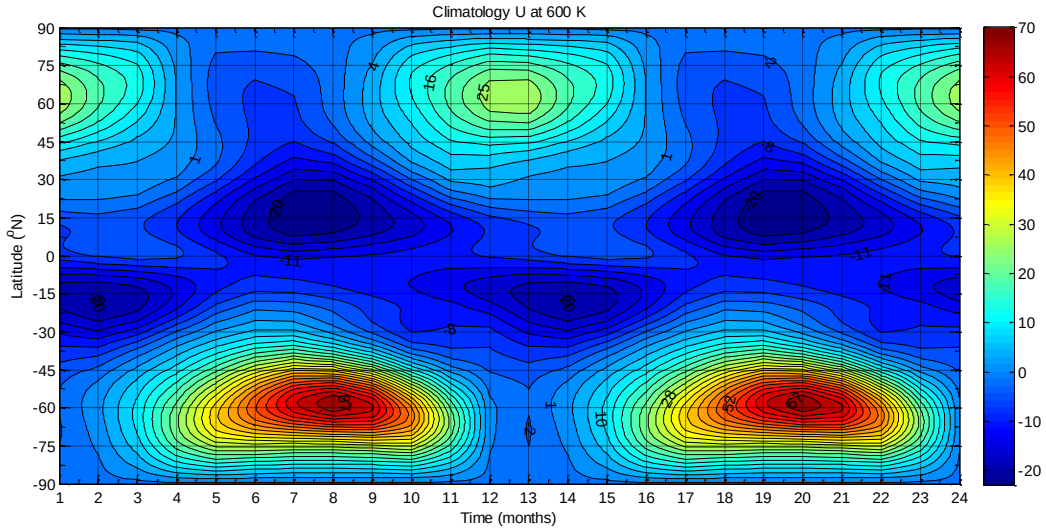

Figure 4.1.4 Climatology of zonal mean zonal wind (U in ms^{-1}) on the 600 K isentrope for January until December for the period 1979–2013. Two years are plotted for clarity. Contour interval is 2 ms^{-1}.

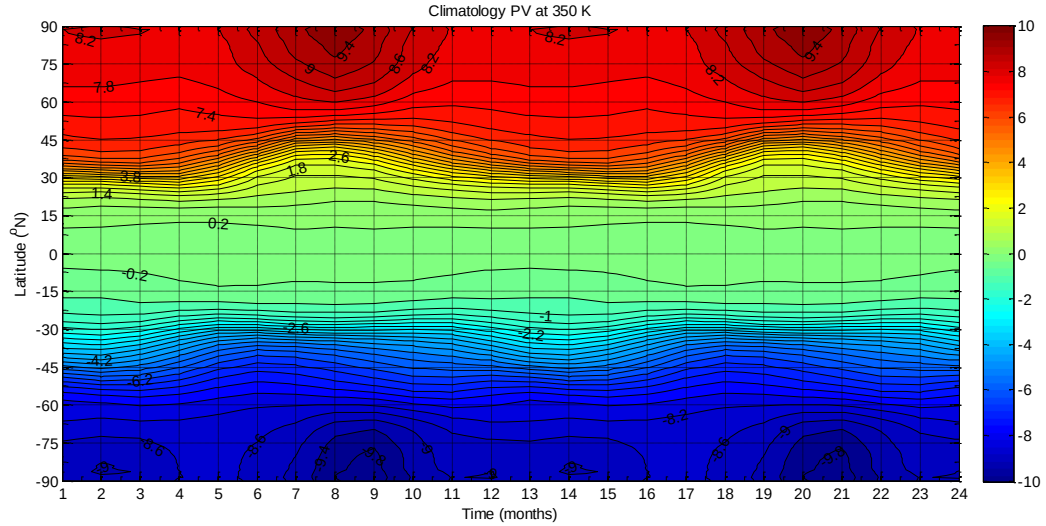

Figure 4.1.5 Climatology of PV (in PVU) on the 350 K isentropic surface for January until December for the period 1979 – 2013. Two years are plotted for clarity. Contour interval is 0.4 PVU.

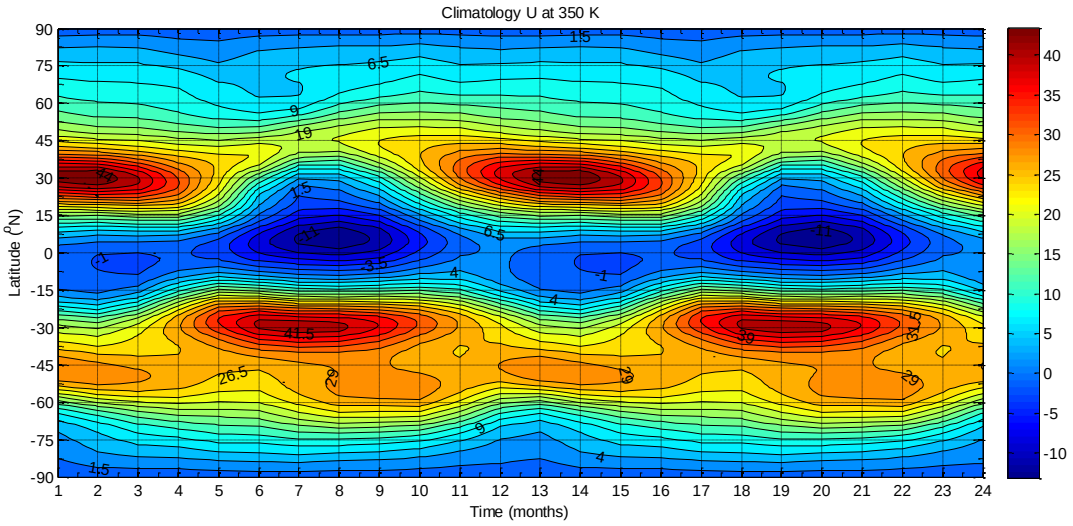

Figure 4.1.6 Climatology of zonal mean zonal wind (U in ms^{-1}) on the 600 K isentrope for January until December for the period 1979 – 2013. Two years are plotted for clarity. Contour interval is 2.5 ms^{-1}.

4.2 Potential vorticity on the 600K isentropic surface (PV600K)

Potential vorticity on the 600 K isentropic surface has been already analyzed by Baldwin and Dunkerton in order to characterize weak and strong stratospheric polar vortex events (Baldwin and Dunkerton, 1998). In this section, the stratospheric variability will also be studied using PV on the 600 K isentrope but with no constraints with respect to the northern or southern hemisphere, instead, the full domain of the PV field will be used including the tropics for the full period of time between 1979 and 2013. For this purpose a cross-correlation matrix (normalized covariance matrix) is calculated using zonal mean monthly mean PV at 600 K for the full period 1979-2013. As already mentioned in section 4.1, cross-correlation matrices are a useful tool to display simultaneous correlations between variables within a data set. **Figure 4.2.1** shows a contour plot of such a matrix for potential vorticity on the 600 K. PV anomalies including the seasonal cycle (hence anomalies with respect to the mean) are shown only for comparison with PV anomalies with seasonal cycle filtered out (in this case, anomalies with respect to the climatology as already mentioned in section 3.1).

Focusing on the results of the PV anomalies with the seasonal cycle filtered out (lower triangle) we see immediately two regions with strong anticorrelations. One at higher latitudes between 48°N and 73.5°N (r = - 0.82) in the NH, another which is symmetric about the equator between 8.25°S

and 8.25°N (r = - 0,98) and a third one with lower correlation coefficient (r = -0.41) in the SH between 45.5°S and 69.75°S. Following the same reasoning as Li and Wang (2003), one may argue that these maximum in anticorrelation represent a transfer of PV anomalies between mid and high latitudes in the extratropics of both hemisphere as well as in a narrow region about the equator.

As discussed in sections 2.2 and 2.6, the main mode of climate variability in the extratropical stratosphere of both hemispheres is the NAM (in NH) and the SAM (in the SH), while the tropical stratosphere is dominated by the by the QBO. It is expected, therefore, that these main modes of climate variability in the stratosphere are captured by the PV distribution on the 600 K. Since PCA is an adequate method to determine main modes of variability, hence teleconnections (section 3.2), PCA is applied to the zonal mean monthly mean PV on the 600 K (standardized) anomaly field. The eigenvectors and eigenvalues are therefore determined from the cross correlation matrix.

Figure 4.2.2 shows the leading eigenvector of PV on the 600 K isentrope (EOF1PV600K) as well as the regression of the QBO time series at 30 mb on the PV anomaly field also on the 600 K isentrope. Recall that negative (positive) values of the QBO represent westward (eastward) winds at 30 hPa over Singapore.

The leading eigenvector of PV on the 600 K isentrope (EOF1PV600K), which explains 24.4% of the total variance, shows a distinct pattern in both hemispheres, with negative PV anomalies between the equator and 36.75°N and positive ones in the SH between the equator and approximately 50°S. Although the positive PV anomalies extend to the midlatitudes in the SH, the highest variance (as seen by the correlation coefficients) comes from within the tropical stratosphere in both hemispheres. The spatial pattern of the QBO projected on the PV600K anomaly field is a clear mirrored image of the leading eigenvector (EOF1PV600K). In the tropics the eastward phase of the QBO (QBO positive) is associated with positive PV anomalies in the NH hemisphere and negative PV anomalies in the SH, while the opposite occurs for the westward phase (QBO negative). Recall that the spatial pattern of the EOFs is displayed in terms of the correlation coefficient resultant from the regression of the PV anomaly field (with the seasonal cycle filtered out and normalized) upon the standardized PCs (section 3.2, equation 3.2.1). Also that positive (negative) PV anomalies in the SH are equivalent to negative (positive) PV anomalies in the NH due to the fact that, by definition, PV is negative in the SH. Therefore positive PV anomalies in the SH (less negative) and negative ones in the NH (less positive) within the tropics represent below average PV in this region. Conversely, negative PV anomalies in the SH and positive ones in the NH are associated with above average PV

in the tropics. These PV anomalies can arise by (adiabatic) transport of PV along isentropes or, if diabatic processes are involved, by cross isentropic transport of mass which dilutes (decreases) or concentrates (increases) PVS (PV) (van Delden, 2014), as explained in section 2.7.

The QBO time series and the time series associated with the leading eigenvector (PC1PV600K) are shown in **figure 4.2.4**. The high (anti) correlation (r = -0.85) between these two time series is thus a confirmation of the strong connection between the QBO and PV variability in the tropical stratosphere. When the QBO is westward (QBO negative), PV is below average in the tropics of both hemispheres. Conversely when the QBO is eastward (QBO positive), PV is above average in that region of both hemispheres.

Although the correlation coefficient between the QBO and PC1PV600K is very high, it is of interest to understand how the QBO leads to PV anomalies in the tropical stratosphere. Taking a closer look at the structure of EOF1PV600K (**figure 4.2.2**), one may argue that (adiabatic) along isentrope transport of PV does not appear to play a significant role. The reason is that, if PV had to be transported from the tropics into the subtropics (and the other way around), one would expect to find a dipole structure such as the one found in **figure 4.2.3** which, as will be shown later, represents transport of PV between mid and higher latitudes in both hemispheres. However, from **figure 4.2.2** one sees more of a monopole structure, located in the tropics, rather than a dipole one. Furthermore, the below average PV observed during the westward QBO cannot be explained in terms of horizontal mixing of PV due to RWB and that is because extratropical RW, which tend to propagate equatorward and upward if the background flow is weakly eastward, will dissipate when then encounter westward winds. This implies that in the westward QBO, the tropical stratosphere is isolated from mixing due to RWB. Since the appearance of local PV anomalies may be associated with dilution and concentration of PVS, which in turn is associated with cross isentropic mass fluxes (section 2.7), the relationship between PC1PV600K, the QBO and PVS is further analyzed.

Figure 4.2.5 shows the cross correlation between PC1PV600K and the QBO (30 mb) with the PVS anomaly field on the 600 K isentropic surface. The maximum correlation between the QBO and PVS in the SH is equal to -0.88 at lag -1 (hence, QBO leads by 1 month) at 9°S and in the NH the maximum correlation is equal to 0.89 at 12°N also with the QBO leading by one month. However, at lag zero the correlation coefficient for both hemispheres is of the order of 0.85 (negative in the SH and positive in the NH) implying that PVS and the QBO are simultaneously correlated. Therefore the

eastward QBO is associated with concentration of PVS (positive PVS anomalies) and the westward QBO with dilution of PVS (negative PVS anomalies).

PC1PV600K and PVS are also strongly correlated at lag zero, with a maximum of 0.92 in the SH at 11.25°S and -0.91 for the NH at 12.75°N. In summary, these results imply that the westward QBO is associated with dilution of PVS and below average PV in the tropics of both hemispheres. Conversely, the eastward QBO is associated with concentration of PVS and above PV in the same regions. The SMC (section 2.6, figure 2.6.2) predicts that at the level of maximum westward (eastward) winds, air must diverge poleward (converge equatorward). Therefore one may argue that the divergence (convergence) of air, might lead to dilution (concentration) of PVS, hence to a decrease (increase) of PV at the level of maximum winds which lies close to the 600 K for both phases of the QBO. These changes in PVS must in turn be associated with cross isentropic transport of mass (section 2.7). In agreement with the SMC induced by the QBO, the above results suggest that the observed PV anomalies of the tropical stratosphere might be a result of the SMC rather than RWB.

Although explaining very little variance, also evident from **figure 4.2.2** is the influence of the QBO at mid and high latitudes. In this case, the westward (eastward) phase of the QBO is associated with positive (negative) PV anomalies at midlatitudes and negative (positive) ones at higher latitudes. Although the correlation coefficient between the QBO and the PV anomaly field on the 600 K at these latitudes is rather low, it is consistent with the results of Holton and Tan (1980) who suggested that during the westward phase of the QBO, the subtropical zero wind line (where the zonal mean zonal wind is zero) is positioned in the NH subtropics leading to an increase of wave activity in the extratropics and hence strong PV mixing at the pole (weak polar vortex). This relationship between polar latitudes and the QBO is less clear in the SH.

The second (EOF2PV600K) and third (EOF3PV600K) eigenvectors (**figure 4.2.3**) which represent, respectively 23.2% and 15.0% of the total variance are almost perfectly mirrored with EOF2PV600K representing variability in the NH and EOF3PV600K variability in the SH. **Figure 4.2.3** is remarkably similar to figure 2 of Baldwin (2001) being the only difference the fact that Baldwin's research was concerned with the NAM at the surface. In the NH, strong negative PV anomalies between 24.75°N and 57.75°N are associated with strong positive ones at higher latitudes between 57.75°N and the pole. The SH also shows a similar dipole pattern with negative PV anomalies between 21.75°S and 55.5°S, associated with positive ones between 55.5°S and the pole. The maximum of the PV

anomaly is found at 71.25°N in the NH and 72.75°S in the SH, and the minimum 45.75°N in both hemispheres. To a less extent, some variability is also found around the equator but it is very low compared with the maxima and minima of PV anomalies at higher latitudes in both hemispheres, suggesting that EOF2PV600K and EOF3PV600K represent mainly variability in the PV anomaly field on the 600 K isentrope between middle and polar latitudes.

The second eigenvector (EOF2PV600K, **figure 4.2.3**) clearly represents variability in the extratropical NH and the principal mode of variability in the NH extratropics is the NAM (section 2.2). It is therefore expected to capture the NAM in the PV distribution on the 600 K isentrope. **Figure 4.3.6** shows the correlation matrix between the NAM indices calculated individually at different pressure levels from the surface until 10 hPa and the PV anomaly field on the 600 K isentrope. The NAM indices were calculated using the same approach as Li and Wang (2003), as explained in section 2.2, and they are defined in Appendix. The goal of this analysis is to find at which altitude the PV anomalies on the 600 K and the NAM indices are better correlated.

From the pole to approximately 74°N, PV is positively correlated with the NAM mainly above the 100 hPa level with correlation coefficients above 0.7, while between approximately 57°N and 46°N the correlation becomes negative. The highest values are also found above the 100 hPa level with correlation coefficients superior to 0.6. This result implies that a strong polar vortex (positive NAM) is associated with positive PV anomalies poleward of 74°N and with negative PV anomalies at midlatitudes. In case of a weak vortex (negative NAM), the situation is reversed and there are negative PV anomalies at polar latitudes associated with positive PV anomalies at midlatitudes.
The maximum in correlation between PV at 600 K and the stratospheric NAM indices is found at 20 hPa (r = 0,903) at 76.5°N and the maximum in anticorrelation is also found at 20 hPa (r = -0.88) at 47.25°N, thus negative values imply higher geopotential height at the poles and a positive ones the reverse. Since the NAM index defined in the stratosphere represents the strength of the polar vortex, from **figures 4.2.7** and **4.2.8** it is clear that PC2PV600K also does. Positive (negative) values of PC2PV600K represent negative (positive) PV anomalies at midlatitudes and associated positive (negative) PV anomalies at higher latitudes. Therefore, a weak polar vortex (negative phase of the NAM) is represented by PV transport from the polar region into the midlatitudes (negative values of PC2PV600K) which, according to McIntyre and Palmer (1984), is due to RWB. As mentioned in section 2.7, RW are able to propagate upwards from the troposphere into the stratosphere and break there if their amplitude is large enough. In this situation meridional PV gradients become

distorted and PV transport or mixing can occur. On the other hand, when the polar vortex is strong, Rossby waves tend to propagate equatorward, therefore PV transport along isentropes is weak (positive values of PC2PV600K) due to the strong PV gradients.

The above results clearly show that PC2PV600K may be viewed as an index which measures the strength of polar vortex in the NH stratosphere, where positive (negative) values represents strong (weak) polar stratospheric extreme events (Baldwin, Dunkerton, 2001; Charlton and Polvani, 2006). The SSWs (around the central date) are clearly captured by the negative values of PC2PV600K and, in agreement with theory (e.g. Baldwin and Holton, 1987), are associated with PV being transported out of the polar region into midlatitudes due to RWB, hence a strongly disturbed polar vortex. These results are in agreement with the ones of Waugh and Polvani (2010) as well as Rongcai and Cai (2006) who used potential vorticity instead of geopotential height and found a maximum correlation between, what they called polar vortex oscillation (PVO), which measured strong and weak polar vortex events in the NH, and the stratospheric NAM at 20 hPa.

The zonal mean zonal wind at 60°S in the stratosphere is a measure of the strength of the polar vortex in the SH. By convention, stronger (weaker) than normal zonal flow along 60°S (and associated lower (higher) than normal geopotential heights over the pole), represents the positive (negative) SAM index, thus a stronger (weaker) polar vortex (Thompson et al., 2004). Using the same approach as for EOF2PV600K, **figure 4.2.9** shows the correlation between the zonal mean zonal wind anomalies at 60°S and at different pressure levels and the PV anomaly field on the 600 K isentrope. There is a strong anticorrelation between the zonal wind and PV on the 600 K at polar latitudes (with a maximum r = -0.83 at 69.75°S) and a less strong positive correlation at midlatitudes (with a maximum r = 0.57 at 47.25°S). Both maxima are located at 20 hPa. Since PV is negative in the SH, positive (negative) PV anomalies at the pole associated with negative (positive) ones in midlatitudes implies transport of PV out (into) of the higher latitudes into the lower ones. Therefore, positive values of PC3PV600K are associated with transport of PV out of the polar region, while negative values of PC3PV600K are associated with PV transport into polar latitudes.
The above results thus imply that, although positive values of PC3PV600K are associated with below average zonal winds at polar latitudes and above average zonal winds at midlatitudes (with the opposite for negative values of PC3PV600K), the main effect of the zonal winds at 60°S on the polar vortex is at higher latitudes.

From **figure 4.2.10** and **4.2.11** one sees that PC3PV600K and U_20 are highly negatively correlated, thus positive (negative) values of PC3PV600K are associated with below (above) average zonal wind at 60°S and 20 hPa, hence with the negative (positive) phase of the SAM. The only known SSWs of the SH in September 2002 is clearly captured. Therefore, a strong polar vortex is associated with weak PV mixing and vice-versa. Since EOF3PV600K represents variability at higher latitudes in the stratosphere in the SH (**figure 4.2.3**) and is strongly correlated with the stratospheric SAM we conclude that its time series, PC3PV600K, represents variability in the southern stratospheric polar vortex strength, with positive values associated to weak polar events (transport of PV out of the polar region into midlatitudes) and positive ones to strong polar events.

Section summary

The cross correlation matrix of potential vorticity on the 600 K isentropic surface shows three maxima in anticorrelation in the stratosphere associated with simultaneous changes in the PV600K anomaly field; one in the tropics and two at higher latitudes in both hemispheres (**figure 4.2.1**).
By applying PCA to zonal means of monthly means of potential vorticity anomalies on the 600 K isentropic surface including all months and both hemispheres, we are able to identify the three main modes of variability in the stratosphere, the QBO in the tropics, the NAM in the NH and the SAM in the SH, as expected from the cross correlation matrix, by using the first three eigenvectors which together explain 62.7% of the total variance of the PV600K field.

The leading eigenvector (EOF1PV600K, 24.4%) represents mainly PV variability in the tropical stratosphere in the both hemispheres. Its associated time series (PC1PV600K) shows a correlation of -0.85 with the QBO index at 30 mb (at lag 0). According to **figure 4.2.2** positive values of PC1PV600K are associated with below average PV in the tropics of both hemispheres and with the westward phase of the QBO and negative values of PC1PV600K (above average PV in the tropics of both hemispheres) are associated with the eastward phase of the QBO. The structure of EOF1PV600K suggests that horizontal transport of PV might not be the main cause for the observed PV anomalies in the tropical stratosphere since the variance explained by the extratropics (mainly in the NH) of this eigenvector is very low. Since the QBO induces a SMC, it is argued that horizontal divergence (convergence) of air poleward (equatorward) at the level of maximum westward (eastward) winds leads to dilution (concentration) of PVS, thus, a decrease (increase) of PV at this level. This is confirmed by the strong correlation between the QBO time series and the PVS anomaly

field on the 600 K isentropic surface (**figure 4.2.5**). These results are consistent with other studies which focused primarily on transport of chemical species in the stratosphere, such as ozone and methane (e.g. Pommrich et al., 2014; Plunge et al., 2009).

The second eigenvector (EOF2PV600K, 23.2%) represents variability in the NH stratosphere and its associated time series represents the strength of the polar vortex which is confirmed by the strong correlation between PC2PV600K and the NAM index defined at 20 hPa (r = 0.93). Therefore, strong PV mixing (negative PC2PV600K), thus a weaker polar vortex, will be associated with the negative phase of NAMI_20 (high geopotential height at pole) and vice-versa. Finally the third eigenvector (EOF3, 15%) represents variability in the SH. The third PC (PC3PV600K) is negatively correlated with the zonal mean zonal wind at 60°S and at 20 hPa, hence the SAM index at 20 hPa, with a correlation coefficient of -0,79 and is also a good representation of the strength of the southern polar vortex. The SSW of September 2002 is captured by PC3PV600K as well as by the U_20 time series. Positive PV anomalies at polar latitudes (positive values of PC3PV600K, weak polar vortex in the SH) are associated with the negative phase of the stratospheric SAM (below normal zonal wind) and vice-versa. In both hemispheres strong (weak) PV mixing due to strong wave activity is associated with a weaker (stronger) polar vortex. Therefore a strong (weak) stratospheric polar vortex is associated with strong (weak) PV gradients and the positive (negative) phase of the AMs. This similarity in the results (**figure 4.2.3**) could imply that the physical mechanisms behind the SAM and the NAM are the same in spite of the obvious differences between the NH and SH in terms of wave activity (stronger wave activity in the NH than in the SH due to differences in topography between the two hemispheres).

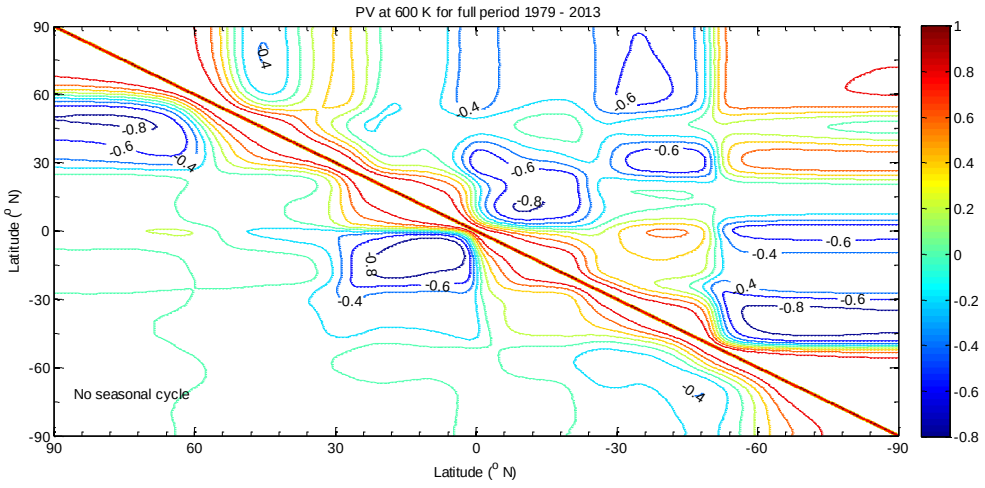

Figure 4.2.1 Cross-correlation matrix of PV at 600 K. The upper triangle shows correlations of PV anomalies including the seasonal cycle (thus anomalies with respect to the mean) and the

lower triangle shows correlations with seasonal cycle filtered out (thus anomalies with respect to the climatology) for the period of time 1979-2013.

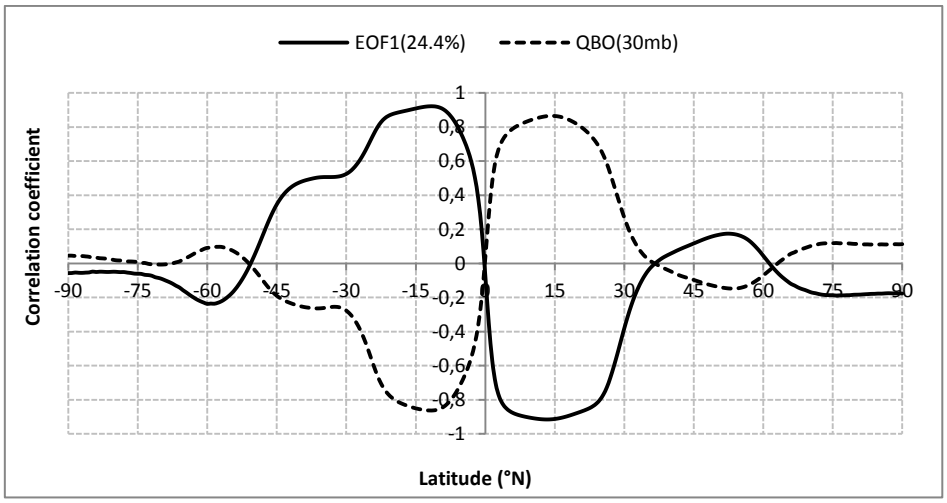

Figure 4.2.2 Leading eigenvector (EOF1PV600K, black solid line) from PCA applied to the PV anomaly filed (with seasonal cycle filtered out and normalized) on the 600 K isentropic surface. The explained variance is shown between parentheses. EOF1PV600K is displayed in terms of the correlation coefficient resultant from the regression of the above mentioned PV field upon the standardized first principal component (PC1PV600K). Also shown is the regression between the same PV anomaly field upon the standardized QBO time series at 30 mb.

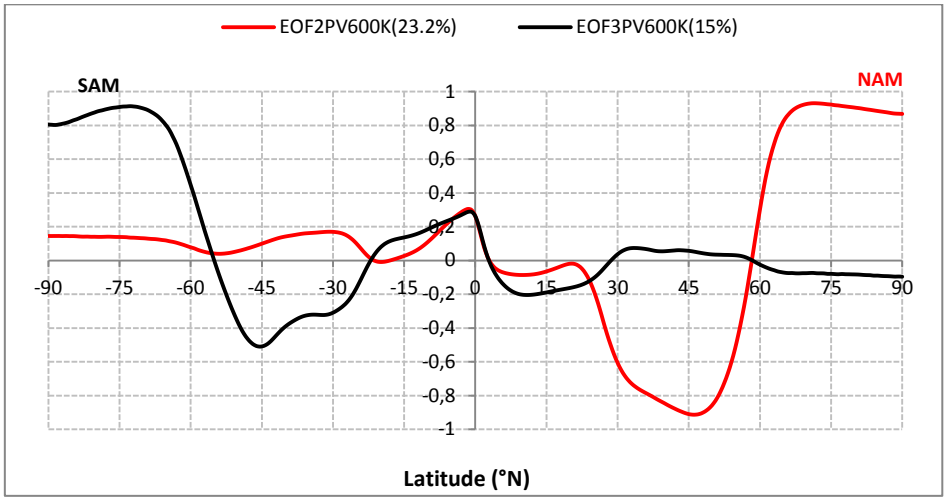

Figure 4.2.3 Second eigenvector (EOF2PV600K, red line) and third eigenvector (EOF3PV600K, black line) from PCA applied to the PV anomaly field (with seasonal cycle filtered out and normalized) on the 600 K isentropic surface. The explained variance is shown between parentheses. EOF2PV600K and EOF3PV600K are displayed in terms of the correlation coefficient resultant from the regression of the above mentioned PV field upon, respectively, the second and third standardized principal components (PC2PV600K and PC3PV600K).

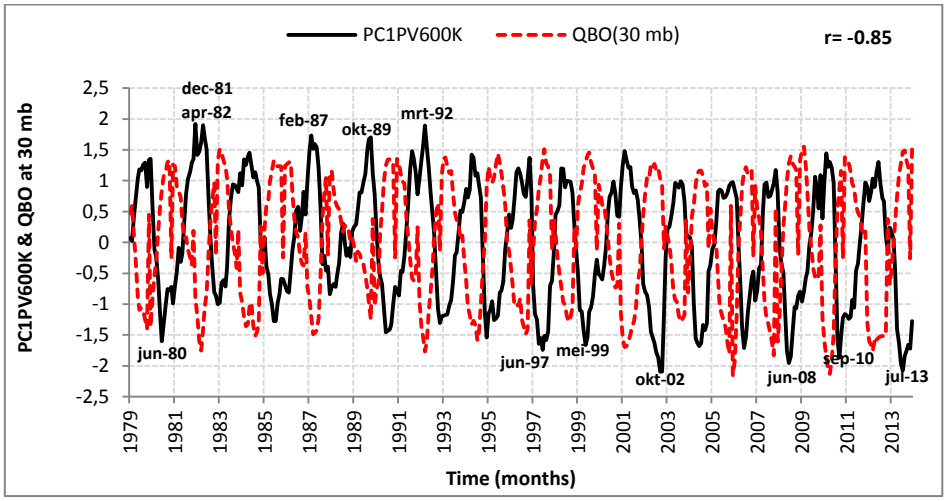

Figure 4.2.4 First principal component (PC1PV600K) and the QBO time series defined at 30 mb. The correlation coefficient between the two time series is r = -0.85 at lag 0. Positive (negative) values of the QBO are representative of eastward (westward) winds.

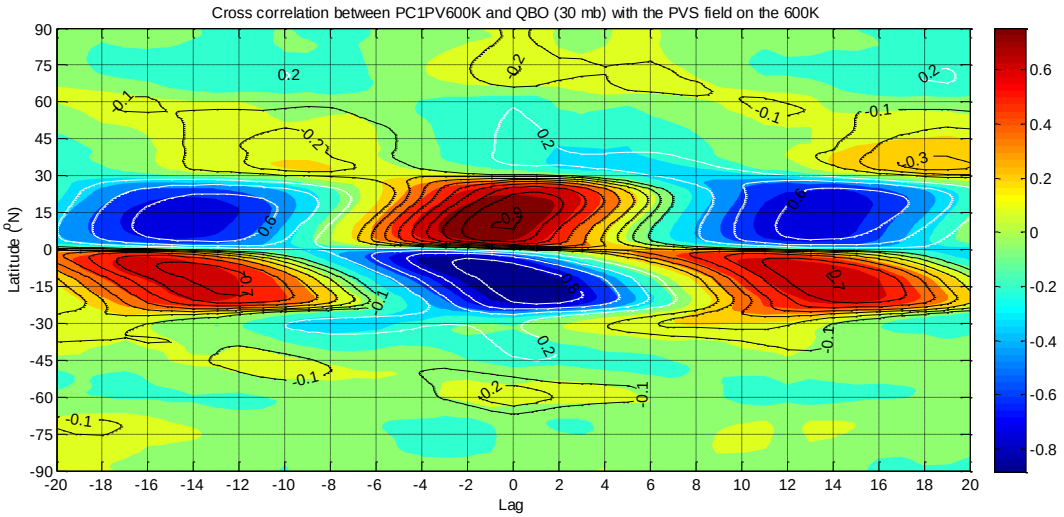

Figure 4.2.5 Cross correlation between the standardized PC1PV600K and the PVS (contours) anomaly field (with seasonal cycle filtered out and normalized) on the 600 K isentropic surface, as well as the QBO time series at 30 mb and the above mentioned PVS anomaly field (colors). Negative lags (in months) means that the PVS leads PC1PV600K and the QBO. Lag in months.

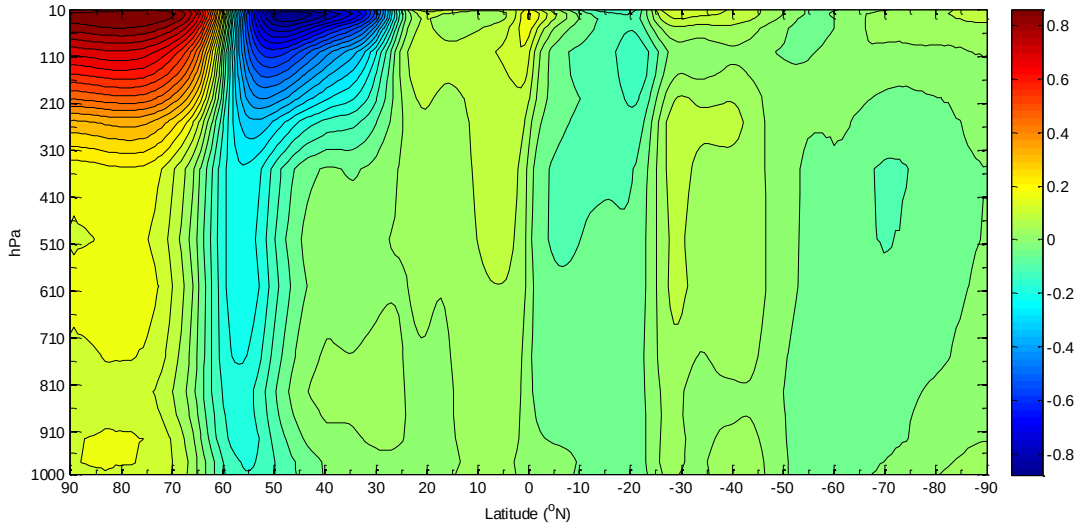

Figure 4.2.6 Correlation between the NAM indices defined at several geopotential heights using the method of Li and Wang (2003), which is explained in section 2.2, and the PV anomaly field (with seasonal cycle filtered out and normalized) on the 600 K isentropic surface.

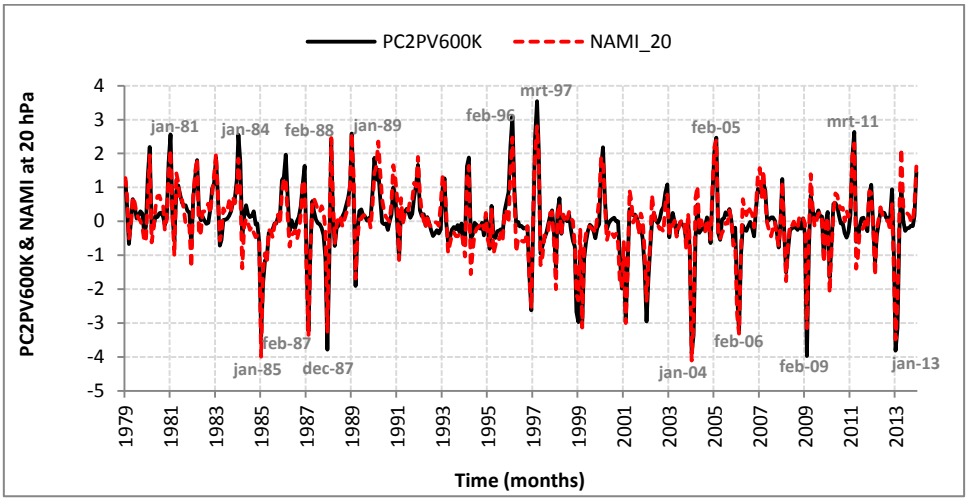

Figure 4.2.7 Time series of the NAM index defined at 20 hPa (NAMI_20) using the method of Li and Wang (2003) and the second principal component (PC2PV600K) from PCA applied to the PV anomaly filed (with seasonal cycle filtered out and normalized) on the 600 K isentropic surface. Dates associated with negative values of PC2PV600K correspond to SSWs.

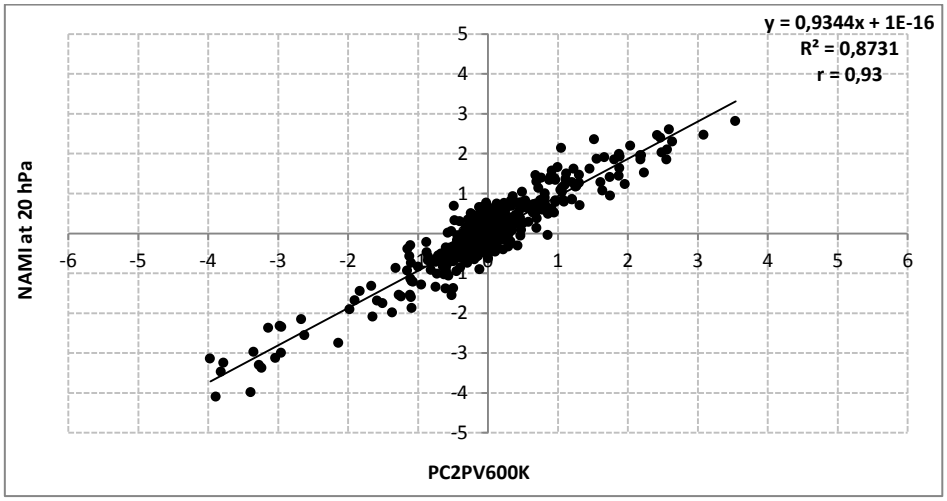

Figure 4.2.8 Scatterplot of the NAM index calculated at 20 hPa (NAMI_20) and the second principal component (PC2PV600K) from PCA applied to the PV anomaly filed (with seasonal cycle filtered out and normalized) on the 600 K isentropic surface.

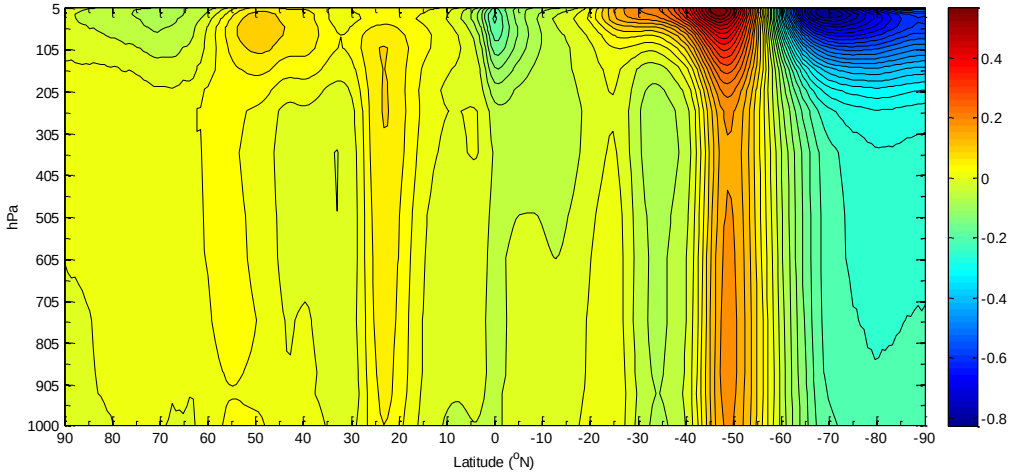

Figure 4.2.9 Same as in **figure 4.2.6** but with the SAM indices calculated with the zonal mean zonal wind at 60°S.

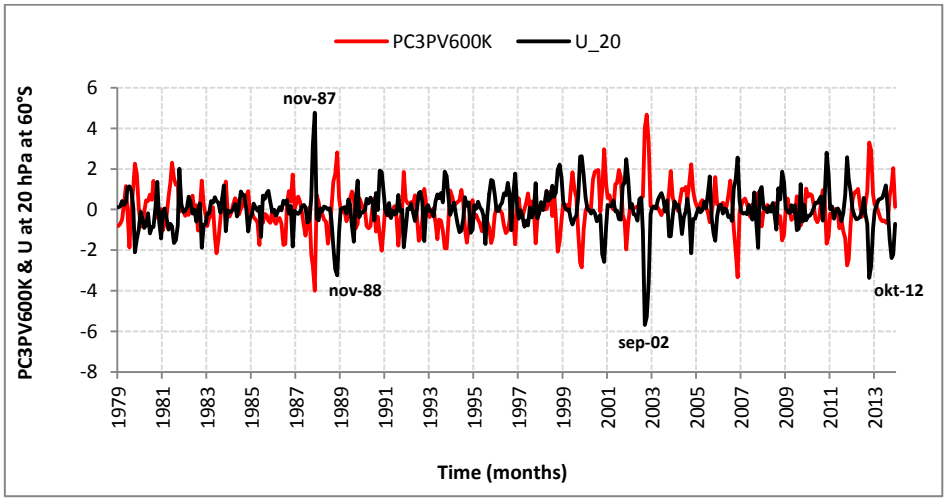

Figure 4.2.10 Time series of the zonal mean zonal wind at 60°S and at 20 hPa (U_20, solid red line) and the third principal component (PC3PV600K, solid black line) from PCA applied to the PV anomaly field (with seasonal cycle filtered out and normalized) on the 600K isentropic surface. The SSW of September 2002 in the SH is captured by both time series.

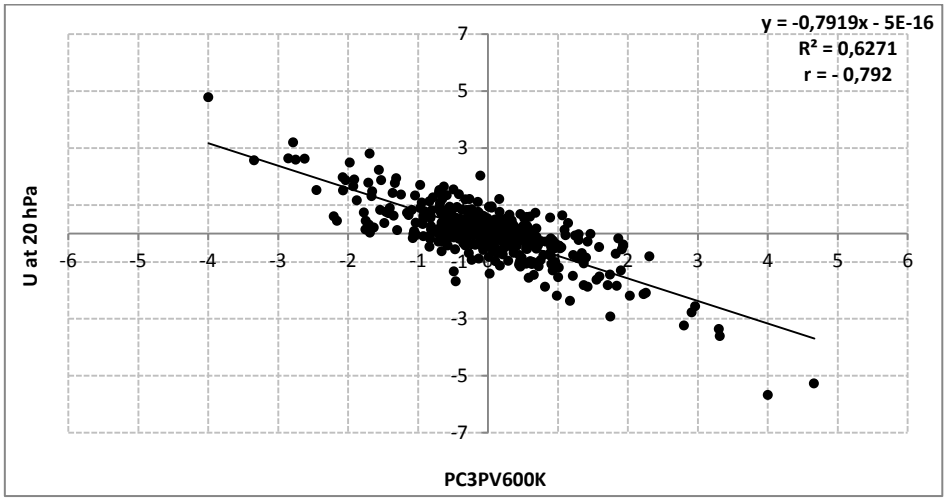

Figure 4.2.11 Scatterplot of the zonal mean zonal wind at 60°S at 20 hPa (U_20) and the third principal component (PC3PV600K) from PCA applied to the PV anomaly field (with seasonal cycle filtered out and normalized) on the 600 K isentropic surface.

4.3 Potential Vorticity on the 350K isentropic surface (PV350K)

In the same way as for PV at on the 600 K isentropic surface, a cross correlation matrix is constructed and PCA is applied to the PV anomaly field on the 350 K isentrope. From **figure 4.3.1** one signal is visible in the tropics around the equator with a maximum in anticorrelation (r= -0.86) between 8.25°N and 9°S and a second one, in the tropics/subtropics, with lower correlation coefficient in the NH (r=-0,57) between 15°N and 34.5°N. Therefore, PV variability on the 350K isentropic surface appears to be strongest in a region near the equator in both hemispheres, and to a less extent in the tropics in the NH with a weaker signal in the SH.

As already mentioned in section 2.1 the isentropes that belong to the Middleworld, such as the 350 K, represent two different parts of the atmosphere with different characteristics and dynamics. According to the cross correlation matrix, it appears that the main simultaneous changes in the PV anomaly field on the 350 K isentrope occur in the upper troposphere. In the same way as in section 4.2, PCA is now applied to the zonal mean monthly mean PV on the 350 K (standardized) anomaly field in order to determine main modes of variability.

The leading eigenvector (EOF1PV350K) represents 19.4% of the total variability of the PV anomaly field on the 350 K isentrope and is shown in **figure 4.3.2**. In the NH there are strong positive PV anomalies between the equator and 27°N with a maximum at 12.75°N and negative PV anomalies poleward of 27°N with a minimum near 35°N, whilst in the SH negative PV anomalies are found between the equator and 26°S and negative ones poleward of 26°S with a minimum at about 44°S. Overall this eigenvector appears to represent PV variability between the tropics and subtropics in both hemispheres. In the NH positive PV anomalies in the tropics are associated with negative ones in the subtropics which imply that air with high PV from the subtropics is transported to the tropics, i.e., there is above average PV in the tropics and below average PV in the subtropics (and vice-versa). Conversely, in the SH, negative PV values in the tropics are associated with positive PV values in the subtropics, which again implies that there is above average PV in the tropics and below average PV in the subtropics (and vice-versa). As already mentioned in the previous section, along isentropic PV transport is associated with adiabatic processes. However, the tropics are a

region of strong diabatic heating variability in which the ENSO and HC play a significant role. Therefore, PV transport in the tropical upper troposphere might occur adiabatically, i.e. along isentropes and by cross isentropic flow (section 2.7) where diabatic processes are involved.

The first principal component (PC1PV350K) associated with the leading eigenvector is shown in **figure 4.3.3** where positive values of PC1PV350K represent above average PV in the tropics and below average in the subtropics, while negative ones represent below average PV in the tropics and above average in the subtropics in both hemispheres. From **figure 4.3.3**, the El Niño's of 1983 and 1998 stand out for negative values of PC1PV350K, which implies that not only there might be a strong connection between this principal component and the SOI (section 2.3), but also that the El Niño will be associated with below average PV in the tropics. In fact, the correlation between PC1PV350K and the SOI is 0.52 at lag 0 with a slight increase at lag -1 (r = 0.56) when SOI leads, which implies that El Niño and La Niña events will indeed affect PV variability in the tropics/subtropics.

To gain further insight about PC1PV350K, PCA is applied to the zonal wind, the cross isentropic flow on the 350 K isentropic surface (U350K and CrIs350K respectively) and tropical precipitation (PrecpT). As in the same way for the PV analysis, all the data were centralized by subtracting the climatological mean (monthly means) and further normalized by division by its standard deviation. The full period is used, i.e. there is no restriction to seasons but the domain will differ between data sets depending of the goal of the analysis.

For the analysis of the zonal wind the full domain (from 90°S to 90°N) will be used. The reason for this choice is that the maximum in eastward winds associated with the tropospheric jet is located on the 350 K isentropic surface near 30° latitude (**figure 4.1.5**, section 4.1). Therefore, the analysis of the zonal wind at this isentrope can provide information about the tropical and extratropical circulation. For the cross isentropic flow on the 350 K as well as precipitation we restrict the analysis to the tropics between 30°S and 30°N, with the intent of capturing the Hadley circulation (HC) via cross isentropic flow and probable connections with the other atmospheric variables. In an attempt to keep the interpretation of the results as clear as possible, the EOFs and associated principal components (PCs) of the zonal wind, the cross isentropic flow and total precipitation that are analyzed throughout this section are only the ones that showed to have strong correlations with the EOFs and PCs of PV350K. The correlation coefficients found throughout this section, i.e.

between PC1PV350K and the other atmospheric variables are listed in table 1. An overview of the PCs (negative and positive values) is given in table 2.

To analyze the role of diabatic processes, PCA is applied to the cross isentropic flow on the 350 K isentropic surface and tropical precipitation. The leading eigenvector of the cross isentropic flow (EOF1CrIs350K) is shown in **figure 4.3.4** and the associated time series (PC1CrIs350K) in **figure 4.3.5**. The leading eigenvector of precipitation (EOF1PrecpT) is shown in **figure 4.3.6** and its associated time series (PC1PrecpT) in **figure 4.3.7**.

From **figure 4.3.4**, one sees that between 12°S to 6°N the cross isentropic flow is above average and poleward of 12°S and of 6°N the cross isentropic flow is below average. Therefore positive values of PC1CrIs350K are associated with anomalous diabatic heating between 12°S to 6°N and anomalous diabatic cooling elsewhere. The opposite is true for negative values of PC1CrIs350K. The leading eigenvector of tropical precipitation (EOF1PrecpT) shows that above average precipitation is found between about 10°S and 5°N and below average precipitation between 5°N and 24°N and 10°S to 30°S. Therefore, positive values of PC1PrecpT are associated with above average precipitation around the equator and below average precipitation poleward of that. The correlation between PC1CrIs350K and PC1PrecpT is 0.53 at lag 0. The above results imply that anomalous diabatic heating (PC1CrIs350K positive) in a narrow region around the equator is associated with above average precipitation (PC1PrecpT positive) within the same region. At the same time, poleward of that and within the tropics, anomalous diabatic cooling (PC1CrIs350K negative) is associated with below average precipitation (PC1PrecpT negative) and vice-versa. This result suggests that the enhanced diabatic heating and associated above average precipitation around the equator are linked to the ascending branch of the HC, hence with the ITCZ. Since latent heat release associated with precipitation in the ITCZ drives the HC (van Delden, 2012), one may argue that the leading eigenvector of CrIs350K (EOF1CrIs350K) is representative of the HC strength. Therefore, positive (negative) values of PC1CrIs350K are associated with a stronger (weaker) HC. Furthermore, PC1PrecpT is also significantly correlated with the SOI (**figure 4.3.8** and **4.3.9**). Although the correlation between PC1CrIs350K and the SOI is somewhat low (r= -0.41 at lag 0 with a slight increase at lag -2, r= -0.46, with SOI leading), in general one may conclude that above average precipitation in a region around the equator (PC1PrecpT positive) associated with the El Niño (SOI negative) is also associated with enhanced diabatic heating (PC1CrIs350K negative), hence a stronger HC.

The correlation between PC1PV350K and PC1CrIs350K is -0.43 (**figure 4.3.9** and **4.3.5**) and with PC1PrecpT is -0.57 (**figure 4.3.9** and **4.3.7**) implying that tropical precipitation strongly affects PV variability in the upper troposphere. The highest correlation of PC1PV350K was, however, found to be with the second PC of the zonal wind on the 350 K (PC2U350K, r=-0.69, at lag 0) and not with the first PC, thus the latter is not shown here.

The second eigenvector of the zonal mean zonal wind at 350 K (EOF2U350K) is shown in **figure 4.3.10** and the associated time series (PC2U350K) in **figure 4.3.11**. In the NH, positive wind anomalies are found between 3°N to about 40.5°N with a maximum near 25°N and negative wind anomalies poleward of 40.5°N with a minimum near 50°N. In the SH the pattern is the same; positive wind anomalies are found between 1.5°S and 44°S with a maximum near 21°S and negative ones poleward of 44°S with a minimum at about 52°S.

The overall picture is that, for both hemispheres, tropical positive wind anomalies are associated with weak negative wind anomalies at midlatitudes and vice-versa. Therefore, we can argue that PC2U350K represents the relative strength of the subtropical and the midlatitude jets. Positive (negative) values of PC2U350K are associated with above (below) average wind anomalies in the tropics/subtropics and below (above) average wind anomalies at midlatitudes, which implies a strong (weak) subtropical jet and a weak (strong) midlatitude jet in both hemispheres. However**,** by comparison with the climatology of the zonal wind on the 350 K isentrope (**figure 4.1.5**) it appears that the wind maxima in the subtropics is shifted equatorward, i.e., from 30°N to 25°N and from 30°S to 21°S, thus one may not rule out the possibility of an equatorward shift of the subtropical jet. Recent studies showed that the El Niño is associated with a stronger and equatorward shifted tropical jet (e.g. Seager et al., 2003). In fact, the correlation between PC2U350K and the SOI is -0.55 at lag 0 which confirms that a strong subtropical jet (PC2U350K positive) is associated with the El Niño (SOI negative), and further indicates that the effect of the SOI on the zonal flow is nearly simultaneous. A strong simultaneous correlation is also found between PC2U350K and PC1PrecpT (r=0.54) as well as with PC1CrIs350K (r=-0.45). The above results suggests that, above average PV in the tropics and below average in the subtropics (PC1PV350K positive) is mainly associated with a weak subtropical jet (PC2U350K negative), La Niña events (SOI positive), and tends to be mainly associated with a weaker HC (PC1CrIs350K negative) and below average tropical precipitation (PC1PrecpT negative), (**figure 4.3.12** and **4.3.13**). Conversely, below average PV in the tropics and above average in the subtropics (PC1PV350K negative) is associated with a strong subtropical jet

(PC2U350K positive), El Niño events (SOI negative) and a stronger HC (PC1CrIs350K positive) associated with above average tropical precipitation (PC1PrecpT positive).

In the same way as for the analysis of EOF1PV600K (section 4.2), it is of interest to have further insight on how these PV anomalies, which are associated with different processes, occur in the tropical upper troposphere.

The dynamical link between strong PV gradients (associated with weak mixing) and a strong subtropical jet is nowadays well established; strong winds are co-located in regions of strong PV gradients (e.g. Martius et al, 2011). When the subtropical jet is strong (PC2U350K positive) planetary waves are inhibited to penetrate deep into the tropics leading to less PV mixing there (PC1PV350K negative, strong PV gradients), which implies that the tropics should be well isolated from the extratropics. Conversely, weak PV gradients (PC1PV350K positive, strong PV mixing) are associated with a weak subtropical jet (PC2U350K negative) which in this case allows waves to propagate into the tropics and even break there, resulting in above average PV anomalies in that region. This is because the likelihood of RWB in weak eastward flows is higher than when the eastward flow is strong.

One may argue, therefore, that the observed positive PV anomalies associated with a weaker HC due to reduced diabatic heating during La Niña events and a weak subtropical jet might arise from RWB which are able to mix air with high PV from the subtropics into the tropics. Under these conditions, there is above average PV in the tropics and below average PV in the subtropics (PC1PV350K positive). On the other hand, in cases when the HC and subtropical jet are stronger, hence during El Niño events, PV mixing between the tropics and subtropics should be inhibited. The below average tropical PV anomalies seen in this situation might therefore be associated with the intensified HC. Following the same reasoning as for the PV anomalies associated with the SMC (EOF1PV600K, section 4.2), one may argue that mass is transported in the intensified upward branches of the HC, and diverges in the upper horizontal branches. This will lead to dilution of PVS, hence a decrease of PV. The relation between strong PV mixing and La Niña events is in agreement with the results of Waugh and Polvani (2000) who found that wave activity in the deep tropics was more frequent during NH winter and during La Niña events.

As mentioned before, PC2U350K represents the relative strength between the subtropical and midlatitude jets. Since the annular modes (AM) are coupled with changes in the zonal flow (Thompson and Lorenz, 2004), a connection between PC2U350K and the NAM/SAM is expected.

Figure 4.3.14 shows the time lag correlation between the NAM indices defined at 15 different pressure levels and PC2U350K. From the surface (r=-0.36) to 100 hPa (r=-0.35) the NAM is negatively correlated with PC2U350K, with a maximum at 750 hPa (r=-0.52), 600 hPa (r=-0.51) and 500 hPa (r=-0.52) at lag 0. With respect to the SAM (**figure 4.3.15**), there is little variation in the correlation coefficient from the surface (r=-0.44) until 100 hPa (r=-0.49). However a maximum is found at 150 hPa (r=-0.51) also at lag 0. **Figure 4.3.16** shows PC2U350K associated with the ten maximum and minimum values of the NAM index at 750 hPa, the SAM index at 150 hPa (since these were the levels of maximum simultaneous correlation between PC2U350K and the AMS, **figure 4.3.14**) and the SOI. A strong subtropical jet (PC2U350K positive) is clearly associated with the El Niño, and the negative phase of the NAM index at 750 hPa, thus a weak subtropical high and a weak subpolar low. A weak subtropical jet, hence stronger midlatitude jet (PC2U350K negative) is again clearly associated with the positive phase of the NAM index at 750 hPa. La Niña events appear to be clustered between 2008 and 2012, and the positive phase of the SAM at 150 hPa appears to be well (negatively) correlated with the weak subtropical jet since 1999 with exception of December 2001. Although PC2U350K is significantly correlated with the SOI, the correlation between the latter and the AMs is very low at any lag. The same applies to PC1CrIs350K, PC1PrecpT as well as PC1PV350K, which are also not correlated with the AMs (**table 1**). However, since the maximum in correlation was found between PC1PV350K and PC2U350K, one would expect a possible link between PV transport in the tropics and the AMs through the subtropical jet. In theory, one could argue that during the positive phase of the AMs, the subtropical jet is weak which could allow PV transport from the subtropics into the tropics (above average PV in the tropics and below average PV in the subtropics by RWB, thus PC1PV350K positive). On the other hand a strong subtropical jet does not favor equatorward propagation of RW, which in turn should lead to very weak along isentropic PV mixing between the tropics and subtropics, hence strong PV gradients in the subtropics.

Although the AMs may have some influence on the PV mixing between the tropics and subtropics through their effects on the strength of the subtropical jet, the results suggest that in the upper troposphere, below average PV in the tropics (PC1PV350K negative) is mainly due to enhanced upward cross isentropic flow (enhanced diabatic heating) associated with the El Niño, hence a strong HC and a stronger subtropical jet. On the other hand, transport of PV into the tropics from the subtropics (PC1PV350K positive) appears to be mainly due to RWB associated with a weak subtropical jet.

The second eigenvector (EOF2PV350K) of PV on the 350 K isentrope explains 14.8% of the total PV350K field variability. **Figure 4.3.17** clearly shows that this eigenvector represents strong variability of PV at high latitudes in the southern hemisphere where strong positive PV anomalies (below average PV) are found between approximately 50°S and the pole with a maximum located at 73.5°S.

This pattern is very similar to the third eigenvector of PV on the 600 K isentrope (EOF3PV600K), especially poleward of 45°S, which is also plotted for comparison. Recall that the principal component associated with the third eigenvector of PV on the 600 K **(**PC3PV600K) had a strong correlation with the SAM defined at 20 hPa and hence it represented fairly well the strength of the southern stratospheric polar vortex, with positive (negative) PC3PV600K associated with a weak (strong) vortex. On the basis of this strong similarity in the patterns of the EOFs associated with PV at 350 K and 600 K, one would expect EOF2PV350K to be also representative of the strength of the polar vortex in the SH lowermost stratosphere, i.e., one would expect a strong correlation between the associated time series. However, further analysis reveals that there is no such correlation between PC2PV350K (**figure 4.3.18**) with any of the SAM indices measured at 15 pressure levels. In fact, there is no significant correlation between PC2PV350K and any of PCs which resulted from the PCA applied to the atmospheric variables used so far. Since an eigenvector may not represent per se a mode of climate variability, PCA is further applied to the PV field on the 350 K isentropic surface only to the SH, thus between 10.5°S and 90°S. **Figure 4.3.20** shows the first eigenvector which represents 30% of the total variability of the PV350K in the SH (EOF1PV350KSH) as well as EOF2PV350K from the previous analysis; **figure 4.3.21** shows their respective time series. Clearly, no matter the domain chosen to apply PCA, this pattern comes through and it appears to be the leading mode of variability of PV on the 350 K isentrope at polar latitudes (thus in the lowermost stratosphere) in the SH. Therefore one may argue that EOF2PV350K and associated time series are not just a mathematical result of PCA.

A closer look at PC2PV350K reveals that, positive values represent mainly variability in the lowermost stratosphere between August and October, while negative values represent variability between June and September. The two extreme positive PC2PV350K values occurred in August 1980 and September 1981, while the extreme negative PC2PV350K values occurred in June 1979, July 1979, September 2007, August 2010 and August 2012. This implies that PC2PV350K represents variability in the lowermost stratosphere in the winter SH, thus at times when the polar vortex in the Overworld is supposed to be strong.

A possible explanation with respect to EOF2PV350K is that it may simply represent the so called stratospheric polar 'sub-vortex'. According to McIntyre (1995), there is a transition zone between the stratospheric polar vortex and the stratosphere below, near the 400 k isentropic surface, to which he called the sub-vortex region. This sub-vortex transition zone is as low as 350 K, during August-November in the SH when the vortex is strong in the middle stratosphere.

Recent studies (e.g. Haynes and Shuckburgh, 2000) show that at levels below 380 K, mixing (between polar and midlatitudes) occurs up to height which is determined by the position of the bottom of the vortex. However, other studies suggest that not only is 350 K isentropic surface laying in the sub-vortex region during winter/spring in both hemispheres but also that there is an impediment to mixing only in the SH during August-October (Santee et al., 2011).

It is clear that there is a strong spatial correlation between the strength of the polar vortex in the middle stratosphere (on the 600 K isentrope) and the PV anomalies in the lowermost stratosphere, as shown by the eigenvectors. However, there is no temporal correlation between the respective PCs, and although the physical mechanisms behind the lowermost stratospheric PV anomalies on the 350 K isentrope cannot be explained with the aid of the zonal wind or geopotential height on a temporal basis at any lag, there is a connection with the cross isentropic flow on the 600 K isentrope specifically at 60°S with a rather low correlation coefficient of -0.35 when the cross isentropic flow leads by three months (**figure 4.3.19**). The 350 K PV anomalies found at higher latitudes cannot, however be solely explained by the cross isentropic flow, although an enhanced downward branch of the BDC could affect the PV distribution in the lowermost stratosphere. From **figure 4.3.17** along isentropic mixing is also a possibility, i.e. transport of PV from the subtropics/midlatitudes to higher latitudes and vice-versa. However the variance explained by subtropical/midlatitude region is also very low. The fact that transport into and out of the lowermost stratosphere can be done at least by three different paths (section 2.1, **figure 2.1.3**) and that these paths cannot be distinguished using PCA, makes the interpretation of the second eigenvector difficult. The true physical mechanisms involving EOF2PV350K remains, thus, unclear.

The third eigenvector explains 13.3% of the total PV on the 350 K isentropic surface (EOF3PV350K) (**figure 4.3.22**) and although the explained variance of EOF3PV350K is very close to the one explained by EOF2PV350K they show distinct spatial patterns as well as distinct associated principal components. While in the case of the second eigenvector the main variability was found at high latitudes in the SH, EOF3PV350K shows main variability at high latitudes in the NH. This suggests

that the local variance explained by EOF2PV350K and EOF3PV350K is similar in their respective hemispheres and within the same region, i.e., poleward of about 45°S and poleward of about 45°N. In the NH, in the same manner as in the SH, PV is above average between 47°N and the pole. The variance explained between approximately 15°N and 47°N appears not to play a significant role in this eigenvector (EOF3PV350K). It also appears from **figure 4.3.22** that there is a relatively small influence of the SH subtropics in EOF3PV350K.

Figure 4.3.23 shows the time series associated with EOF3PV350K (PC2PV350K), where positive values of PC3PV350K (**figure 4.3.23**) are mainly associated with positive PV anomalies in the region between 47°N and the pole, whilst the opposite is true for negative values of PC3PV350K. Since the highest variance comes from the mid and high latitudes, in the same way as for the SH, we look for signals of the NAM. **Figure 4.3.24** shows the correlation between the PC3PV350K and the NAM indices calculated at different pressure levels. The maximum in correlation was found between PC3PV350K and the NAM index defined at 30 hPa and 50 hPa with a value of 0.38 with the stratospheric NAM leading by one month, and between the NAM index defined at 100 and 150 hPa with a correlation coefficient of 0.35 at lag zero. At the surface the maximum in correlation is rather low and equal to 0.27 also at lag zero.

Figure 4.3.25 shows PC3PV350K associated with the ten maxima and minima values of the NAM index defined at 20, 30 and 50 hPa at lag -1 where the NAM indices lead. It appears from the figure, that there is a better agreement between the negative phase of the stratospheric NAM indices and negative values of PC3PV350K implying that negative PV350K anomalies between 47°N and the pole are associated with a weak polar vortex (negative phase of the stratospheric NAM indices). On the other hand, positive values of PC3PV350K are better related with the positive phase of the NAM but at the levels 150 and 100 hPa as well as with the NAM index defined at the surface (**figure 4.3.26**). In summary, at lag -1 (when the stratospheric NAM leads) there are significant correlations between the stratospheric NAM indices above 50 hPa, especially for negative values of PC3PV350K with no connection to the surface, while at lag 0, with relatively lower correlations, the relationship between PC3PV350K and the NAM indices occurs from the surface to near 50 hPa and are mainly observed for positive values of PC3PV350K, hence above average PV from mid to polar latitudes.

With respect to the cross isentropic flow, PC3PV350K has a maximum simultaneous correlation on the 350 K at 69°N (r=0.365) and on the 475 K at lag -1 (r=0.372) at 76.5°N, when the cross isentropic flow leads by one month. The maximum correlation between PC2PV600K, which represented the strength of the stratospheric polar vortex in the NH (section 4.2), and the cross

isentropic flow is also on the 475 K, at lag 0, with r = 0.74 at 76.5°N. Since on average and especially in the northern winter, the cross isentropic flow on the 475 K is downward (negative), a stronger polar vortex (positive PC2PV600K, thus positive phase of the stratospheric NAM), will be associated with positive anomalies of cross isentropic flow on the 475 K isentrope at 76.5°N, i.e. with reduced diabatic cooling at this latitude, and vice-versa.

It is clear from **figure 4.3.28** that although the correlation coefficient between PC3PV350K and the cross isentropic flow on the 350 K and 475 K is very similar, the latter shows a stronger connection mainly for negative values of PC3PV350K.

The above results suggest that below average PV anomalies in polar latitudes in the lowermost stratosphere (negative values of PC3PV350K) is mainly associated with the negative phase of the stratospheric NAM (weak polar vortex) and enhanced diabatic cooling, specifically on the 475 K isentrope at 76.5°N (**figure 4.3.28**), when both lead by one month. From figures **4.3.25** and **4.3.28** one can see that for March 2009 (minimum value of PC3PV350K) was characterized by an extreme negative phase of the stratospheric NAM as well as with enhanced diabatic cooling. Also, in January/February 1985, at the time of a major SSW in the NH, the negative NAM anomalies are not only seen in the stratosphere but also at the surface. Therefore negative values of PC3PV350K must be associated with strong wave activity events.

On the other hand, above average PV at polar latitudes of the lowermost stratosphere (positive values of PC3PV350K) appears to be mainly associated with the positive phase of NAM from the surface until 50 hPa and to a less extent, with reduced diabatic cooling on the 475 K at 76.5°N. From **figure 4.3.25** it is clear that the link between a strong stratospheric polar vortex as measured by PC2PV600K (which is simply the NAM index defined at 20 hPa, NAMI_20) is less obvious for positive values of PC3PV350K. Since in the positive tropospheric NAM RW tend to propagate upward and equatorward, one may argue that the above PV anomalies found on the 350 K at higher latitudes are so due to weak wave activity in these regions. However, the exact pathway by which PV is transported into and out of the stratospheric part of the Middleworld remains unclear. As in the lowermost part of the stratosphere in the SH, both cross isentropic flow and PV transport along isentropes are possibilities which cannot be distinguished in this analysis.

Section summary

The first three eigenvectors resulting from applying PCA to the PV anomaly field on the 350 K isentropic surface account for 47.6% to the total variability. The first eigenvector (EOF1PV350K, 19.4%) represents mainly variability in the tropical/subtropical upper troposphere of the Middleworld. Positive upper tropospheric PV anomalies are associated with a weaker HC due to reduced diabatic heating (below average tropical precipitation) during La Niña events and a weak subtropical jet. Under these conditions RW are able to propagate through the weak eastward flow and probably break in the tropics leading to above average PV in that region and below average PV in the subtropics. On the other hand, in cases when the HC and subtropical jet are stronger due to enhanced diabatic heating (above average tropical precipitation) during El Niño events, it appears that the negative PV anomalies are mainly due to PV transport associated with the HC. In this scenario, mass is transported by the enhanced upward cross isentropic flow, leading to dilution of PVS in the upper horizontal branches of the HC and PV values must decrease. Therefore it is argued that in the tropical upper troposphere PV anomalies might be generated by RWB as well as by the HC in cases when it is stronger, thus when cross isentropic flow is enhanced.
The AMs are not captured directly by PC1PV350K but could play a role in the tropical PV transport (or the other way around) since both AMs and PC1PV350K are strongly correlated with the tropospheric jet: the negative phase of the NAM/SAM is associated with a strong subtropical jet which inhibits equatorward propagating planetary waves leading to strong meridional PV gradients, hence weak PV mixing in the tropics. The opposite is true for the positive phase of the AMs.

The second eigenvector accounts for 14.8% of the total variance and it represents strong variability at high latitudes in the southern hemisphere. Until the end of this project, the true physical mechanism behind this eigenvector remained unclear. It appears that there is a connection between the Overworld polar vortex and PC2PV350K in terms of latitudinal position, as shown by the eigenvectors, but with no temporal correlation, and with the cross isentropic flow on the 600K playing a minor role.

The third eigenvector explains 13.3% of the total variability and it is confined to the high latitudes but in the northern hemisphere. The associated time series (PC3PV350K) shows significant correlations between the NAM indices defined in the stratosphere, as well as with the cross isentropic flow on the 475 K isentrope when both lead by one month. Although the tropospheric

NAM indices are also captured, the correlations are somewhat lower but simultaneous. Below average PV at higher latitudes (between about 47°N and the pole) in the lowermost stratosphere (negative PC3PV350K) are mainly associated with the negative phase of the stratospheric NAM (weak polar vortex) and enhanced diabatic cooling on the 475 K isentrope at 76.5°N. In this case, the tropospheric NAM is not captured, with January/February 1985 being an exception. On the other hand, above average PV in the higher latitudes of the lowermost stratosphere (positive PC3PV350K) is mainly associated with the positive phase of the NAM from the surface to about 50 hPa and to a less extent reduced diabatic cooling on the 475 K isentrope. The connection between PC3PV350K and the polar vortex as measured by PC2PV600K is more evident for negative values of the former, thus for a disturbed vortex, which must be associated with strong wave activity in the stratosphere. In this case, there are negative PV anomalies at higher latitudes on the 350 and 600 K isentropic surfaces. Interesting is the fact that the maximum correlation between PC2PV600K, hence the NAMI at 20 hPa, and the cross isentropic flow is also on the 475 K isentrope at the same latitude (76.5°N) with a correlation coefficient of r=0.74 at lag zero.

From the above results, one may argue that, first the NAM anomalies appear in the stratosphere and propagate downward to the troposphere in cases when the stratospheric polar vortex is strong in the middle stratosphere. In cases of a weak polar vortex, enhanced diabatic cooling appears to play a role and only the stratospheric NAM is captured by PC3PV350K.

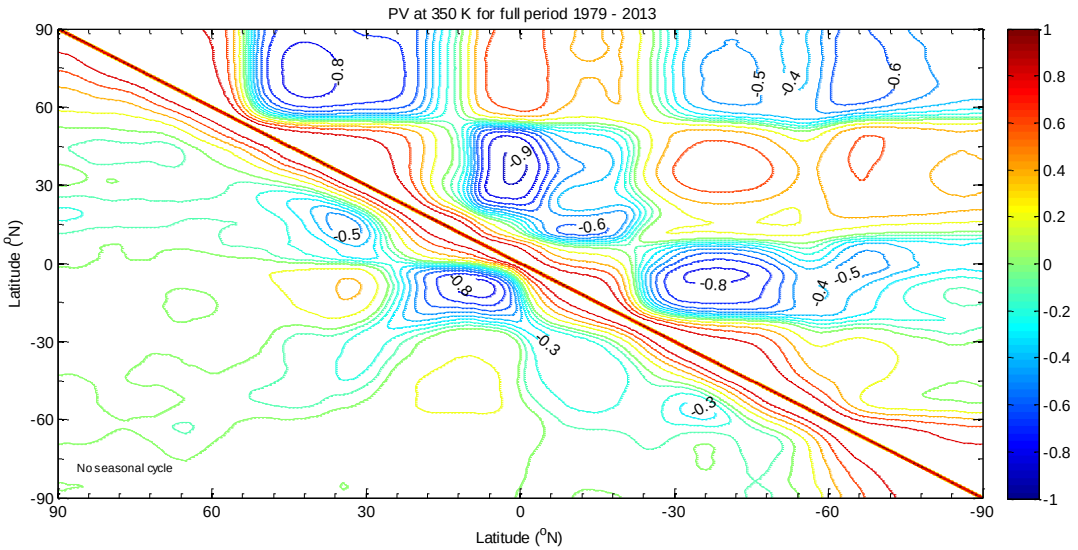

Figure 4.3.1 Cross-correlation matrix of PV at 350 K. The upper triangle shows correlations of PV anomalies including the seasonal cycle and the lower triangle shows correlations with seasonal cycle filtered out by subtracting the PV data from the climatology (monthly means with respect to the 1979-2013 time period).

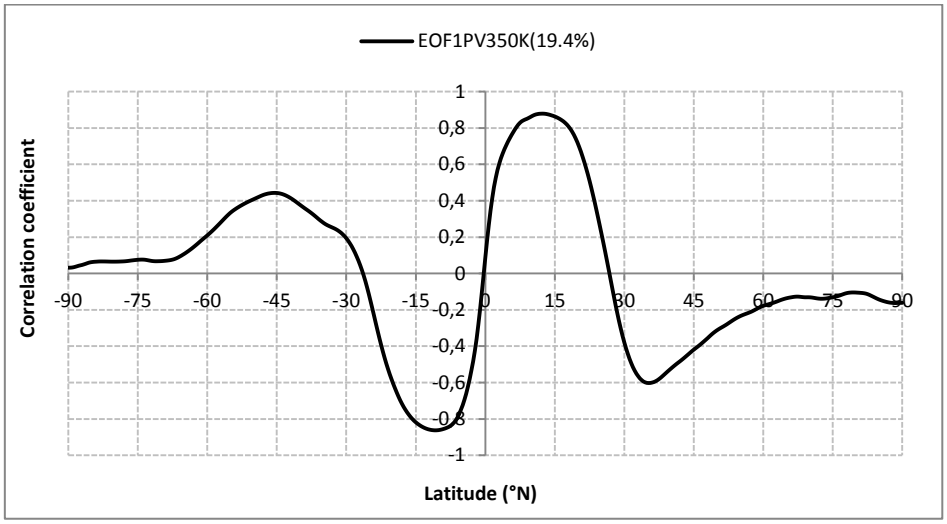

Figure 4.3.2 Leading eigenvector (EOF1PV350K) from PCA applied to the PV anomaly field (with seasonal cycle filtered out and normalized) on the 350 K isentropic surface. The explained variance is shown between parentheses. EOF1PV350K is displayed in terms of the correlation coefficient resultant from the regression of the above mentioned PV field upon the standardized first principal component (PC1PV350K).

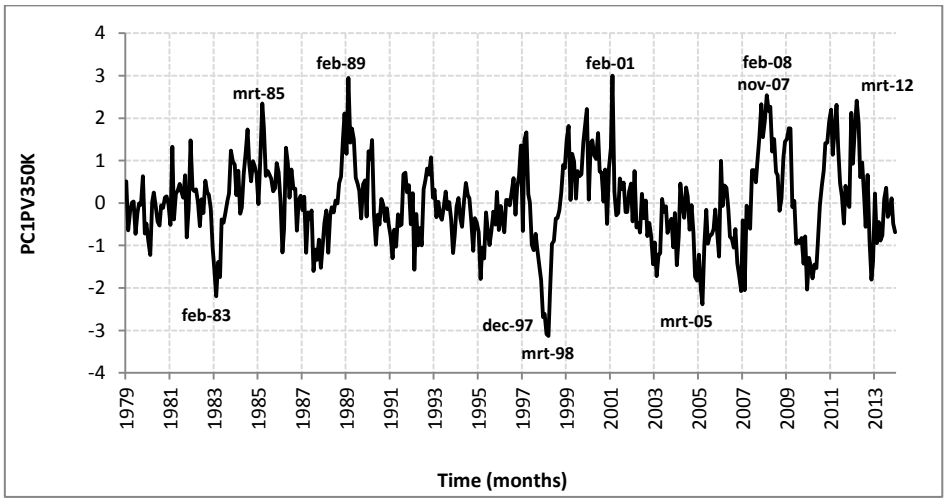

Figure 4.3.3 Time series of the first principal component (PC1PV350K) from PCA applied to the PV anomaly filed (with seasonal cycle filtered out and normalized) on the 350 K isentropic surface.

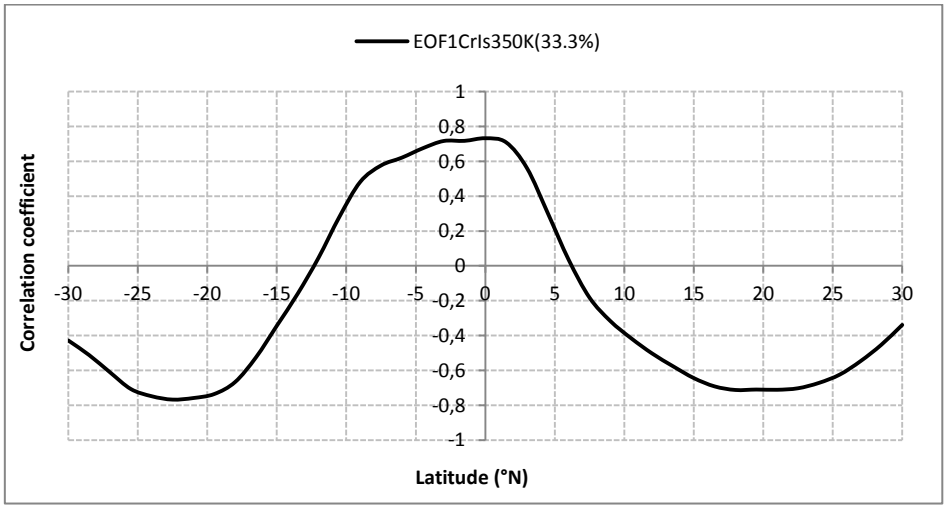

Figure 4.3.4 Leading eigenvector (EOF1CrIs350K) from PCA applied to the cross isentropic flow (CrIs) anomaly filed (with seasonal cycle filtered out and normalized) on the 350 K isentropic surface. The explained variance is shown between parentheses. EOF1CrIs350K is displayed in terms of the correlation coefficient resultant from the regression of the above mentioned CrIs flow field upon the standardized first principal component (PC1CrIs350K). The explained variance is shown between parentheses.

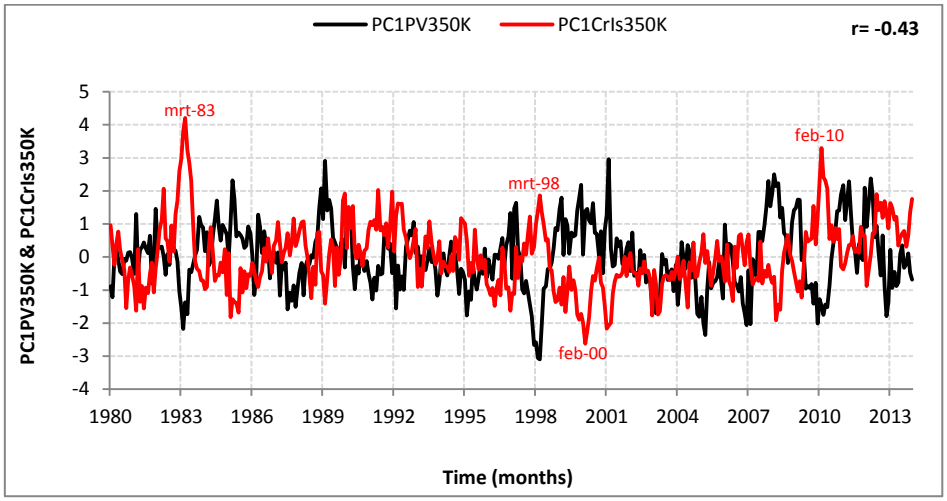

Figure 4.3.5 Time series of the first principal component (PC1PV350K, black line) from PCA applied to the PV anomaly field (with seasonal cycle filtered out and normalized) on the 350 K isentropic surface and the first principal component (PC1CrIs350K, red line) from PCA applied to the CrIs flow anomaly field (with seasonal cycle filtered out and normalized) on the 350 K isentropic surface. The correlation between the two time series is r= -0.43 at lag 0. Note that the time domain is now from 1980 until 2013 since this is the period of time available for the cross isentropic flow.

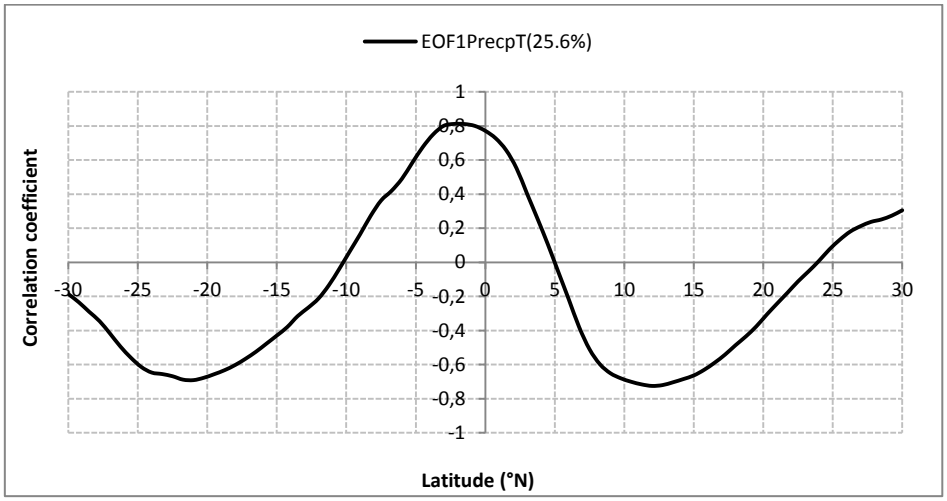

Figure 4.3.6 Leading eigenvector (EOF1PrecpT) from PCA applied to the tropical precipitation anomaly filed (between 30°N and 30°S with seasonal cycle filtered out and normalized). The explained variance is shown between parentheses. EOF1PrecptT is displayed in terms of the correlation coefficient resultant from the regression of the above mentioned tropical precipitation field upon the standardized first principal component (PC1PrecpT). The explained variance is shown between parentheses.

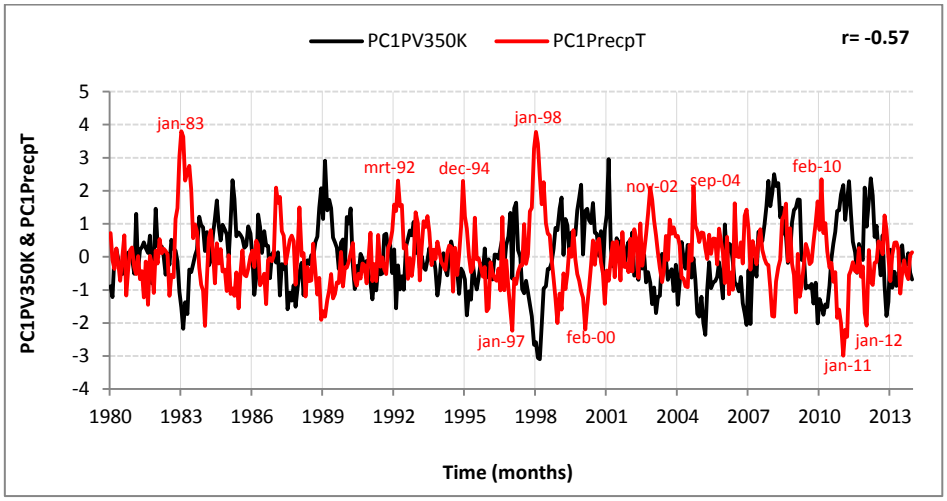

Figure 4.3.7 Time series of the first principal component (PC1PV350K, red line) from PCA applied to the PV anomaly field (with seasonal cycle filtered out and normalized) on the 350 K isentropic surface and the first principal component (PC1PrecpT) from PCA applied to the tropical precipitation flow anomaly field (with seasonal cycle filtered out and normalized). The correlation between the two time series is r=-0.57 at lag 0.

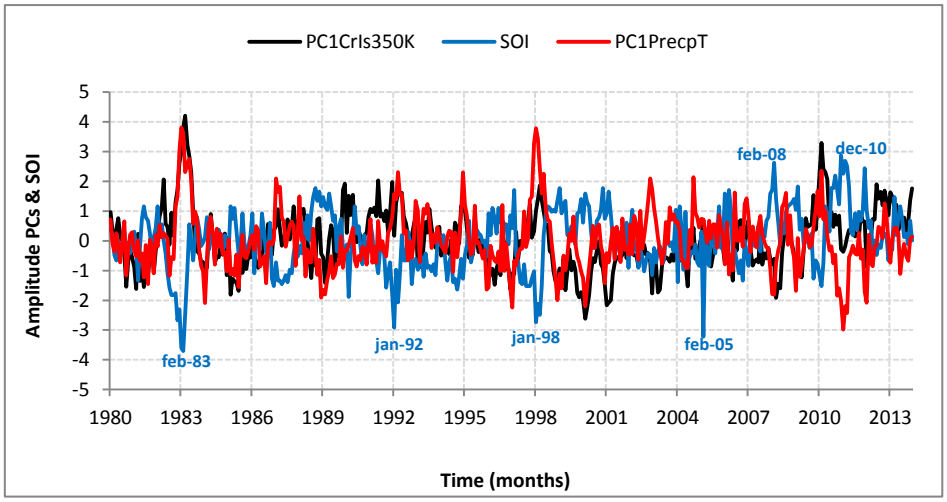

Figure 4.3.8 Time series of the first principal component (PC1PV350K, red line) from PCA applied to the PV anomaly field (with seasonal cycle filtered out and normalized) on the 350 K isentropic surface, time series of the first principal component (PC1PrecpT, black line) from PCA applied to the tropical precipitation flow anomaly field (with seasonal cycle filtered out and normalized) and the SOI (blue line).

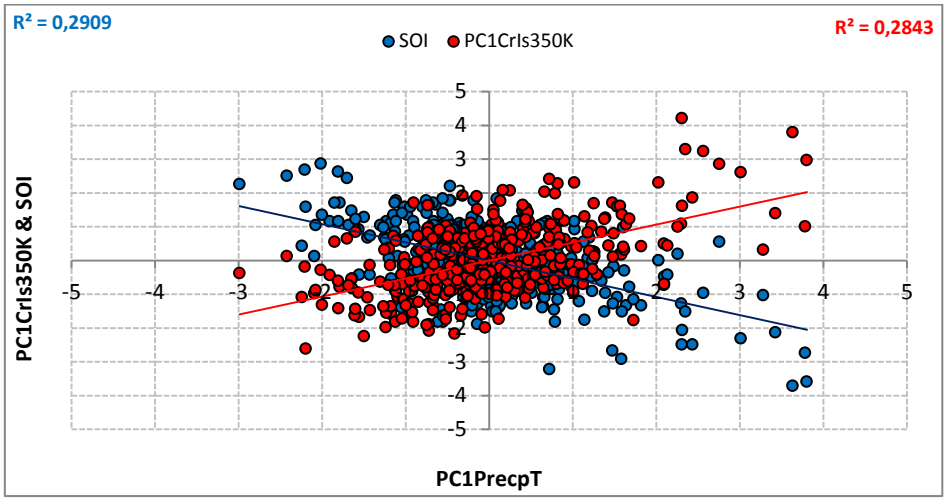

Figure 4.3.9 Scatterplot of PC1PrecpT and PC1CrIs350K (red dots) and PC1PrecpT and the SOI (blue dots); the associated correlation coefficients are in red and blue respectively.

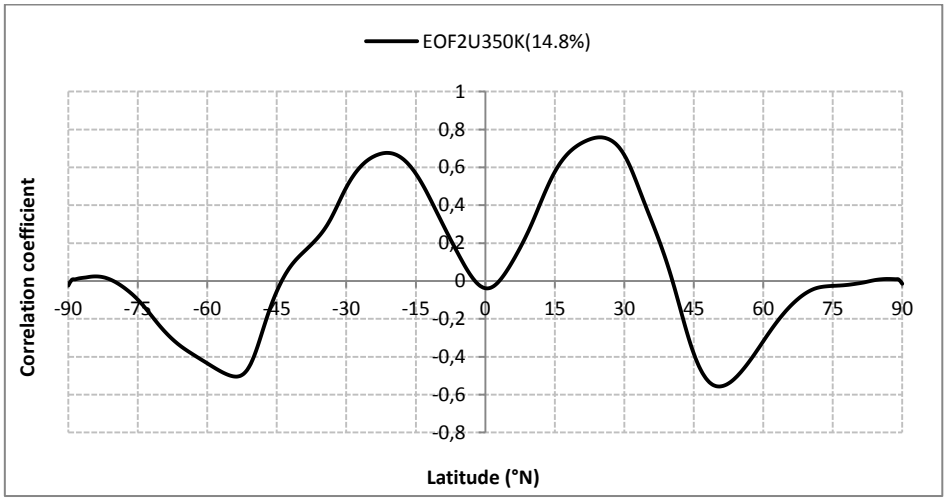

Figure 4.3.10 Second eigenvector (EOF2U350K) from PCA applied to the zonal wind (U) anomaly filed (with seasonal cycle filtered out and normalized) on the 350 K isentropic surface. The explained variance is shown between parentheses. EOF1U350K is displayed in terms of the correlation coefficient resultant from the regression of the above mentioned U field upon the standardized second principal component (PC2U350K). The explained variance is shown between parentheses.

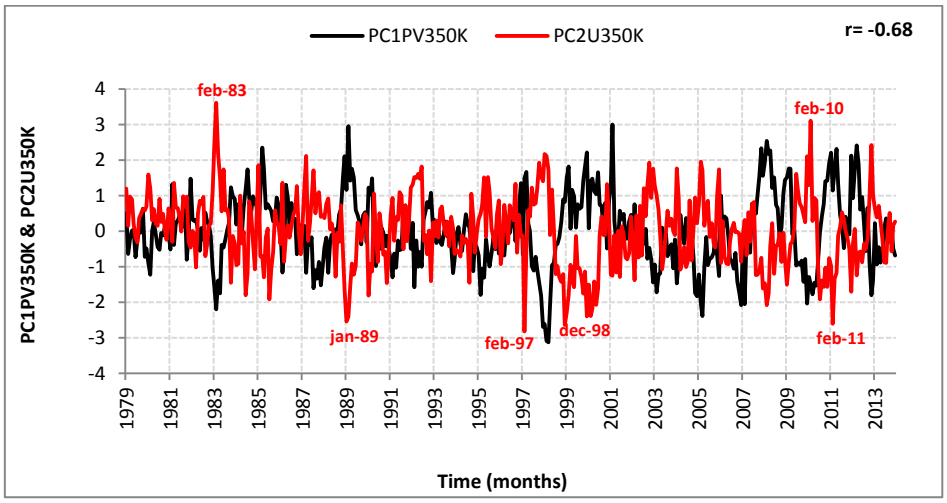

Figure 4.3.11 Time series of the first principal component (PC1PV350K) from PCA applied to the PV anomaly field (with seasonal cycle filtered out and normalized) on the 350 K isentropic surface and the second principal component (PC2U350K) from PCA applied to the U anomaly field (with seasonal cycle filtered out and normalized) on the 350 K isentropic surface. The correlation between the two time series is r=-0.68 at lag 0.

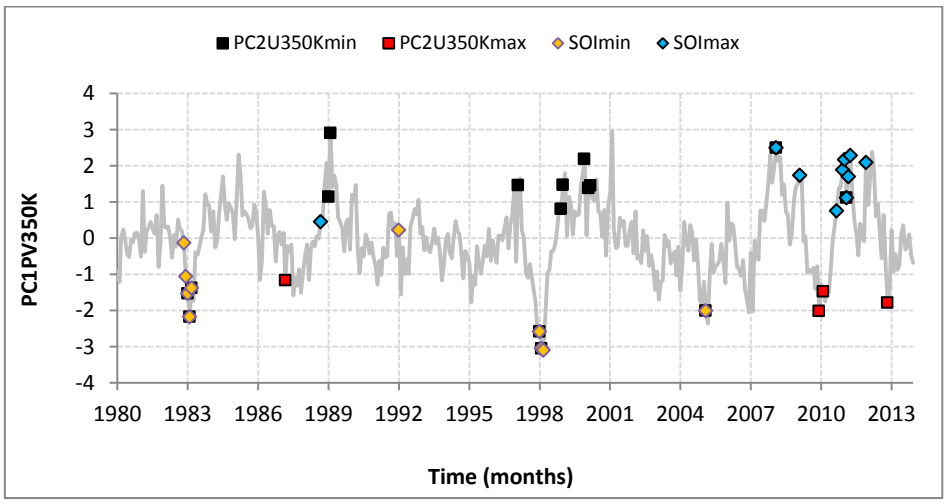

Figure 4.3.12 Top ten maxima and minima of PC2U350K (PC2U350Kmin corresponds to a strong subtropical jet; PC2U350Kmax corresponds to a weak subtropical jet) and the SOI (SOImin corresponds to El Niño events; SOImax corresponds to La Niña events) associated with PC1PV350K (grey line).

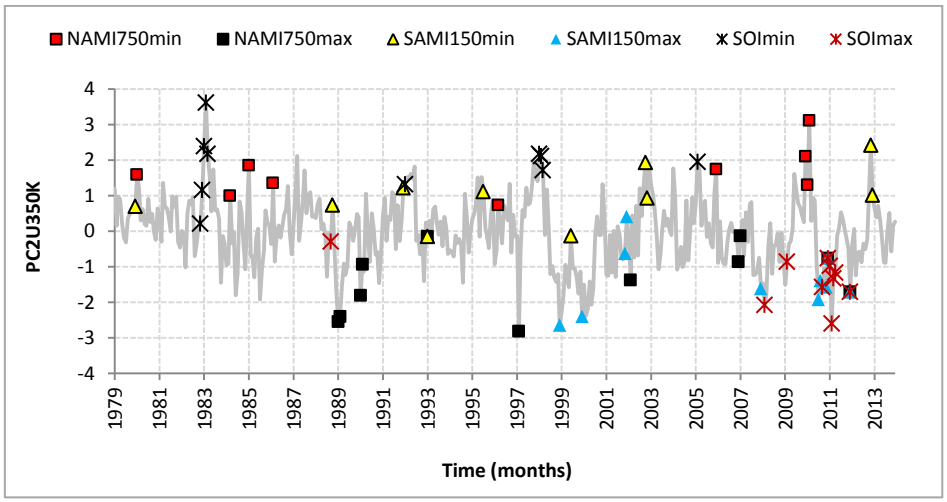

Figure 4.3.13 Top ten maxima and minima of the NAM index defined at 750 hPa (respectively NAMI750min and NAMI750max), the SAM index defined at 150 hPa(SAMI150min and SAMI150max) and the SOI (SOImin corresponds to El Niño events; SOImax corresponds to La Niña events) associated with PC2U350K (grey line).

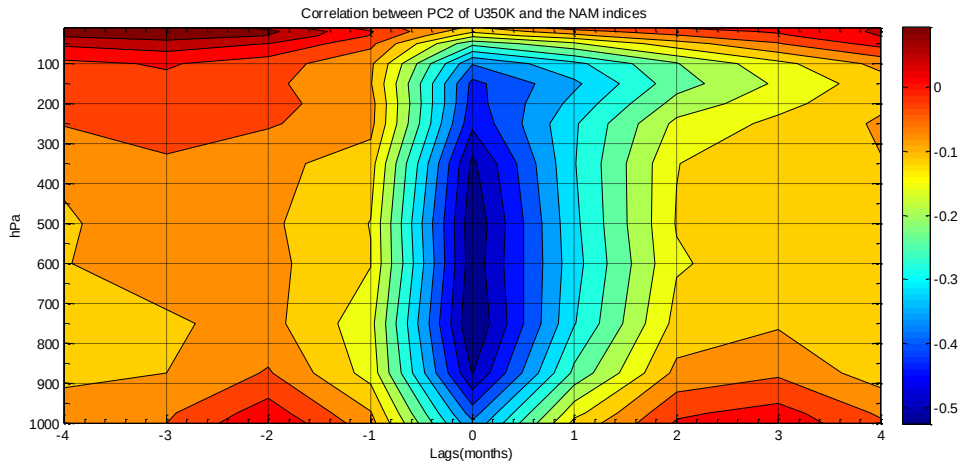

Figure 4.3.14 Correlation matrix between PC2U350K and the NAM indices defined at several geopotential heights using the method of Li and Wang (2003). Negative lags (in months) means that the NAM leads PC2U350K.

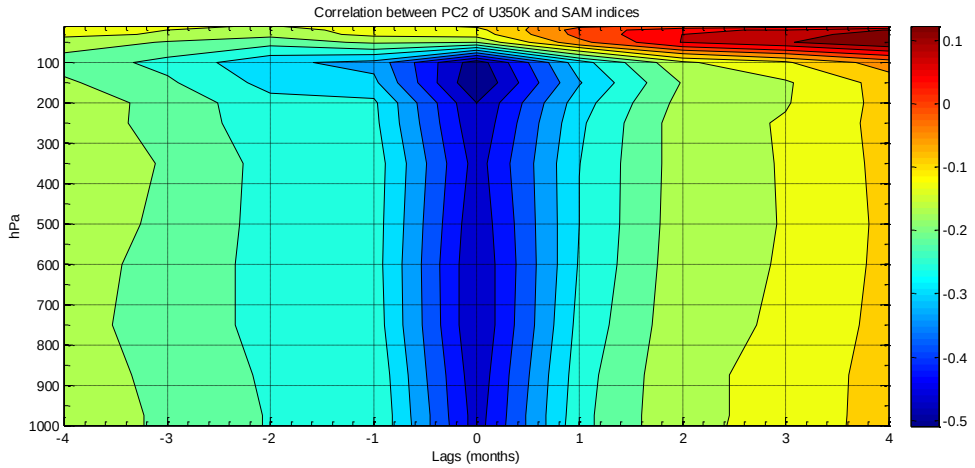

Figure 4.3.15 Same as in **figure 4.3.14** but with the SAM indices instead of the NAM.

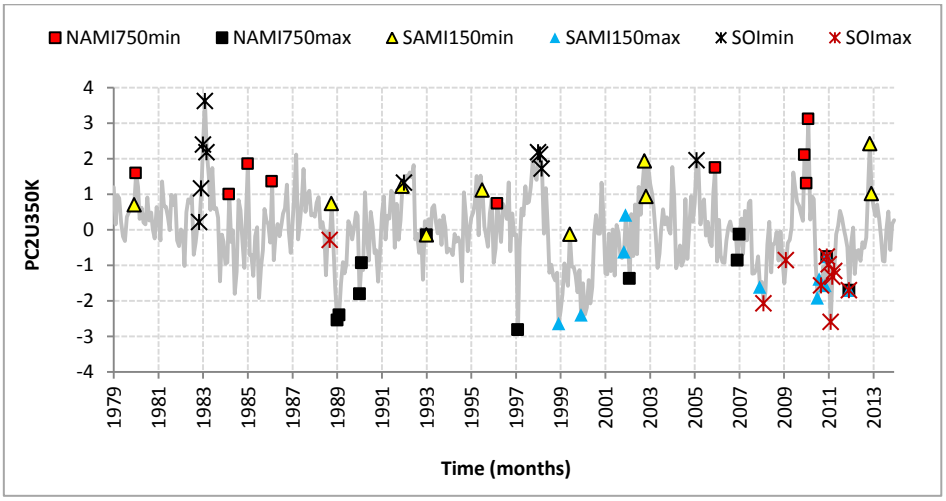

Figure 4.3.16 Top ten maxima and minima of the NAM index defined at 750 hPa (respectively NAMI750min and NAMI750max), the SAM index defined at 150 hPa(SAMI150min and SAMI150max) and the SOI (SOImin corresponds to El Niño events; SOImax corresponds to La Niña events) associated with PC2U350K (grey line).

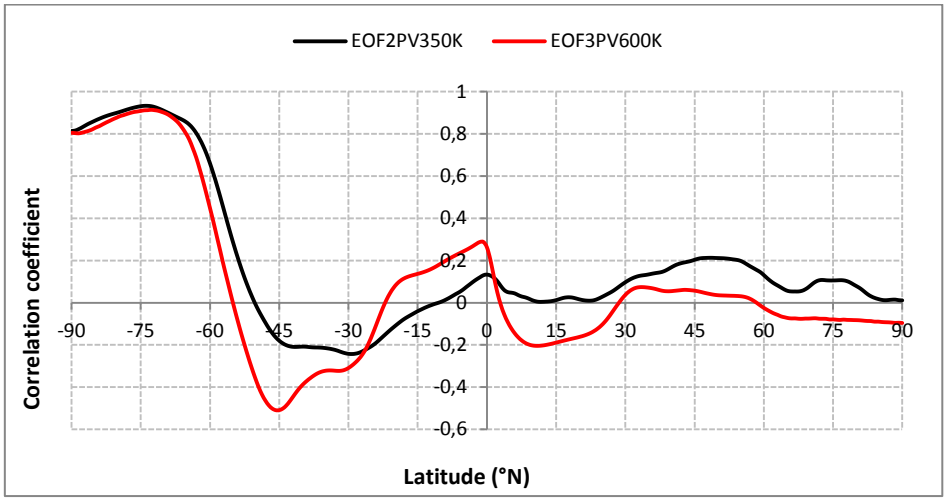

Figure 4.3.17 Second eigenvector (EOF2PV350K, black line) from PCA applied to the PV anomaly filed (with seasonal cycle filtered out and normalized) on the 350 K isentropic surface and EOF3PV600K (section 4.1, **figure 4.2.3**). EOF1PV350K is displayed in terms of the correlation coefficient resultant from the regression of the above mentioned PV field on the 350 K isentrope upon the standardized second principal component (PC2PV350K). The explained variance is shown between parentheses.

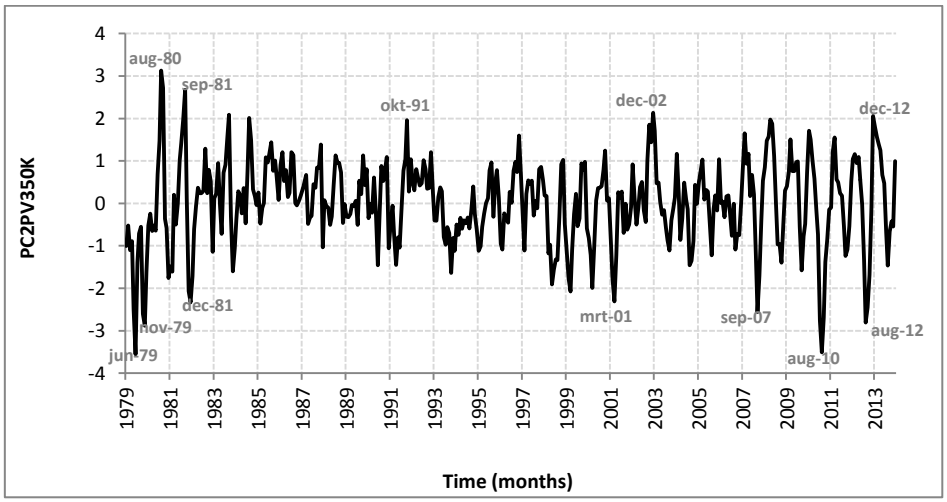

Figure 4.3.18 Time series of the second principal component (PC2PV350K) from PCA applied to the PV anomaly field (with seasonal cycle filtered out and further normalized) on the 350 K isentropic surface.

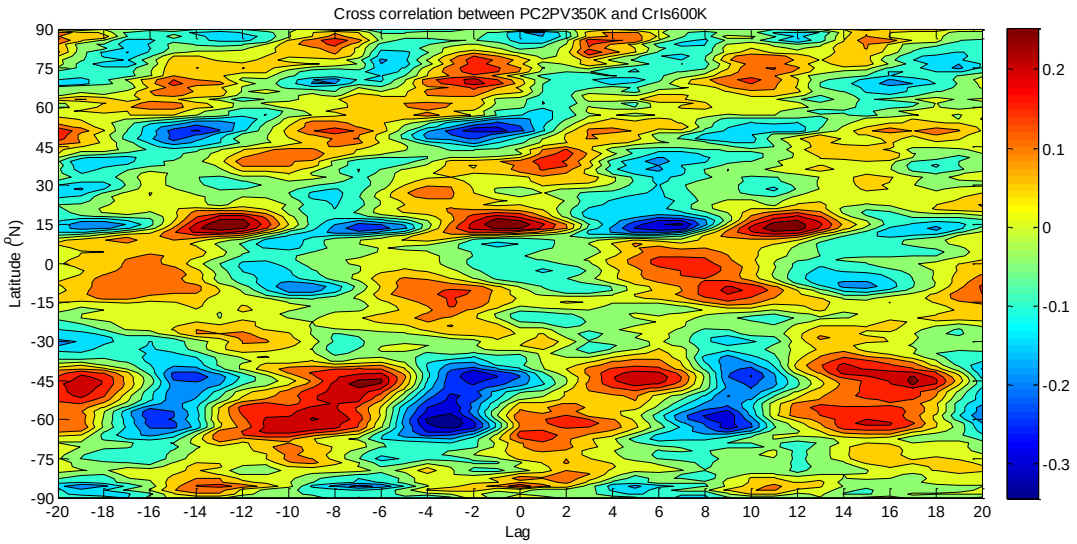

Figure 4.3.19 Cross correlation between PC2PV350K and the cross isentropic flow on the 600K (CrIs600K) isentropic surface. Negative lags (in months) means that the cross isentropic flow leads. Lag in months.

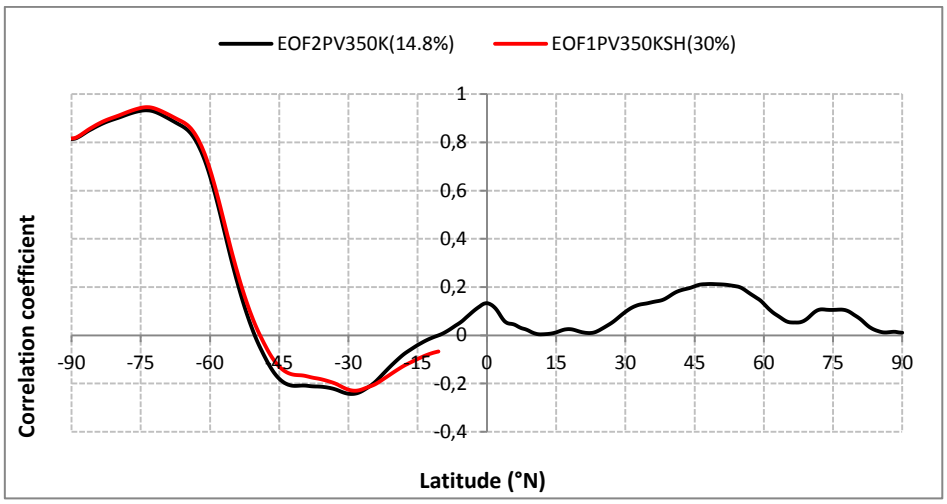

Figure 4.3.20 Second eigenvector of PV350K for full domain, from 90°N to 90°S (EOF2PV350K) and the leading eigenvector of PV350K for the domain 10.5°S to 90°S (EOF1PV350KSH) from PCA applied to the PV anomaly filed (with seasonal cycle filtered out and normalized) on the 350 K isentropic surface. The explained variance is shown between parentheses.

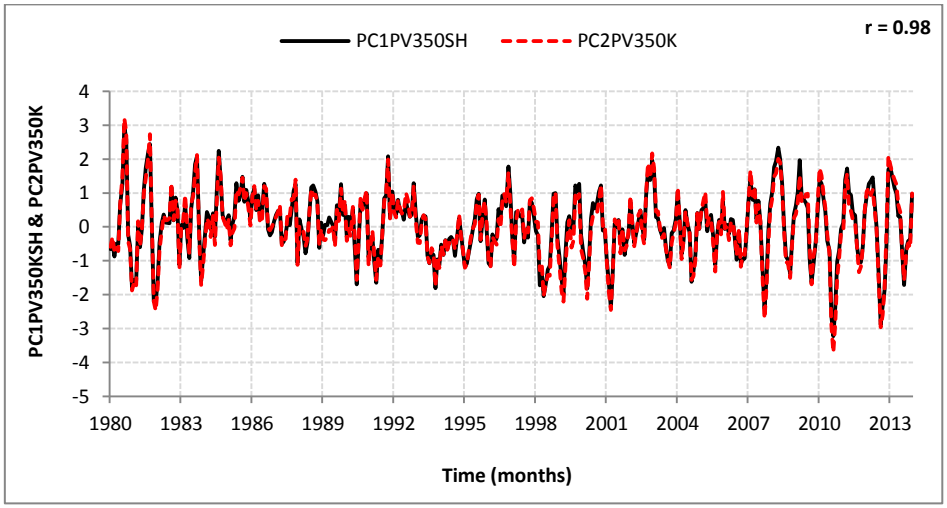

Figure 4.3.21 Time series of the PC2PV350K (red dotted line) and the time series of PC1PV350SH from PCA applied to the SH. The latter is only shown for comparison.

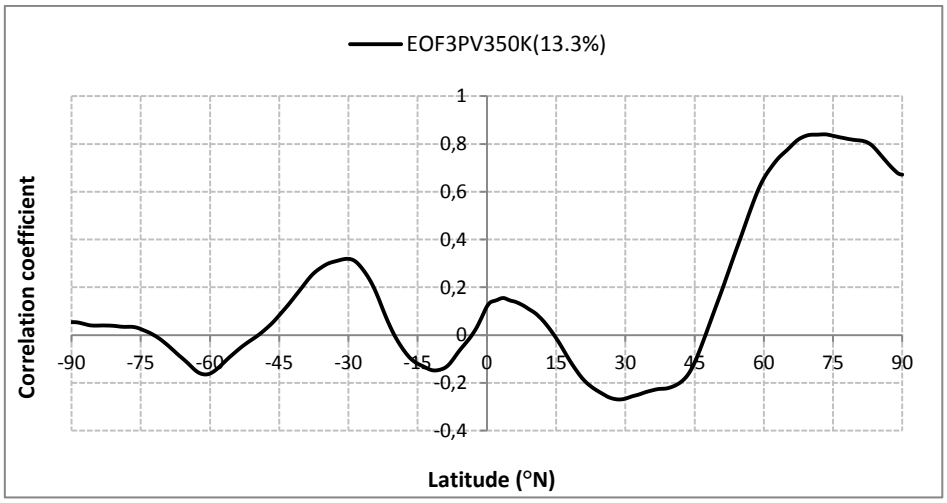

Figure 4.3.22 Third eigenvector (EOF3PV350K) from PCA applied to the PV anomaly filed (with seasonal cycle filtered out and normalized) on the 350 K isentropic surface. The explained variance is shown between parentheses. EOF3PV350K is displayed in terms of the correlation coefficient resultant from the regression of the above mentioned U field upon the standardized second principal component (PC3PV350K). The explained variance is shown between parentheses.

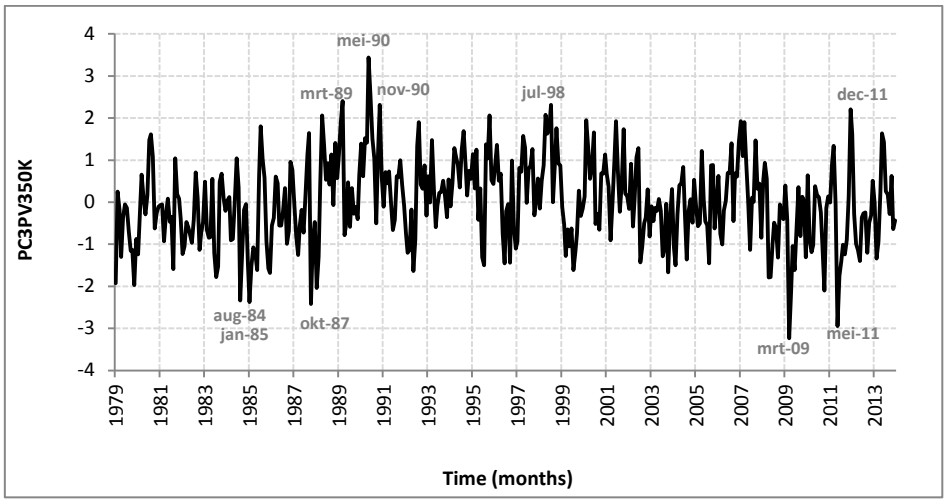

Figure 4.3.23 Time series of the third principal component (PC3PV350K) from PCA applied to the PV anomaly field (with seasonal cycle filtered out and further normalized) on the 350 K isentropic surface.

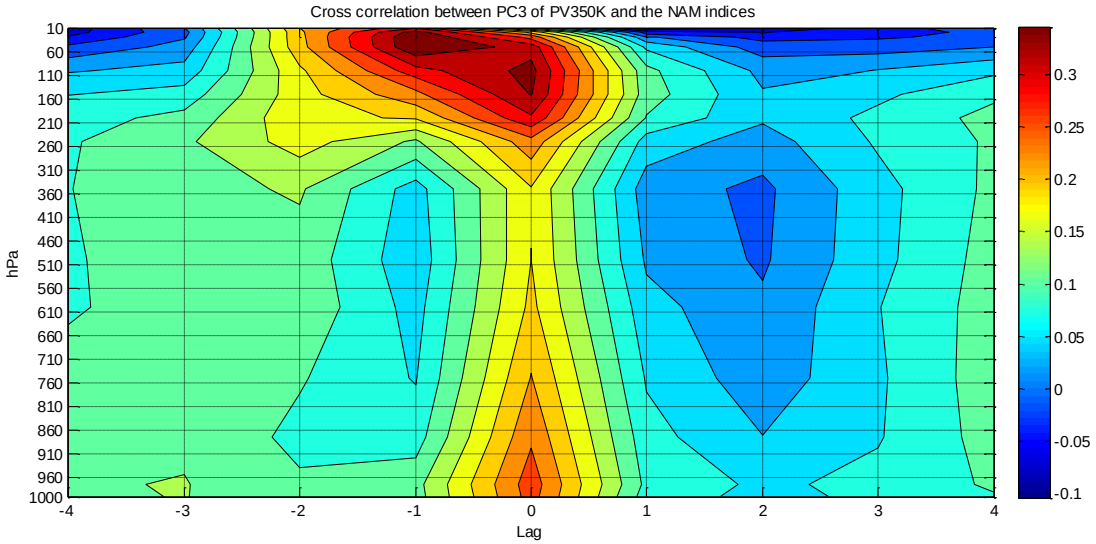

Figure 4.3.24 Cross correlation between PC3PV350K and the NAM indices defined at different pressure levels. Negative (positive) lag means NAM leads (lags). Lag in months.

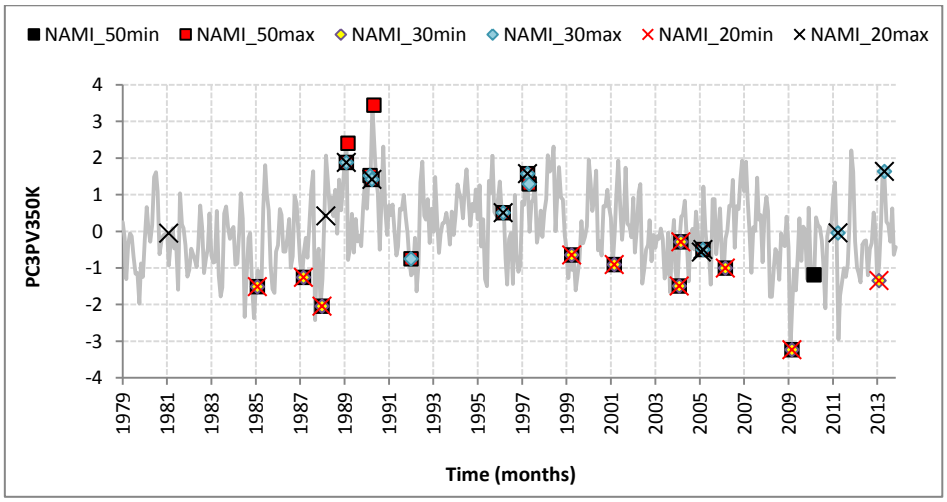

Figure 4.3.25 Top ten maxima and minima values of the NAM indices (at lag -1 when the NAM leads) defined at 50 hPa (NAMI_50), 30 hPa (NAMI_30) and 20 hPa (NAMI_20) associated with PC3PV350K (grey line).

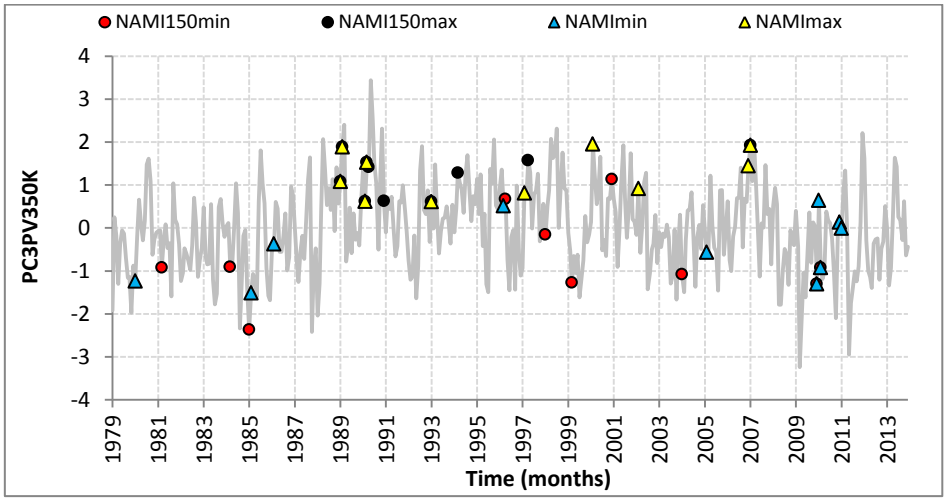

Figure 4.3.26 Top ten maxima and minima values of the NAM indices (at lag 0) defined at 150 hPa (NAMI_150) and at the surface (NAMI) associated with PC3PV350K (grey line).

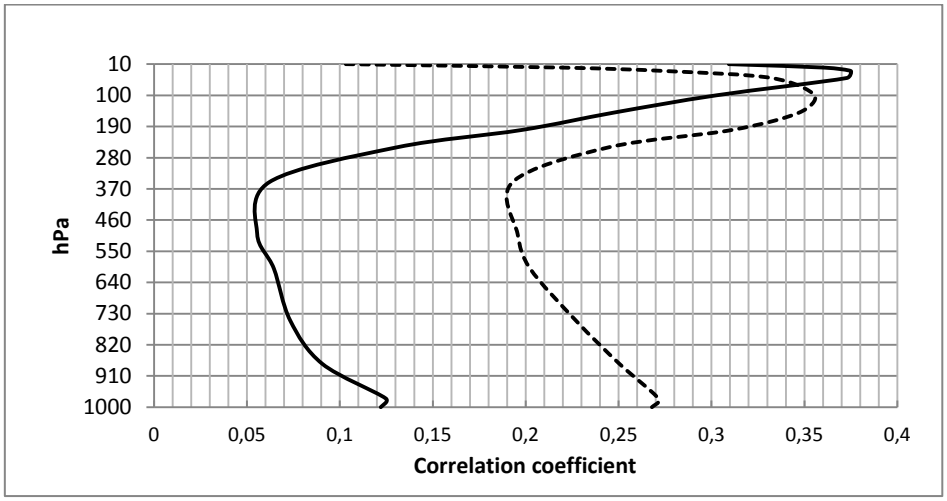

Figure 4.3.27 Correlation coefficient between PC3PV350 and the NAM indices (defined at different pressure levels) at lag -1 (solid line) and at lag 0 (dotted line) with height.

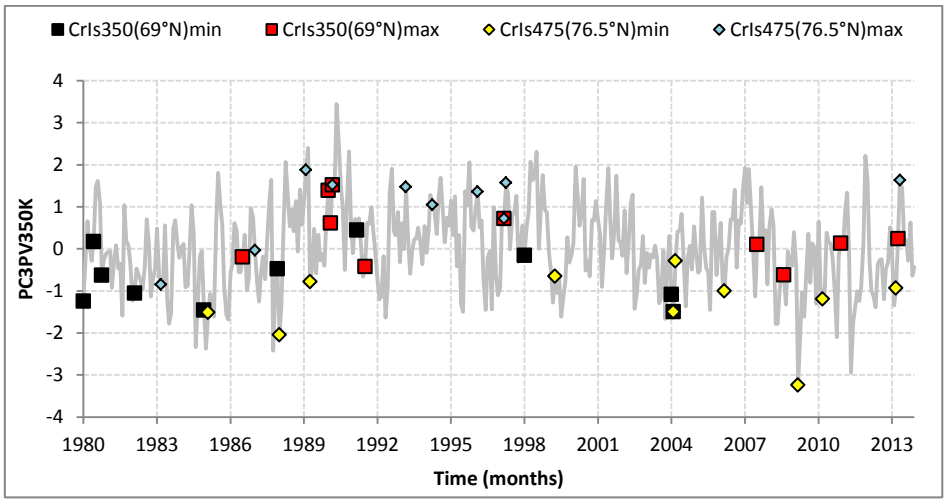

Figure 4.3.28 Top ten maxima and minima values of the cross isentropic flow on the 350 K isentrope at 69°N (CrIs350(69°N)min and max at lag 0) and on the 475 K isentrope at 76.5°N (CrIs475(76.5°N)min and max at lag -1 when CrIs475K leads by one month) associated PC3PV350K (grey line).

Table 1 Correlation coefficients (r) at lag zero between the principal components of PV, cross isentropic flow and the zonal wind on the 350 K isentropic surface (respectively PC1PV350K, PC1CrIs350K and PC2U350K), tropical precipitation (PC1PrecpT), SOI and the AMs (NAM and SAM). N.S. stands for not significant. (1) at lag -1, r=0.57 with PC1PrecpT leading; (2) at lag 1, r=-0.61 with SOI leading; (3) at lag -2, r=0.46 with SOI leading. Lags in months.

	PC1PV350K	PC2U350K	PC1PrecpT	PC1CrIs350K	SOI	NAM	SAM
PC1PV350K	**1**	-0.69	-0.57	-0.43	0.52	N.S.	N.S.
PC2U350K	-0.69	**1**	0.54 (1)	-0.45	-0.55	-0.52	-0.51
PC1PrecpT	-0.57	0.54	**1**	0.53	-0.54 (2)	N.S.	N.S.
PC1CrIs350K	-0.43	-0.45	0.53	**1**	0.41 (3)	N.S.	N.S.
SOI	0.52	-0.55	-0.54 (2)	0.41	**1**	N.S.	N.S.
NAM	N.S.	-0.52	N.S.	N.S.	N.S	**1**	N.S
SAM	N.S.	-0.51	N.S.	N.S.	N.S.	N.S.	**1**

Table 2 Short description of the positive and negative values of the principal components (PCs) resultant from PCA applied to PV, cross isentropic flow and zonal wind on the 350 K and 600 K isentropic surfaces as well as the PCs resultant from PCA applied to climate indices for the NH.

Section 4.2: PCA applied to PV on the 600 K isentropic surface		
Principal Components(PC)	**Positive**	**Negative**
PC1PV600K	• Westward phase QBO (QBO < 0) • Below average PV (tropics both hemispheres) • Below average PVS (tropics both hemispheres)	• Eastward phase QBO (QBO > 0) • Above average PV (tropics both hemisphere) • Above average PVS (tropics both hemispheres)
PC2PV600K	• Positive phase NAM at 20 hPa • Positive PV anomalies at midlatitudes & Negative PV anomalies at polar latitudes • Strong polar vortex	• Negative phase NAM 20 hPa • Negative PV anomalies at midlatitudes & Positive PV anomalies at polar latitudes • Weak polar vortex
PC3PV600K	• Positive phase SAM at 20 hPa • Positive PV anomalies at midlatitudes & Negative PV anomalies at polar latitudes (in absolute value) • Strong polar vortex	• Negative phase SAM at 20 hPa • Negative PV anomalies at midlatitudes & Positive PV anomalies at polar latitudes (in absolute value) • Weak polar vortex
Section 4.3: PCA applied to PV on the 350 K isentropic surface		
PC1PV350K	• Strong PV mixing • Weak subtropical jet (PC2U350K negative) • SOI positive (La Niña) • PC1CrIs350 negative (anomalous diabatic cooling between 12°S and 6°N & anomalous diabatic heating elsewhere; weak HC) • PC1PrecpT negative (below average precipitation between 10°S and 5°N	• Weak PV mixing • Strong subtropical jet (PC2U350K positive) • SOI negative (El Niño) • PC1CrIs350 positive (anomalous diabatic heating between 12°S and 6°N & anomalous diabatic cooling elsewhere; strong HC) • PC1PrecpT positive (above average precipitation between 10°S and 5°N

	& above precipitation elsewhere)	& below precipitation elsewhere)
PC2PV350K	• Unclear	• Unclear
PC3PV350K	• PV transport into the region 47°N and the pole • In general positive phase of the tropospheric NAM (at lag zero) • Positive CrIs475K (reduced diabatic cooling at 76.5°N)	• PV transport out of the region 47°N and the pole • In general negative phase of the stratospheric NAM (when the latter leads by one month) • Positive CrIs475K (enhanced diabatic cooling at 76.5°N)
Section 4.4: PCA applied to climate indices for the NH		
PC1CI	• Positive PC2PV600K	• Negative PC2PV600K
PC2CI	• Negative PC1PV350K	• Positive PC1PV350K
PC3CI	• Negative NAM (surface) • U350I positive (strong subtropical jet, weak midlatitude jet)	• Positive NAM (surface) • U350I negative weak subtropical jet, strong midlatitude jet)
PC4CI	• CrIs600IBD positive (enhanced heating at 13.5°N, reduced at 1.5°N) • CrIs600I positive (westward QBO)	• CrIs600IBD negative (reduced heating at 13.5°N, enhanced at 1.5°N)) • CrIs600I negative (eastward QBO)

4.4 PCA applied to Climate Indices (CI)

So far we have been analyzing the potential vorticity fields on the 350 K and 600 K isentropic surface and their relations with other atmospheric variables such as the zonal winds, cross isentropic flow, as well as with the annular modes using the full domain, thus from 90°N to 90°S. In this section we will focus only on the northern hemisphere and define climate indices for potential vorticity, zonal wind, cross isentropic flow and the NAM in order to have a better understanding of their relationship. The method used for the calculation of the indices is the one developed by Li and Wang (2003) which defined the NAM index by finding the maximum in anticorrelation in normalized mean sea level pressure which they found to be between 35°N and 65°N. The NAM index was then defined as the difference in sea level pressure between those latitude bands (section 2.2). The same approach is used here, thus for each atmospheric variable we calculate the cross correlation matrix, find the latitudes of maximum anticorrelation and the respective indices are then the difference between those latitudes (**table 3**). The domain used is from 10.5°N until 90°N with exception for the cross isentropic flow on 350 K (CrIs350K) and 600 K (CrIs600K) isentropic surfaces where the equator is included. For the case of CrIs350K the domain used is from 0° until 90°N, while for CrIs600K both domains will be used, i.e., from 0° to 90°N and from 10.5°N to 90°N. The time period is from 1980-2013 including all months for all atmospheric variables. Furthermore, tropical precipitation will be also analyzed and defined as the time series associated

with the leading eigenvector (PC1PrecpT) found in the previous analysis with PV on the 350K isentropic surface (section 4.3). Although this PC was found by applying PCA to precipitation between 30°S and 30°N, there are no significant changes in case PCA is applied to precipitation only in the northern hemisphere tropics. . In the same way as in the previous sections, all data sets are normalized by subtracting the climatology, i.e., the seasonal cycle is filtered out, and further divided by their standard deviation. Therefore all the climate indices are dimensionless

4.4.1 Climate Indices – Overview

4.4.1.1 PV600I

The maximum in anticorrelation for the PV anomaly field on the 600 K isentrope belongs to the mid and polar latitudes, i.e. between 48°N and 73.5°N. These two latitudes were already captured when the cross correlation matrix was calculated for PV on the 600 K for the full domain (section 4.2, **figure 4.2.1**). It follows that the PV index on this isentropic surface, PV600I, is then defined as the difference in PV between 48°N and 73.5°N (**table 3** and **figure 4.4.1**). In section 4.2 it was found that the second eigenvector of PV on the 600 K (EOF2PV350K) represented PV anomalies between mid and polar latitudes, with the associated PC (PC2PV350K) representing strong and weak stratospheric polar vortex events. As seen in **figure 4.4.2,** the very strong correlation between PV600I and the PC2PV600K (r=0.95) and the NAM index at 20 hPa (r=0.93) implies that PV600I also represents variability in the polar vortex of the NH. The obvious conclusion is therefore that positive (negative) values of PV600I are representative of strong (weak) polar vortex events, hence associated with positive (negative) PV anomalies at polar latitudes and with negative (positive) ones at midlatitudes.

4.4.1.2 PV350I

With respect to PV on the 350 K isentrope (PV350I, **table 3** and **figure 4.4.3**), the maximum in anticorrelation is found between the tropics (15°N) and subtropics (34.5°N), which again were the latitudes already found when the cross correlation matrix was calculated for PV on the 350 K for the full domain (section 4.3, **figure 4.3.1**). From section 4.3 it was argued that the leading eigenvector, EOF1PV350K (section 4.3, **figure 4.3.2**) represented PV variability between the tropics and subtropics. In fact, the correlation between PC1PV350K and PV350I is -0.83 at lag 0 (**figure 4.4.3**). This strong anticorrelation simply implies that positive values of PV350I (negative values of PC1PV350K) are associated with a stronger HC, thus a strong subtropical jet, due to enhanced

diabatic heating associated with the El Niño. Conversely, negative values of PV350I (positive values of PC1PV350K) should be associated with a weaker HC, a weaker subtropical jet and La Niña events.

4.4.1.3 U350I

The tropospheric zonal flow consists of two distinct jets, the subtropical jet and the midlatitude jet (Eichelberger and Hartmann, 2007). The subtropical jet is located approximately at 30° latitude on the 350 K isentrope and is driven mainly by transfer of angular momentum by the HC, while the midlatitude jet is eddy driven. Hartmann (2007) found that in the extratropics two maxima of eddy momentum flux exits in both hemispheres: a poleward one centered at 30° - 40° latitude and an equatorward one located at higher latitudes. The former dominates and its role is to transfer angular momentum from the tropics to the extratropics which sustain the eastward midlatitude winds (Hartmann, 2007).

The maximum in anticorrelation for the zonal wind was found be between the subtropics (32.5°N) and midlatitudes (51°N). Therefore, according to the theory above, one can think of the monthly mean zonal mean wind index on 350 K isentrope, U350I (**table 3**, **figure 4.4.4**) as being a measure of the strength of the eddy-driven jet relative to the subtropical jet (and vice-versa). A negative zonal wind index (U350I negative) will represent a stronger eddy (weaker subtropical) jet while a positive index will represent a weaker eddy (stronger subtropical) jet. A similar conclusion about the relative strength of the subtropical and the midlatitude jets was already found in section 4.2 when PCA was applied to the full domain of the zonal wind on the 350 K isentrope, i.e., for PC2U350K. However, in the latter it appeared that the subtropical jet was shifted equatorward. In fact, the correlation between U350I and PC2U350K is equal to 0.61 at lag zero, which implies that the latter is indeed coupled with the strength of the subtropical jet.

In the stratosphere, the zonal mean wind on the 600 K index (U600I), has a maximum anticorrelation between 27.75N and 56.26N. The strong correlation between U600I and PV600I (**table 4**) implies that the former is representative of the polar night jet.

4.4.1.4 CrIs350I, CrIs600I and CrIs600IBD

The latitudes of maximum anticorrelation for the cross isentropic flow on the 350 K isentropic surface is at the equator and 13.5°N (**table 3**). In the same way as above, the cross isentropic flow index on the 350 K, CrIs350I, is then the difference in cross isentropic flow between the equator and 13.5°N. On average, the cross isentropic flow at the equator is positive (diabatic heating) while at 13.5°N is negative (diabatic cooling, in the winter hemisphere). From **table 4** it is clear that CrIs350I and tropical precipitation (PC1PrecpT) are strongly correlated (r=0.63). As already

mentioned, latent heat release associated with tropical precipitation drives the HC. Therefore, one may argue that the cross isentropic flow on 350 K index, CrIs350K (**figure 4.4.6**) represents the strength of the HC. Positive (negative) values of CrIs350I are representative of a stronger (weaker) HC which in turn is associated with above (below) average tropical precipitation. This reasoning is reinforced by the strong correlation between CrIs350I and PC1CrIs350K (section 4.3) which is shown in **figure 4.4.6**.

With respect to the cross isentropic flow index at 600 K (CrIs600I, **table 3** and **figure 4.4.7**), the latitudes of maximum anticorrelation (including the equator) were found between 1.5°N and 22.5°N. On average, there is diabatic heating at both latitudes, therefore a positive index implies stronger diabatic heating at 1.5°N and weaker diabatic heating (or probably diabatic cooling) at 22.5°N (the inverse for negative values). As we will see later, this index is well correlated with the QBO at 50 mb.

By changing the domain of the cross isentropic flow at 600 K for 10.5°N to 90°N the equator is excluded and the latitudes associated with the maximum in anticorrelation change to be between 13.5°N and 52.5°N. On average, there is diabatic heating in the tropics (at 13.5°N) and diabatic cooling at higher latitudes (at 52.5°N), therefore we have ascending in the tropics, descending at high latitudes and in between, due to conservation of mass, a meridional poleward transport in the stratosphere. This circulation, represented by this index (CrIs600IBD), can be used as a measure of the Brewer Dobson circulation (BDC). Positive values of the CrIs600 index (CrIs600IBD positive) will give indication of a stronger upward branch (and a corresponding stronger BDC) while a negative index will give indication of the opposite. Although the maximum in anticorrelation associated with the above mentioned latitudes is somewhat low (**table 3**), this index is included for better insight with respect to the extratropical stratospheric diabatic circulation and its possible effects on the troposphere.

4.4.2 Climate Indices – PCA results

In this section, in the same way as in the previous ones, the goal is to evaluate a general behavior within a network of climate indices, thus PCA is used to identify the leading patterns of simultaneous variability with all the indices defined above. In this analysis, the NAM index defined at 150 hPa will also be included since it appears, from the previous results, to be well correlated with the stratospheric NAM and with the NAM defined at the surface.

The leading eigenvector (EOF1CI) explains 30% of the total variability mainly in the stratosphere. From **table 4**, it is clear that the first PC (PC1CI) is strongly correlated with the stratospheric NAM calculated at 20 hPa (r=0.91), with PV600I (r=0.87) as well as with U600I (0.87), implying that this principal component represents variability in the stratospheric polar vortex in the NH. Interesting is the fact that PC1CI is also strongly correlated with the NAM index calculated at 150 hPa (r=0.83) being surface NAM also captured by EOF1CI as well as the zonal mean wind index (U350I). From **Figure 4.4.9** one can see that PC1CI is correlated with NAM from the surface until 10 hPa, although with correlations much higher in the stratosphere than in the troposphere. Furthermore, a maximum in correlation was found between PC1CI and the cross isentropic flow on the 475 K isentropic surface (r=0.69) at lag zero and at 79.5°N (**figure 4.4.11**). This implies that a strong polar vortex (positive PC1CI, positive phase of the stratospheric NAM) must be associated with reduced diabatic cooling on the 475 K, while a weak polar vortex (negative PC1CI, negative phase of the stratospheric NAM) must be associated with enhanced diabatic cooling on the same isentropic surface and at 79°N. However, from **figure 4.4.10** we see that the simultaneous NAM anomalies at the surface and in the stratosphere are mainly seen in case of a strong polar vortex (PC1CI positive). This result is similar to the one found in the analysis of PV on the 350 K isentrope (section 4.3) where it was shown that positive values of the time series associated with the third eigenvector (PC3PV350K), thus above average PV in the region between 47°N and the pole, were better associated with the positive phase of the NAM indices defined at 150 hPa as well as at the surface, while negative PC3PV350K values were in general not associated with the surface NAM but with the stratospheric NAM. The enhanced diabatic heating on the 475 K isentrope also appeared to play a role in the latter result, with PV anomalies on the 350 K lagging the cross isentropic flow by one month.

The second eigenvector (EOF2CI) explains 22.9% of the total variance. From table 6 it is clear that the time series associated with this eigenvector (PC2CI) is strongly correlated with PV350I (r=0.78), with tropical precipitation (PC1PrecpT, r=0.75), with the SOI (r=-0.71), with CrIs350I (r=0.73) and to a less extent, with the strength of the subtropical jet (U350I, r=0.47). It is interesting to note that although the correlation between U350I and PC2U350K (section 4.3) is equal to 0.61, the highest correlation is found to be between PC2CI and PC2U350K (r =0.74 at lag zero) and not with U350I. Recall that U350I positive is associated with stronger eastward winds at 32.5°N and weaker winds at 51°N, while positive PC2U350K was associated with stronger eastward winds at 25°N and weaker

winds at 50°N. The difference between U350I and PC2U350K resides therefore on the latitude of the stronger tropical/subtropical jet since the latitudes of the midlatitude jet are very close. This result implies that when the winds are stronger at 32.5°N they are also stronger at 25°N, therefore one may argue that, while U350I represents the strength of the subtropical jet relative to the midlatitude one, PC2U350K may represent an equatorward shift of the subtropical.

Figure 4.4.12 shows the regressions of PC2CI, the SOI, CrIs350I, PC1PrecpT and PV350I upon the PV anomaly field on the 350 K isentropic surface. As expected, EOF2CI is clearly associated with tropical/subtropical variability which is not restricted to the NH. Since the highest correlation is found between PC2CI and the PV350I (see also **table 5**), one may conclude that EOF2CI and associated time series represent mainly the effect of the SOI, the HC strength (as measured by CrIs350I) and tropical precipitation (PC1PrecpT) on PV transport in the tropical and subtropical upper troposphere. Indeed, from **figures 4.4.12, 4.4.13 and 4.4.14,** the extreme positive PC2CI values are clearly associated with below average PV in the tropics and above average in the subtropics (PV350Imax), the El Niño (SOImin), and strong tropical precipitation (PC1PrecpTmax). Under these conditions a strong subtropical jet (as measured by U350Imax) as well as its (argued) equatorward shift (PC2U350Kmax) is also captured by positive PC2CI.With respect to the maximum in the cross isentropic flow on the 350 K index (CrIs350max) associated with PC2CI, it appears to be clustered specifically at the end of 1982 until February 1983, the time of one of the strongest El Niño's of history, implying that before and during this event, the HC (as measured by CrIs350I) was anomalously strong.

Extreme negative values of PC2CI correspond to transport of PV into the tropics (PV350Imin). In this case, the results seem less obvious. With respect to the positive SOI events (La Niña), they appear in **figure 4.4.13** as a cluster between March 2008 and December 2011 and are mainly associated with below average tropical precipitation and a weaker HC.

Overall, EOF2CI and associated time series (PC2CI) represents mainly the effect of the El Niño/La Niña and associated changes in the strength of the HC, hence the strength of the subtropical jet, due to enhanced/reduced diabatic heating in the tropics in the NH. As expected, the correlation between PC2CI and PC1PV350K is -0.735 at lag 0 (recall that negative values of PC1PV350K were associated with transport of PV out of the tropics, while in the present analysis PV transport out of the tropics is associated with positive PC2CI values, hence PC2CI and PC1PV350K are negatively correlated). Therefore the conclusions regarding PC2CI are the same as the ones regarding PC1 of PV350K.

The third eigenvector (EOF3CI) explains 13.3% of the total variance. **Table 6** shows that the correlation between PC3CI with the NAMI (r = -0.71) is the highest followed by the tropospheric jet (r = 0.56), and to a less extent tropical precipitation (PC1PrecpT, r=-0.42). Therefore it appears that PC3CI represents mainly the link between the surface NAM and the relative strength of the subtropical and midlatitude jets (with no connection with PC2U350K) with some influence of tropical precipitation. However the cross isentropic flow, on both the 350 and 600 K isentropes, as well as the SOI also appear to play a role. **Figure 4.4.15** and **4.4.16** show the PC3CI time series associated with the maximum and minimum values of the NAM index calculated at the surface (NAMI), U350I, the SOI and the cross isentropic flow on the 350 K and 600 K isentropic surface indices (CrIs350I and CrIs600I). Positive values of PC3CI are clearly associated with the negative phase of the NAMI (NAMImin) and a strong subtropical jet (U350Imax) as well as a minimum in tropical precipitation (PC1PrecpTmin). The El Niño's (SOImin) do appear to be associated with negative values of PC3CI as well as maximum values of CrIs350I (which represent a strong HC) and a maximum in tropical precipitation specifically in 1983 (**figure 4.4.16**). Negative values of PC3CI are also associated with the positive surface NAM (NAMImax), a weak subtropical jet (U350Imin) and above average tropical precipitation (**figure 4.4.15**). For positive values of PC3CI, mainly with respect to December 2010/January 2011, a year marked by a strongly negative NAM, La Niña is captured as well as a minimum in tropical precipitation, with no clear evidence of any influence/effect of/on the subtropical jet. From **figure 4.4.16** it is also visible that the time periods from December 2001 until February 2002 and December 2012 until January 2013 were marked by strong diabatic heating near the equator in the stratosphere as seen by the maximum in CrIs600I which in turn is associated with the QBO defined at 50hPa (**figure 4.4.7**). In fact, and as expected, CrIs600I is strongly correlated with PC1PV600K (section 4.2) at lag 4 (r = -0.7) where the cross isentropic flow index leads (**figure 4.4.8**). Although the tropical stratosphere is captured by EOF3CI, the main contributions are from within the extratropical troposphere. In fact, PC3CI is strongly correlated with the NAM index defined not only at the surface but until about 350 hPa (**figure 4.4.19**).

The main conclusions regarding EOF3CI and its associated time series are therefore that PC3CI represents the relationship between the NAM, the relative strength between the subtropical jet and the midlatitude one and tropical precipitation, i.e. the positive phase of the NAM is associated with a strong subtropical jet (U350I positive) and below average tropical precipitation, and vice-versa.

Finally, the fourth eigenvector represents mainly the strength of the Brewer Dobson Circulation (CrIs600IBD) associated with diabatic heating/cooling within the tropical stratosphere (CrIs600I) which in turn is related with the QBO (**table 4** and **figure 4.4.7**). **Figure 4.4.20** shows the regression of PC4CI on the CrIs600K anomaly field from which is clear that the highest variance explained by this eigenvector belongs mainly to the tropics and subtropics. From section 4.2 it was found that PC1PV600K represented the effect of the QBO (30 mb) on PV variability in the tropical stratosphere associated with diabatic heating/cooling as measured by the cross isentropic flow on the 600 K isentrope. As already mentioned CrIs600I is strongly correlated with PC1PV600K when CrIs600I leads by 4 months (**figure 4.4.8**). Recall that positive (negative) values of the CrIs600I are associated with strong (weak) diabatic heating at 1.5°N (22.5°N), and positive values of CrIs600IBD are associated with strong diabatic heating at 13.5°N and weak cooling at 52.5°N. Therefore, these results imply that the westward phase of the QBO (QBO negative) will be associated with strong (weak) diabatic heating at 1.5°N (22.5°N), hence positive CrIs600I, while the opposite happens for the eastward QBO (QBO positive). However, the correlation between PC4CI and PC1PV600K is somewhat low (r = -0.42, also at lag 4 where PC4CI leads), therefore the QBO is not the main driving force associated with PC4CI. The lag correlation between PC4CI and the PV anomaly field on the 600 K isentrope is shown in **figure 4.4.21**, from where it can be seen that PC4CI leads changes in the PV on the 600 K. The maximum and minimum correlation is found at 6.75°N (r = 0.47, lag 2) and at 3.75°S (r = -0.52, lag 1), implying that the effect of PC4CI on potential vorticity mixing is stronger just poleward of the equator in the southern hemisphere. Since the highest correlation is between PC4CI and CrIs600IDB (r = 0.77), one might be tempted to argue that EOF4CI represents mainly changes in BDC strength due to the QBO; a stronger BDC (CrIs600IBD positive) is associated with enhanced diabatic heating at 13.5°N due to the QBO westward (which is associated in turn with positive values of CrIs600I), while a weaker BDC (CrIs600IBD) is associated with weak diabatic heating at 1.5°N in the eastward QBO. These results are in agreement with Flury et al. (2013) who showed that variability in the BDC depends on the phase of the QBO, with enhanced (reduced) vertical speeds in case of westward (eastward) QBO. The fact that PC4CI and PC1PV600K have a lower correlation might be due to the fact that while PC1PV600K represented the effect of the QBO on PV mixing, PC4CI represents the effect of the QBO on the BDC.

Section summary

Together, the first four eigenvalues resulting from applying PCA to the climate indices account for 75.6% of the total variance. The leading eigenvector (EOF1CI, 30.3%) clearly represents stratospheric variability, specifically the stratospheric polar vortex. These results confirm, not only that the PV600K index (PV600I) is an obvious measure of the polar vortex strength, but that PC2PV600K (section 4.2) also is. This is confirmed by the strong correlation between PC1CI and PV600I with the NAMI at 20 hPa (table 3), as well as with PC1CI and PC2PV600K with a correlation coefficient of 0.85 at lag 0.

The second eigenvector (EOF2CI, 22.9%) represents tropical variability. The time series associated with this eigenvector (PC2CI) is mainly associated with the PV350I, the SOI, the HC strength, tropical precipitation and to a less extent, the strength of subtropical jet (U350I) but with a strong correlation with PC2U350K which might reflect an equatorward shift of the subtropical jet. These results were already found in section 4.3, and the same conclusions regarding PC2PV350K apply to PC2CI: below average PV in the tropics is mainly associated with the El Niño, a maximum in tropical precipitation and a stronger HC. Further insight can be taken with respect to EOF1CrIs350K and associated time series (PC1CrIs350K, section 4.3) which shows a correlation of 0.71 with CrIs350I implying that they represent the same phenomenon (recall that positive values of PC1CrIs350K were associated with enhanced diabatic heating at the equator).

The third eigenvector (EOF3CI, 13.3%) represents mainly variability in the tropics/subtropics and midlatitudes. The associated time series (PC3CI) is clearly associated with the surface NAM and the tropospheric jet: the positive phase of the NAM is associated with a weak subtropical jet and to a less extent above average precipitation in the tropics, with the opposite for the negative phase of the NAM. Again the relationship between the El Niño, a stronger Hadley cell and increased precipitation is seen (figure **4.4.17** and **4.4.18**).

The forth eigenvector (EOF4, 9.3%) and less straight forward to interpret, represents changes in the cross isentropic flow on the 600K isentropic surface. The associated time series (PC4CI) appears to relate the strength of the BDC with the effect of the QBO on the equatorial diabatic heating. According to the results, a stronger BDC is seen in the westward phase of the QBO, while a weak BDC occurs in the QBO eastward.

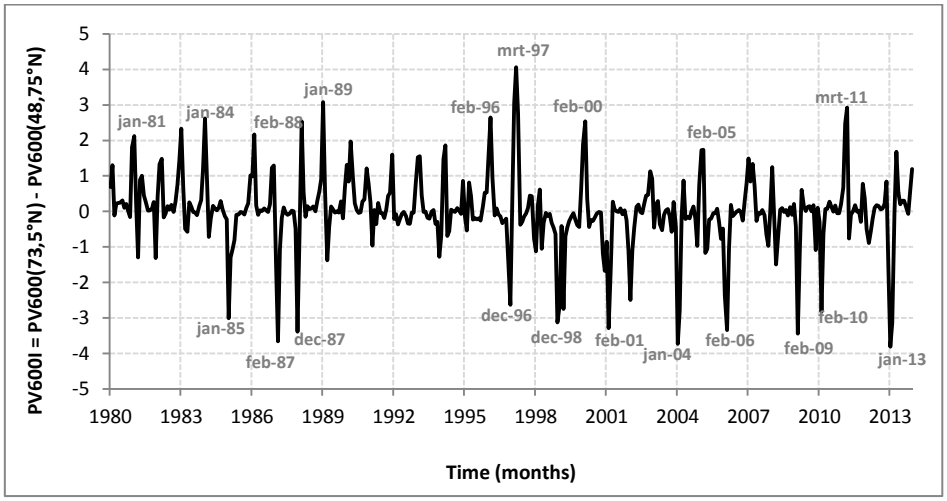

Figure 4.4.1 Time series of the PV600K index (PV600I) which is defined as the difference between the PV anomaly field (with seasonal cycle filtered out and normalized) on the 600 K isentropic surface at 73.5°N and 48.75°N (PV350I=PV(73.5°N)–PV(48.75°N).

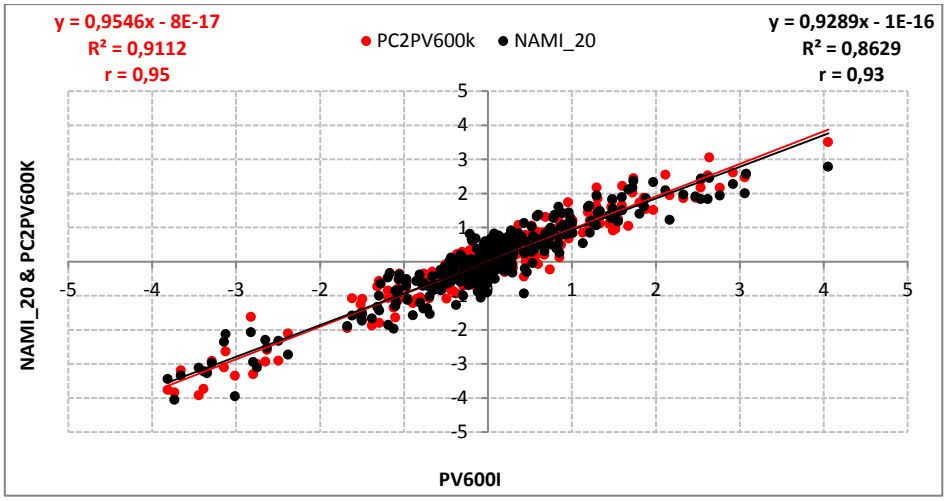

Figure 4.4.2 Correlation between the PV index at 600K (PV600I) and the NAM index defined at 20 hPa (NAMII_20, black circles, r = 0.93) and with PC2 of PV600K (PC2PV600K, red circles, r = 0.95).

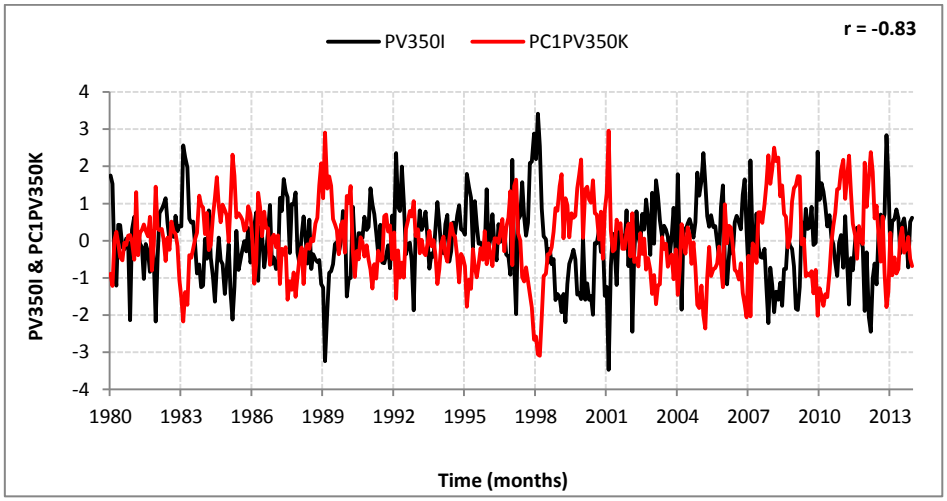

Figure 4.4.3 Time series of the PV350K index (PV350I) which is defined as the difference between the PV anomaly field (with seasonal cycle filtered out and normalized) on the 350 K

isentropic surface at 34.5°N and 15°N (PV350I=PV350(34°N)–PV350(15°N) and PC1PV350K (section 4.3). The correlation coefficient between the two time series is -0.83 at lag 0.

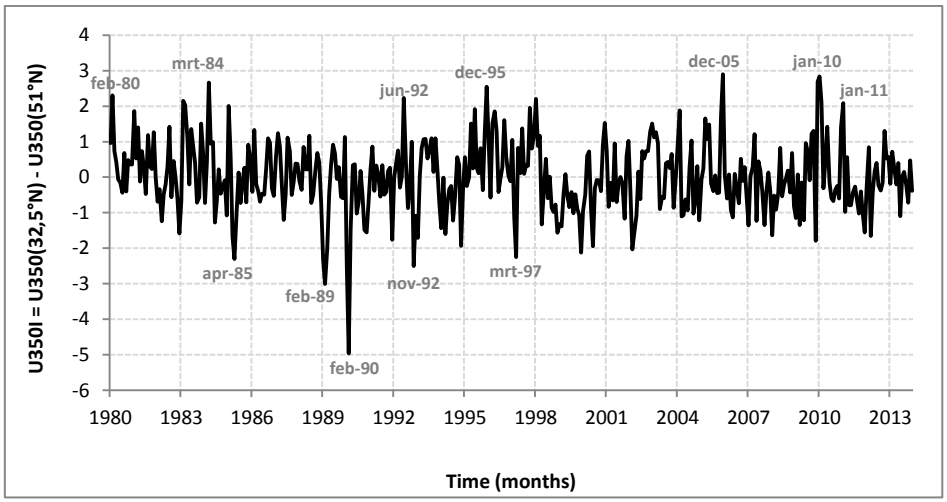

Figure 4.4.4 Time series of the zonal wind index on the 350K isentrope (U350I) which is defined as the difference between the zonal wind (U) anomaly field (with seasonal cycle filtered out and normalized) on the 350 K isentropic surface at 32.5°N and 51°N N (U350I=U350(32.5°N)-U350(51°N)).

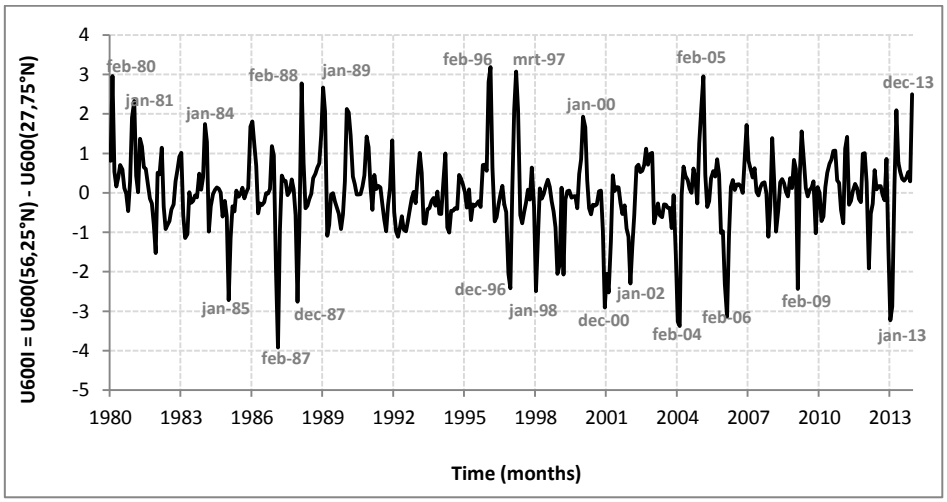

Figure 4.4.5 Time series of the zonal wind index on the 600K isentrope (U600I) which is defined as the difference between the zonal wind (U) anomaly field (with seasonal cycle filtered out and normalized) on the 600 K isentropic surface at 56.25°N and 27.75°N (U600I=U600(56.25°N)-U600(27.75°N)).

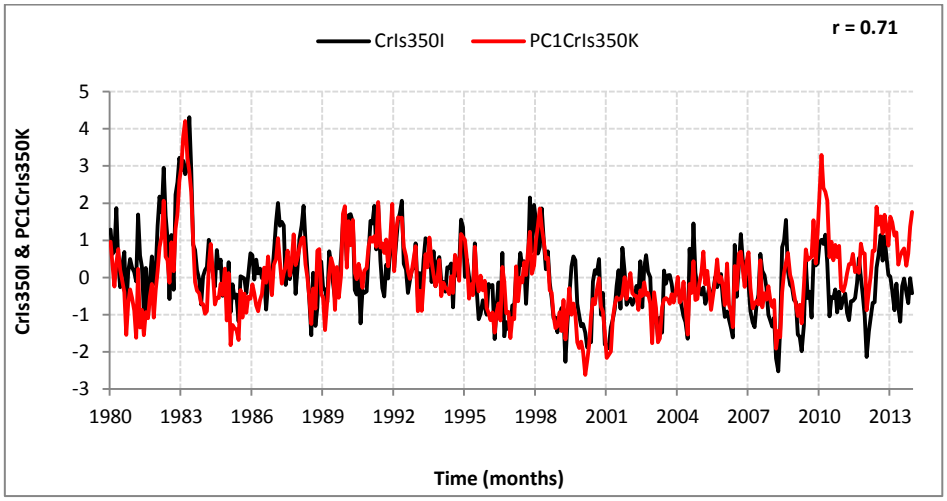

Figure 4.4.6 Time series of the CrIs350K index (CrIs350I) which is defined as the difference between the cross isentropic flow (CrIs) anomaly (with seasonal cycle filtered out and normalized) on the 350 K isentropic surface at 0° and 13.5°N (CrIs350I=CrIs350(0°) – CrIs350(13.5°N), black line) and PC1CrIs350K (red line, section 4.3, **figures 4.3.9** and **4.3.10**). The correlation between the two time series is 0.71 at lag 0.

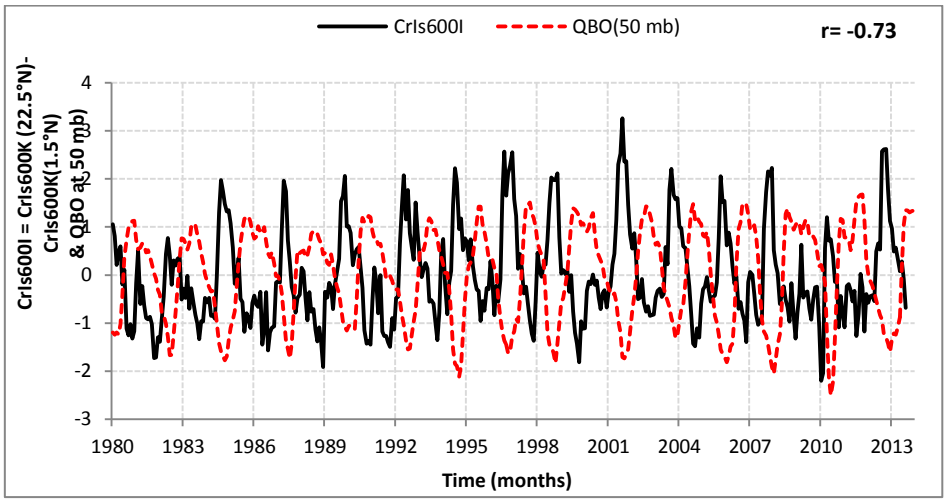

Figure 4.4.7 Time series of the CrIs600K index (CrIs600I) which is defined as the difference between the cross isentropic flow (CrIs) anomaly (with seasonal cycle filtered out and normalized) on the 600 K isentropic surface at 22.5°N and 1.5°N. Also plotted is the time series of the QBO at 50 mb. The maximum correlation between the two time series is -0.73 where the QBO leads by 4 months. At lag 0 the correlation coefficient is r=-0.35.

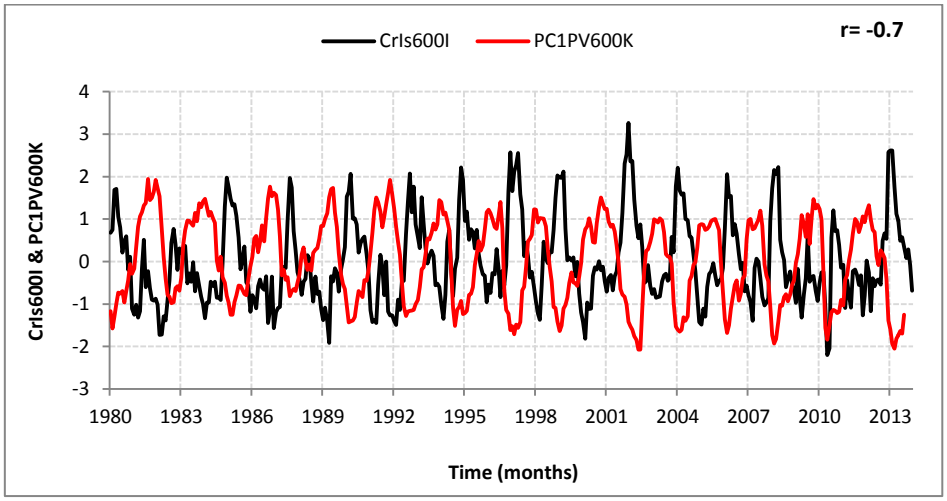

Figure 4.4.8 Time series of the CrIs600K index (CrIs600I) which is defined as the difference between the cross isentropic flow (CrIs) anomaly (with seasonal cycle filtered out and normalized) on the 600K isentropic surface at 22.5°N and 1.5°N. Also plotted is the time series of the principal component of PV on the 600K isentrope (PC1PV600K, see section 4.2). The correlation between the two time series is -0.7 where the CrIs600I leads by 4 months. At lag zero the correlation coefficient is r=-0.39.

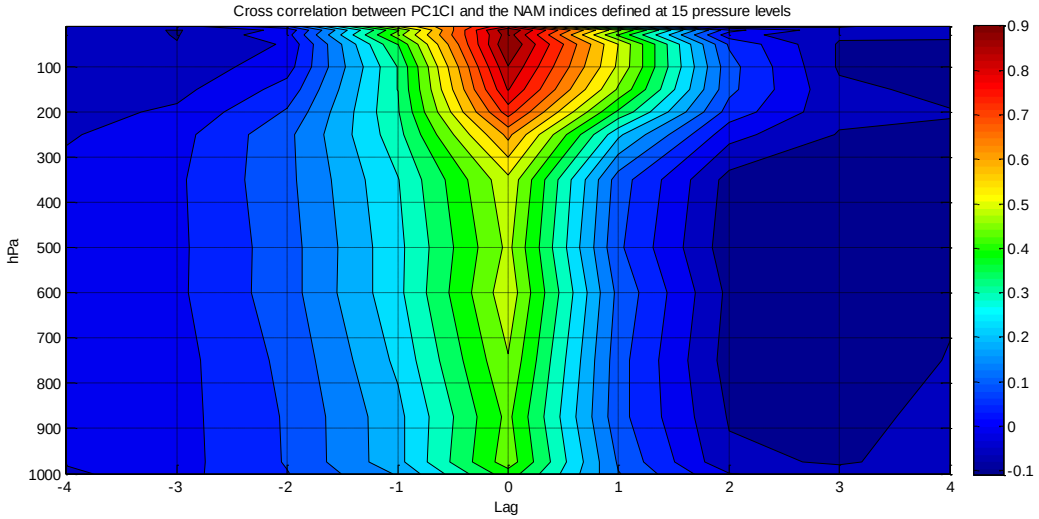

Figure 4.4.9 Cross correlation between the first principal component resulting from the PCA applied to the climate indices (PC1CI) and the NAM indices defined at 15 different pressure levels. Negative (positive) lag means NAM leads (lags). Lag in months.

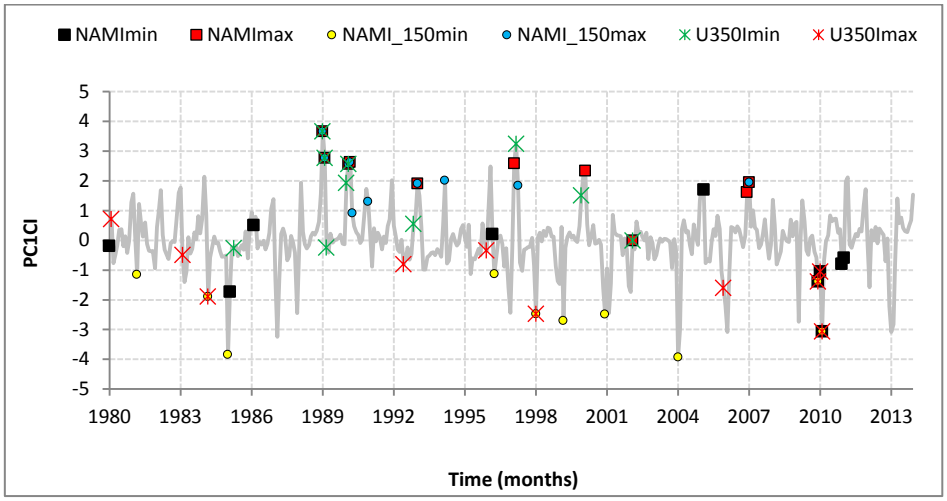

Figure 4.4.10 Top ten maxima and minima values of the NAM indices (at lag 0) defined at the surface (NAMI) and at 150 hPa (NAMI_150) as well as the zonal wind index on the 350 K isentropic surface(U350I) associated with the first principal component resulting from PCA applied to the climate indices (PC1CI, grey line). See also **figure 4.4.11** for completeness.

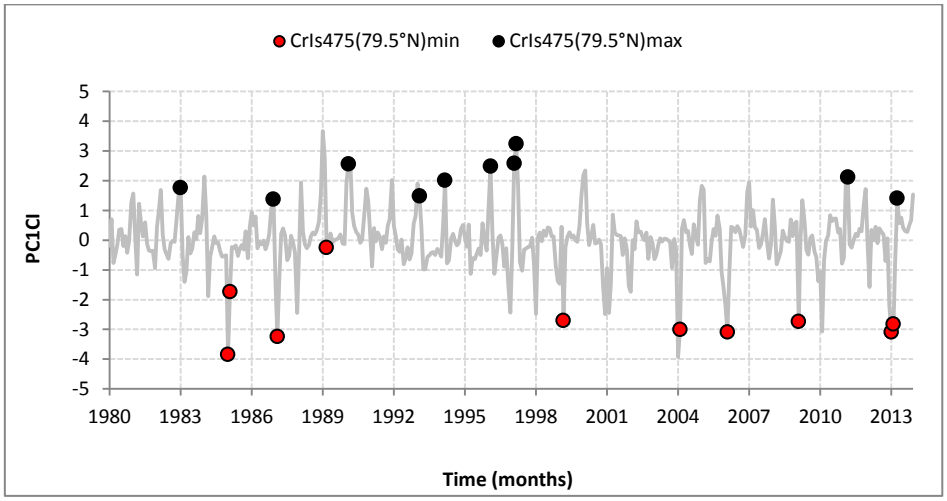

Figure 4.4.11 Top ten maxima and minima values of the cross isentropic flow on the 475 K isentropic surface (CrIs475K at lag 0) associated with the first principal component resulting from PCA applied to the climate indices (PC1CI, grey line).

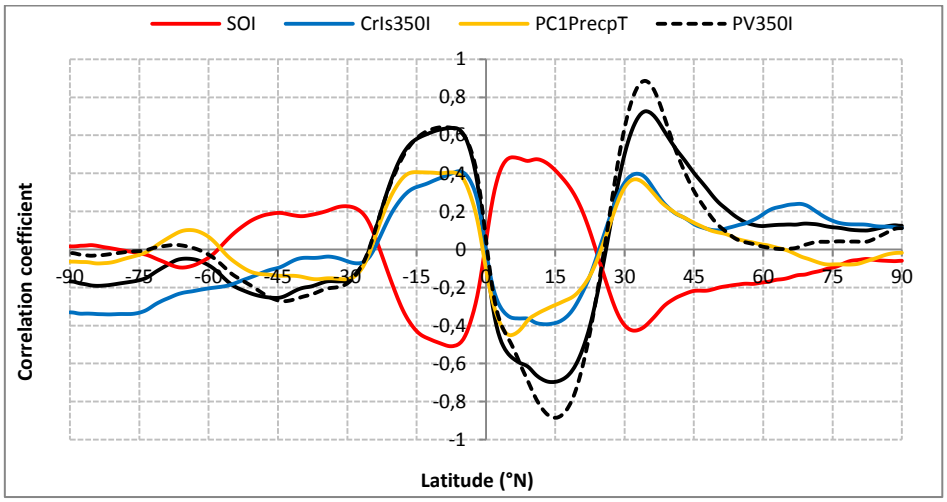

Figure 4.4.12 Regression of PC2CI (black solid line), the SOI, the cross isentropic flow index on the 350K (CrIs350I), tropical precipitation as found in section 4.2 (PC1PrecpT) the PV

index on the 350K isentrope (PV350I) upon the PV anomaly (with respect to the climatology and further divided by the standard deviation) field on the 350 K isentropic surface.

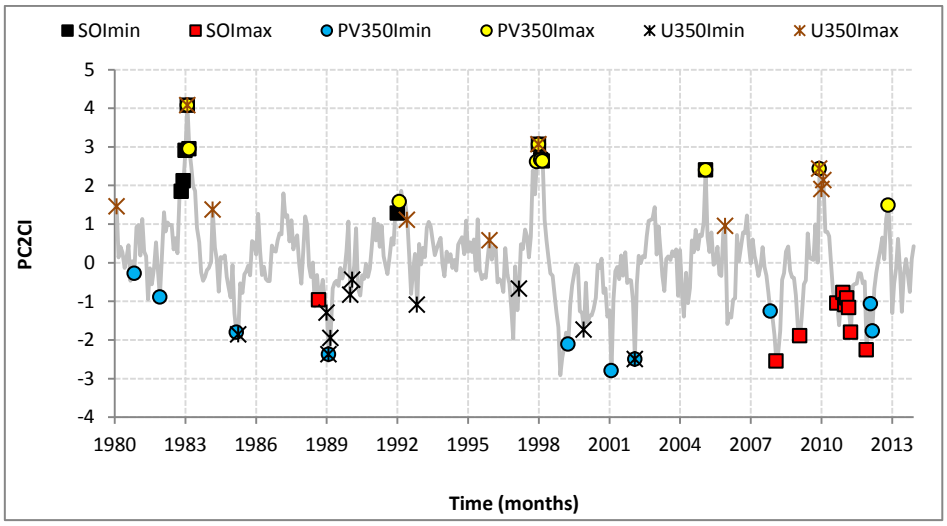

Figure 4.4.13 Top ten maxima and minima values of the SOI, the PV index on the 350K isentrope (PV350I) and the zonal wind index on the 350K isentrope (U350I) associated with the second principal component resulting from PCA applied to the climate indices (PC2CI, grey line).

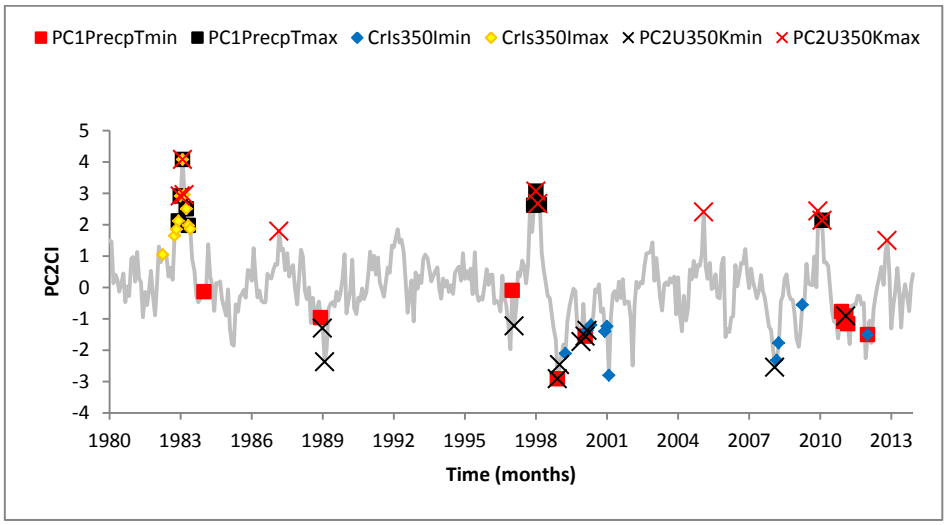

Figure 4.4.14 Top ten maxima and minima values of the first principal component of tropical precipitation (PC1PrecpT found in section 4.2) and the cross isentropic flow index on the 350K isentrope (CrIs350I) associated with the second principal component resulting from PCA applied to the climate indices (PC2CI, grey line).

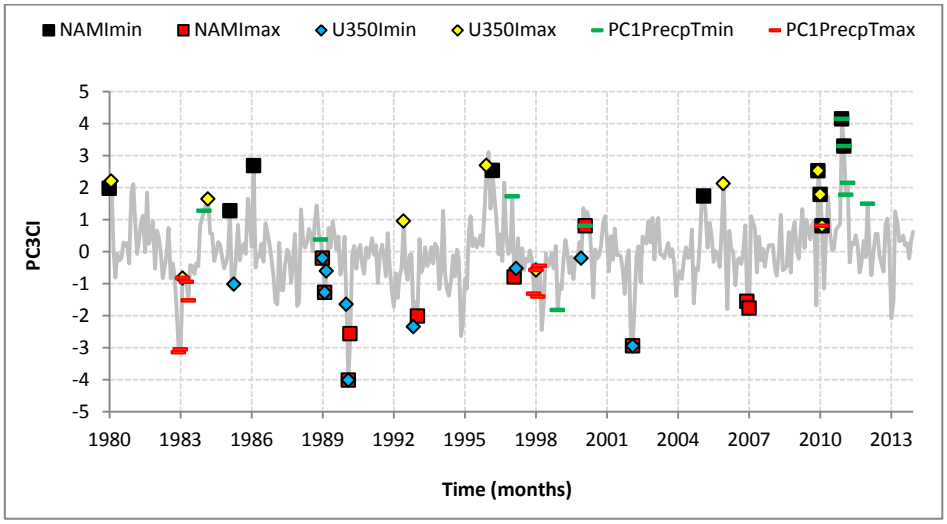

Figure 4.4.15 Top ten maxima and minima values of the NAM index defined at the surface (NAMI), the zonal wind index on the 350K isentropic surface (U350I) and the first principal component of tropical precipitation (PC1PrecpT found in section 4.2) associated with the third principal component resulting from PCA applied to the climate indices (PC3CI, grey line).

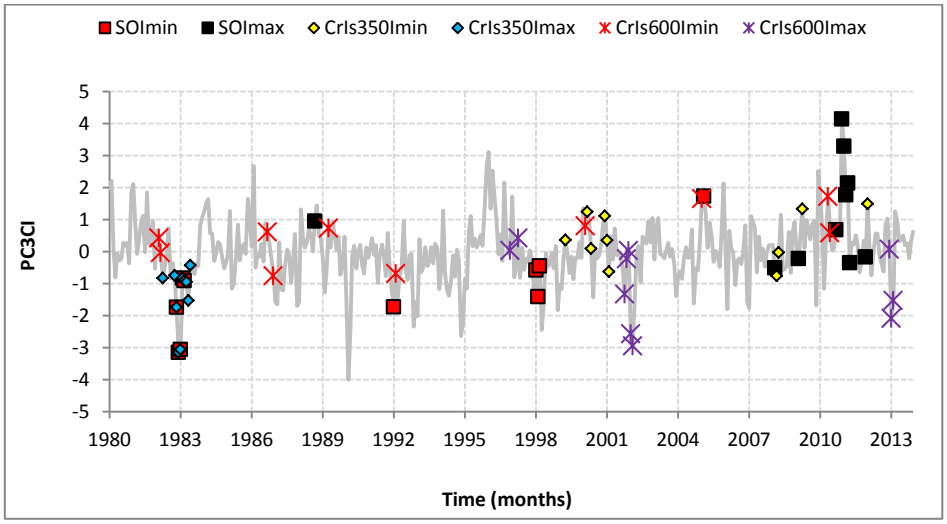

Figure 4.4.16 Top ten maxima and minima values of the SOI, the cross isentropic flow index on the 350K isentropic surface (CrIs350I) , the cross isentropic flow index on the 600K isentropic surface (CrIs600I) associated with the third principal component resulting from PCA applied to the climate indices (PC3CI, grey line).

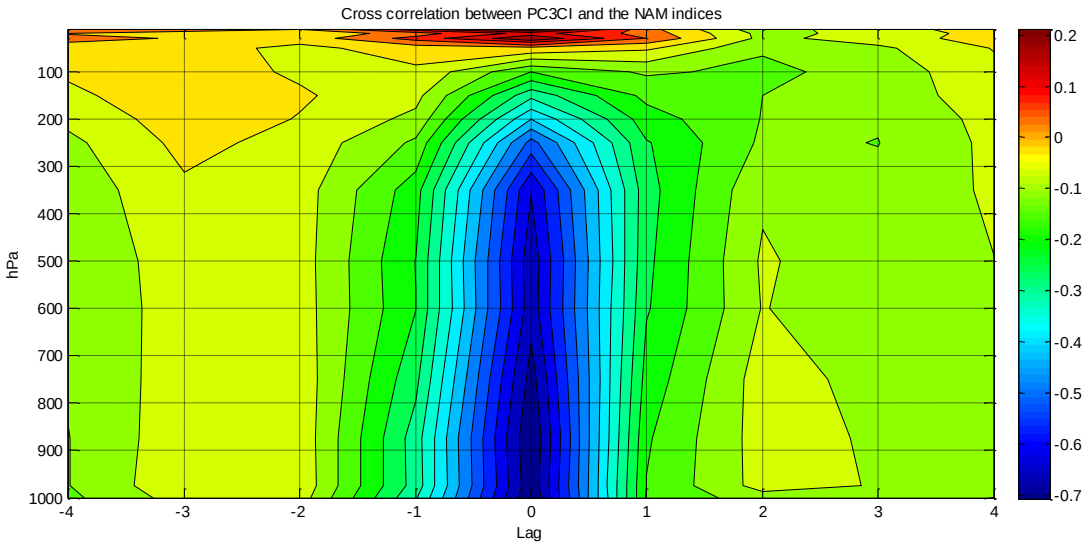

Figure 4.4.17 Cross correlation between the third principal component resulting from the PCA applied to the climate indices (PC1CI) and the NAM indices defined at 15 different pressure levels. Negative (positive) lag means NAM leads (lags). Lag in months.

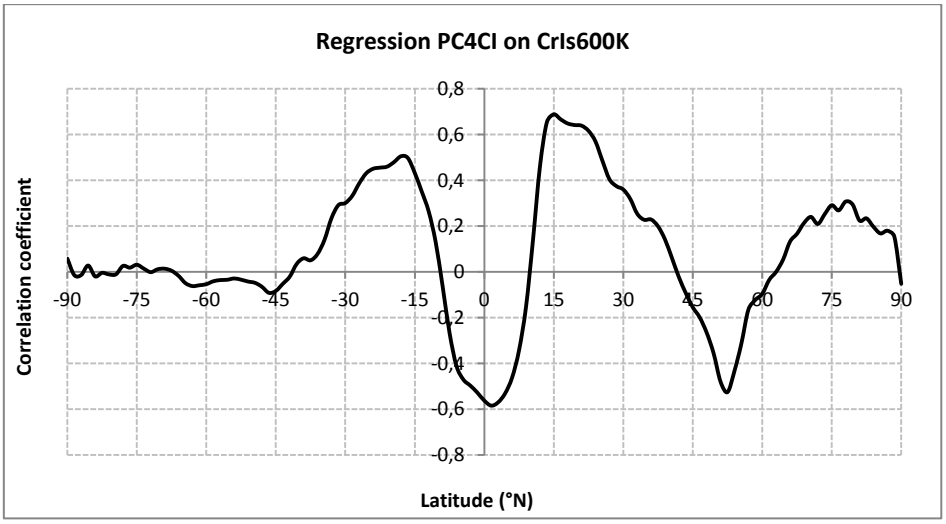

Figure 4.4.18 Regression of the cross isentropic flow anomalies (with seasonal cycle filtered out and normalized) on the 600 K isentropic surface upon the forth standardized principal components (PC4CI).

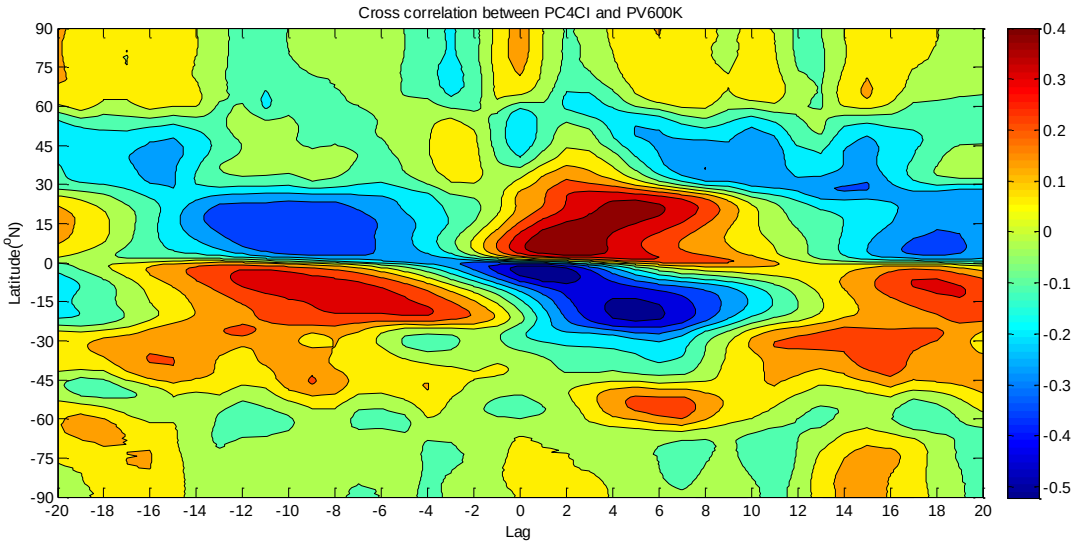

Figure 4.4.19 Cross correlation between the forth principal component resulting from the PCA applied to the climate indices (PC4CI) and the PV anomaly field (with seasonal cycle filtered out and normalized) on the 600 K isentropic surface. Negative (positive) lag means PC4CI leads (lags). Lag in months.

Table 3 Definition of the climate indices for potential vorticity and cross isentropic on the 600K (respectively PV600I and CrIs600I) and potential vorticity, zonal wind and cross isentropic flow on the 350K (respectively PV350I, U350I and CrIs350I) as well as the NAM index defined at the surface(NAMI), in accord with Li and Wang (2003).

	Correlation coefficient	Latitudes	Indices
PV600I	r = -0.82	48°N and 73.5°N	**PV600I=PV600(73.5°N) - PV600(48°N)**
PV350I	r = -0.57	15°N and 34.5°N	**PV350I=PV350(34°N) - PV350(15°N)**
U350I	r = -0.70	32.25°N and 51°N	**U350I=U350(32.25°N) - U350(51°N)**
U600I	r = -0.56	27.75N and 56.25N	**U600I= U600(56.25°N) - U350(27.75°N)**
CrIs350I	r = -0.59	0° and 13.5°N	**CrIs350I=CrIs350(0°) - CrIs350(13.5°N)**
CrIs600I	r = - 0.66	1.5°N and 22.5°N	**CrIs600I=CrIs600(22.5°N) - CrIs600(1.5°N)**
CrIs600BD	r = - 0.3	13.5°N and 52.5°N	**CrIs600I=CrIs600(13.5°N) - CrIs600(52.5°N)**
NAMI	r = -0.59	26.25°N and 63.75°N	**NAMI=MSLP(26.25°N) - MSLP(63.75°N)**

Table 4 Correlations between the climate indices. Values in bold are different from 0 with a significance level α=0.05.

Variables	NAMI	NAMI_150	NAMI_20	SOI	PV350I	PV600I	U350I	U600I	CrIs350I	CrIs600I	Cr600IBD	PC1PrecpT
NAMI	**1**	**0,50**	**0,18**	-0,02	**-0,27**	**0,12**	**-0,54**	**0,12**	0,04	0,03	-0,09	0,04
NAMI_150	**0,50**	**1**	**0,64**	**0,10**	**-0,10**	**0,57**	**-0,59**	**0,57**	-0,02	-0,03	**-0,32**	**-0,11**
NAMI_20	**0,18**	**0,64**	**1**	-0,07	**0,14**	**0,93**	**-0,19**	**0,88**	**0,14**	**-0,27**	**-0,15**	-0,04
SOI	-0,02	**0,10**	-0,07	**1**	**-0,47**	-0,06	**-0,17**	0,04	**-0,47**	0,03	-0,09	**-0,54**
PV350I	**-0,27**	**-0,10**	**0,14**	**-0,47**	**1**	**0,14**	**0,42**	0,08	**0,40**	**-0,11**	0,05	**0,46**
PV600I	**0,12**	**0,57**	**0,93**	-0,06	**0,14**	**1**	**-0,12**	**0,86**	**0,14**	**-0,24**	**-0,16**	-0,05
U350I	**-0,54**	**-0,59**	**-0,19**	**-0,17**	**0,42**	**-0,12**	**1**	**-0,23**	0,10	**-0,13**	**0,16**	**0,21**
U600I	**0,12**	**0,57**	**0,88**	0,04	0,08	**0,86**	**-0,23**	**1**	0,06	**-0,22**	**-0,19**	**-0,11**
CrIs350I	0,04	-0,02	**0,14**	**-0,47**	**0,40**	**0,14**	0,10	0,06	**1**	**-0,14**	0,09	**0,63**
CrIs600I	0,03	-0,03	**-0,27**	0,03	**-0,11**	**-0,24**	**-0,13**	**-0,22**	**-0,14**	**1**	**0,25**	-0,10
Cr600IBD	-0,09	**-0,32**	**-0,15**	-0,09	0,05	**-0,16**	**0,16**	**-0,19**	0,09	**0,25**	**1**	0,01
PC1PrecpT	0,04	**-0,11**	-0,04	**-0,54**	**0,47**	-0,05	**0,21**	**-0,11**	**0,63**	-0,10	0,01	**1**

Table 5 First four eigenvectors (total of 75.5% of the total variance) resulting from PCA applied to the climate indices: NAM index at the surface (NAMI), NAM index at 150 hPa (NAMI_150), NAM index at 20 hPa (NAMI_20), the Southern Oscillation Index (SOI), PV index on the 350K (PV350I) and on the 600K (PV600I) isentropic surfaces, the cross isentropic flow index on the 350K (CrIs350I) and on the 600K isentropic surfaces, including the equator (CrIs600I) and excluding the equator (CrIs600IBD). In total the four eigenvectors represent 75.5% of the total variance.

Eigenvectors:				
	EOF1(30%)	**EOF2(22.9%)**	**EOF3(13.3%)**	**EOF4(9.3%)**
NAMI	0,217	-0,132	-0,560	-0,062
NAMI_150	0,437	-0,093	-0,220	-0,005
NAMI_20	0,475	0,148	0,160	0,160
SOI	0,037	-0,431	0,262	-0,070
PV350I	-0,030	0,472	0,107	0,067
PV600I	0,455	0,154	0,209	0,168
U350I	-0,252	0,286	0,439	0,007
U600I	0,458	0,087	0,209	0,145
CrIs350I	0,025	0,443	-0,282	-0,010
CrIs600I	-0,132	-0,168	-0,253	0,596
Cr600IBD	-0,176	0,052	-0,027	0,731
PC1PrecpT	-0,072	0,451	-0,329	-0,150

Table 6 Correlation between the time series associated with the first four eigenvectors (PC1CI, PC2CI, PC3CI, PC4CI, respectively) with each of the indices defined in table 2. For instance, the correlation between PC1CI and the NAM index defined at 20 hPa (NAMI_20) is equal to 0.905.

Correlations between variables and Principal Components (PCs):				
	PC1CI	**PC2CI**	**PC3CI**	**PC4CI**
NAMI	0.413	-0.219	-0.706	-0.065
NAMI_150	0.833	-0.153	-0.278	-0.005
NAMI_20	0.905	0.245	0.202	0.169
SOI	0.070	-0.714	0.331	-0.074
PV350I	-0.057	0.782	0.136	0.071
PV600I	0.867	0.255	0.264	0.178
U350I	-0.481	0.474	0.555	0.007
U600I	0.874	0.144	0.264	0.153
CrIs350I	0.047	0.733	-0.356	-0.011
CrIs600I	-0.252	-0.279	-0.319	0.630
Cr600IBD	-0.335	0.087	-0.034	0.772
PC1PrecpT	-0.138	0.746	-0.416	-0.159

5 CONCLUSIONS

Principal component analysis (PCA) was extensively used in this study to describe and analyze potential vorticity (PV) variability in the Overworld and in the Middleworld and its association with main modes of climate variability. Special attention was given to the annular modes (AMs), the quasi-biennial oscillation (QBO) and the Hadley cell (HC) due to their role, respectively, in the extratropics throughout the troposphere and stratosphere, tropical stratosphere and tropical upper troposphere. These modes of variability were clearly captured by the PV distribution on the 600 K and 350 K isentropic surfaces which belong, respectively, to the Overworld and to the Middleworld.

In the Overworld, the three main modes of stratospheric variability, the QBO, the stratospheric Northern annular mode (NAM) and the stratospheric Southern annular mode (SAM) were clearly captured. The mechanism by which the QBO induces changes in the PV field is proposed in this thesis to be due to the secondary meridional circulation (SMC). The SMC predicts that at the level of maximum westward winds, air diverges poleward, while at the level of maximum eastward winds, air converges equatorward. This divergence and convergence of air must in turn be associated with vertical motions (cross isentropic flow). The hypothesis is that this divergence of air must lead to dilution of potential vorticity substance (PVS) while the air convergence to a concentration of PVS, due to the impermeability theorem. Thus, at the level of maximum winds, PV values decrease in the westward QBO and increase in the QBO eastward, in accord with the results found in this thesis.

PV on the 600 K also proved to be an important tool for the study of the dynamics of the stratospheric polar vortices in both hemispheres. The stratospheric AMs, the NAM in the Northern hemisphere (NH) and the SAM in the Southern hemisphere (SH), can thus be analyzed in terms of PV distribution, which allows a better understanding of the processes associated with weak and strong polar vortices events. The results of this study showed that a weak polar vortex (negative stratospheric NAM index) is represented by negative PV anomalies at polar latitudes associated with positive ones at midlatitudes, hence mixing of PV due to Rossby wave breaking (RWB) associated with strong wave activity. The opposite is true for cases when the polar vortex is strong. The above conclusions, with respect to the NH, can be taken whether principal component analysis (PCA) is applied to full domain of PV or by calculating a PV index following the method of Li and Wang (2003).

The results associated with the Middleworld, i.e., on the 350 K isentropic surface, showed clearly variability in the tropical upper troposphere and in the lowermost stratosphere in the extratropics of both hemispheres.

In the tropical upper troposphere, during El Niño events, there is enhanced diabatic heating due to above average tropical precipitation which intensifies the HC and the subtropical jet which appears to shift equatorward under these conditions. In this situation, PV is below average in the tropics. It is argue that these PV anomalies are a result of dilution of PVS in the horizontal branches of the HC since a strong subtropical jet and associated strong PV gradients should lead to weak mixing in the tropics. On the other hand, during La Niña events, the HC and the subtropical jet are weak. In this case, RW may break in the tropics leading to above average PV there. Therefore one may argue that in the tropical upper troposphere PV transport is mainly due to both along isentropes and cross isentropic flow. In the same way as for the stratospheric AMs, upper tropospheric tropical variability in the NH is captured whether PCA is applied to the full domain of PV on the 350 K or if a PV index on this isentropic surface is constructed using again the method of Li and Wang (2003).

The results of the stratospheric part of the Middleworld, thus the lowermost stratosphere are not straightforward to interpret. In the NH, negative PV anomalies in the Overworld (negative phase of the stratospheric NAM) are clearly associated with PV anomalies of the same sign in the lowermost stratosphere and enhanced diabatic cooling on the 475 K isentrope (when the stratospheric NAM and cross isentropic flow lead by one month). In general the negative stratospheric NAM has no connection with the tropospheric one except for January/February 1985 where NAM anomalies in the stratosphere are also seen at the surface. The winter of 1985 was marked by a major sudden stratospheric warmings (SSW) in the NH in the beginning of January. During strong vortex events, on the other hand, NAM anomalies appear throughout the troposphere until about 50 hPa. In this case, the cross isentropic flow on the 475 K appears not to play a significant role. These results suggest that the PV anomalies in the lowermost stratosphere may play a role in the connection between the stratosphere and the troposphere or the other way around.

With respect to the extratropics in the SH the results were unclear. Although there is a connection between the cross isentropic flow on the 600 K isentrope and the lowermost stratospheric PV anomalies, no definite conclusions could be taken. It is interesting to notice that the same difficulty in the interpretation of the results arose for the lowermost stratosphere of both hemispheres. The fact that in the NH the NAM was captured may be related to stronger wave activity here which could lead to stronger variability of the NAM compared to the SAM in the SH.

Overall, the results associated with the NH are clearer than the ones associated with the SH, mainly with respect to the stratospheric part of the Middleworld. This could be related to the fact that the maximum in anticorrelation and associated latitudes for the 350 K and 600 K isentropes were calculated for the NH, thus from 10.5°N until 90°N. In fact, if the same method is applied to find the isentropic surfaces with the highest anticorrelation in the SH, the choice had to be the 330 K and the 850 K (see figure in Appendix, section 7.3). Nevertheless, the results of the Overworld and tropical upper troposphere of the Middleworld of both hemispheres clearly showed the advantages of using PV as a diagnostic tool. The fact that the results of the stratospheric part of the Middleworld were not clear should not be taken as a down point but as a starting point for further investigation. Further insight about the dynamics of this fascinating region of the Middleworld may provide valuable information about the extratropical stratosphere and troposphere connection which in turn may be related with the annular modes. According to the results of this project, it appears that indeed PV variability in the NH lowermost stratosphere, in conjunction with the polar stratosphere-troposphere connection in terms of the annular modes and PV variability.

6 REFERENCES

Ambaum M. H. P. and B. J. Hoskins, 2002: The NAO Troposphere-Stratosphere Connection, *American Meteorological Society*.

Baldwin M. P. and D. W.J. Thompson, 2009: A critical comparison of stratosphere-troposphere coupling indices, *Q. J. R. Meteorol. Soc.* **135**: 1661-1672.

Baldwin M. P. and T. J. Dunkerton, 1998: Biennial, quasi-biennial, and decadal oscillations of potential vorticity in the northern stratosphere, *Journal of Geophysical Research*, Vol. 103, NO. D4, Pages 3919-3928.

Baldwin M. P. and T. J. Dunkerton, 1998: Quasi-biennial modulation of the southern hemisphere polar vortex, Geophysical Research Letters, Vol. 25, NO. 17, 3343-3346.

Baldwin M. P. and T. J. Dunkerton, 2001: Stratospheric Harbingers of Anomalous Weather Regimes, *Science*, Vol. 294.

Baldwin M. P., 2001: Annular modes in global daily surface pressure, *Geophysical Research Letters*, Vol. 28, NO. 21, 4115-4118.

Baldwin M. P., D. B. Stephenson and I. T. Jolliffe, 2008: Spatial Weighting and Iterative Projection Methods for EOFs, *Journal of Climate*, Volume 22.

Baldwin M. P., L.J. Gray, T. J. Dunkerton, K. Hamilton, P. H. Haynes, W. J. Randel, J. R. Holton, M. J. Alexander, I. Hirota, T. Horinouchi, D. B. A. Jones, J. S. Kinnersley, C. Marquard, K. Sato, and M. Takahashi, 2001: The Quasi-Biennial Oscillation, *Reviews of Geophysics*, 39, pages 179-229.

Baldwin, M. P., and T. J. Dunkerton, 1999: Propagation of the Arctic oscillation from the stratosphere to the troposphere, *Journal of Geophysical Research*, Vol. 104, NO. D24, Pages 30,937-30,946.

Björnsson H. and S. A. Venegas: A Manual for EOF and SVD analysis of Climatic Data, Department of Atmospheric and Oceanic Sciences and Center for Climate and Global Change Research, McGill University.

Black, R. X. and B. McDaniel, 2009: Submonthly polar vortex variability and stratosphere-troposphere coupling in the Artic, *J. Climate*, 22, 5886-5901.

Charlton, A. J. and L. M. Polvani, 2006: A New Look at Stratospheric Sudden Warmings. Part I: Climatology and Modeling Benchmarks, *American Meteorological Society*.

Dessler, A. E., E. J. Hintsa, E. M. Weinstock, J. G. Anderson and K. R. Chan, 1995: Mechanisms controlling water vapor in the lower stratosphere: “A tale of two stratospheres”, *Journal of Geophysical Research*, Vol. 100, NO. D11, 23,167-23,172.

Dunkerton, T. J., 1997: The role of gravity waves in the quasi-biennial oscillation, *Journal of Geophysical Research*, 102, 26,053-26,076.

Eichelberger S. J. and D. L. Hartmann, 2007: Zonal jet structure and the leading mode of variability, *Journal of Climate*, Vol. 20, 5149-5163.

Feldstein, S. B., C. Franzke, 2006: Are the north atlantic oscillation and the northern annular mode distinguishable?, *Journal of Atmospheric Sciences*, Vol. 63, 2915-2930.

Flury T., D. L. Wu and W. G. Read, 2013: Variability in the speed of the Brewer-Dobson circulation as observed by Aura/MLS, *Atmos. Chem. Phys.*, 13, 4563-4575.

Hamilton, K., 1988: Intermispheric asymmetry and annual synchronization of the ozone quasi-biennial oscillation, *Geophysical Fluid Dynamics Laboratory*, Princeton University, New Jersey, 1019.

Hannachi, A., I. T. Jolliffe, and D. B. Stephenson, 2007: Empirical orthogonal functions and related techniques in atmospheric sciences: A review, *Int. J. Climatol.* **27**: 1119 – 1152.

Hartmann D. L., 2007: The Atmospheric General Circulation and Its Variability, *Journal of the Meteorological Society of Japan,* Vol. 85B, pp. 123-143.

Hartmann D. L., J. M. Wallace, V. Limpasuvan, D. W. J. Thompson and J. R. Holton, 2000: Can ozone depletion and global warming interact to produce rapid climate change?, *Proceedings of the National Academy of Science of the United States of America*, Vol. 97, No. 4, 1412-1417.

Haynes, P. H. and M. E. McIntyre, 1987: On the evolution of vorticity and potential vorticity in the presence of diabatic heating and frictional or other forces, *Journal of the Atmospheric Science*s, Vol. 44, No. 5, 828-840.

Haynes, P. H., 2005: Stratospheric dynamics*, Annual Review of Fluid Mechanics*, 37, 263-293.

Holton, J. R., and R. S. Lindzen, 1972: An updated theory for the quasi-biennial cycle of the tropical stratosphere, *Journal of Atmospheric Sciences*, 29, 1076-1080.

Holton, J. R., P. H. Haynes, M. E. McIntyre, A. R. Douglass, R.B. Rood, L. Pfister, 1995: Stratosphere-troposphere exchange, *Reviews of Geophysics*, 33, 403-439.

Hoskins, B. J., 1991: Towards a PV-θ view of the general circulation, *Tellus*, 43AB, 27-35.

Hurrel, J. W., 1995: Decadal trends in the North Atlantic oscillation: Regional temperatures and precipitation, *Science*, 269, 676-679.

Kushner, P. J., 2010: Annular modes of the troposphere and stratosphere, in The stratosphere: Dynamics, transport and chemistry (eds L. M. Polvani, A H. Sobel and D. W. Waugh), American Geophysical Union, doi: 10.1002/9781118666630.ch4.

Li, J. and J. X. L. Wang, 2003: A modified zonal index and its physical sense, *Geophys. Res. Lett*., 30, NO.12, 1632.

Lindzen, R.S., and J. R. Holton, 1968: A theory of the quasi-biennial oscillation, *Journal of Atmospheric Sciences*, 25, 1095-1107.

Lorenz D. J. and D. L. Hartmann, 2002: Eddy-zonal flow feedback in the Northern Hemisphere Winter, Journal of Climate, Vol. 16.

Lorenz, E. N., 1956: Empirical orthogonal functions and statistical weather prediction, *Scientific Report No. 1, Statistical Forecasting Project*, MIT, Cambridge.

Manney, G . L., R. W. Zurek, A. O'Neill and R. Swinbank, 1994: On the motion of air through the stratospheric polar vortex, *Journal of Atmospheric Sciences*, 51, 2973-2994.

McIntyre M. E. and T. N. Palmer, 1984: The 'surf zone' in the stratosphere, *Journal of Atmospheric and Terrestrial Physics*, Vol. 46, No. 9, 825-849.

McIntyre, M. E., 1981: How well do we understand the dynamics of stratospheric warmings?, *Journal of the Meteorological Society of Japan*, Vol. 60, No.1, 37-64.

Mohanakumar, S., 2008: Stratosphere troposphere interactions: An introduction, *Springer*, ISBN 978-1-4020-8216-0.

Moore, J. T., 1989: Isentropic analysis and interpretation, Air Weather Service (MAC), Scott Air Force Base, Illinois, 62225-5008.

Nguyen, H., A. Evans, C. Lucas, I. Smith, B. Timbal, 2013: The Hadley circulation in reanalysis: climatology, variability, and change, Journal of Climate, Vol. 26, 3357-3375

Oort, A.H., J. J. Yienger, 1996: Observed interannual variability in the Hadley circulation and its connection with ENSO, *Journal of Climate*, Vol. 9, 2751-2767.

Plumb, R. A., 2002: Stratospheric transport, *J. Meteor. Soc. Japan*, 80, 793-809.

Plumb, R. A., and J. D. Mahlman, 1987: The zonally averaged transport characteristics of the GFDL general circulation/transport model, *Journal of the Atmospheric Sciences*, Vol. 44, No.2, 298-327.

Plunge H. J., P. Konopka, M. A. Giorgetta and R. Müller, 2009: Effects of the quasi-biennial oscillation on low-latitude transport in the stratosphere derived from trajectory calculations.

Pommrich R., R. Müller, J. -U. Grooβ, P. Konopka, F. Ploeger, B. Vogel, M. Tao, C. M. Hoppe, G. Günther, N. Spelten, L. Hoffmann, H. –C. Pumphrey, S. Viciani, F. D. D'Amato, C. M. Volk, P. Hoor, H. Schlager, and M. Riese, 2014: Tropical troposphere to stratosphere transport of carbon monoxide and long-lived trace species in the chemical Lagrangian Model of the Stratosphere (cLaMs), *Geosci. Model Dev. Discuss*., 7, 5087-5139.

Rogers, M. J., 1984: The association between the North Atlantic Oscillation in the Northern Hemisphere, *Mon, Wea. Rev*., 112, 1999-2015.

Rongcai R. and M. CAI, 2006: Polar vortex oscillation viewed in an isentropic potential vorticity coordinate, *Advances in Atmospheric Sciences*, Vol. 23, NO. 6, 884-900.

Santee, M. L., G. L. Manney, N. J. Livesey, L. Froidevaux, M. J. Schwartz and W. G. Reed, 2011: Trace gas evolution in the lowermost stratosphere from Aura Microwave Limb Sounder Measurements, *Journal of Geophysical Research*, Vol. 116, D18306.

Santer, B. D., T. M. L. Wigley, J.S. Boyle, D. J. Gaffen, J. J. Hnilo, D. Nychka, D. E. Parker, and K.E. Taylor, 2000: Statistical significance of trends and trend difference in layer-average atmospheric temperature time series, *Journal of Geophysical Research*, Vol. 105, N). D6, 7337-7356.

Seager R., N. Harnik and Y. Kushnir, 2003: Mechanisms of hemispherically symmetric climate variability, *Journal of Climate*, Vol. 16, 2960-2978.

Shuckburgh E., W. Norton, A. Iwi and P. Haynes, 2001: Influence of the quasi-biennial oscillation on isentropic transport and mixing in the tropics and subtropics, Journal of Geophysical Research, Vol. 106, NO. D13, pages 14,321-14,337.

Thompson D. W. J. and D. J. Lorenz, 2004: The Signature of the Annular Modes in the Tropical Troposphere, *Journal of Climate*, Volume 17.

Thompson D. W. J., M. P. Baldwin and S. Solomon, 2004: Stratosphere-Troposphere Coupling in the Southern Hemisphere, *Journal of Atmospheric Sciences*, Vol. 62.

Thompson D. W. J., Sukyoung Lee, Mark P. Baldwin, 2003: Atmospheric processes governing the Northern Hemisphere Annular Mode/North Atlantic Oscillation, *Geophysical Monograph 134.*

Thompson, D. W. J., and D. J. Lorenz, 2004: The signature of the annular modes in the tropical troposphere, *J. Clim.*, Vol.17, 4330-4342.

Thompson, D. W. J., and J. M. Wallace, 2000: Annular modes in the extratropical circulation. Part I: Month-to-month variability, *J. Clim.*, Vol. 13, 1000-1016.

Trenberth K. E. J. M. Caron, D. P. Stepaniak and S. Worley, 2002: Evolution of the El Niño-Southern Oscillation and global atmospheric surface temperatures, *Journal of Geophysical Research*, Vol. 107.

Trenberth, K. E., J. M. Caron, D. P. Stepaniak and S. Worley, 2002: Evolution of the El Niño southern oscillation and global atmospheric surface temperature, *Journal of Geophysical Research*, Vol. 107, NO. D8.

van Delden A. J., 2014: PV-Theta View of Diabatic-Dynamical Interaction in the General Circulation, *Tellus*.

van Delden, A. J. van, 2012: Atmospheric Dynamics, chapter1, section 1.26, Institute for Marine and Atmospheric research Utrecht (IMAU), Utrecht University

Wallace J. M. and D. S. Gutzler, 1980: Teleconnections in the geopotential height field during the Northern Hemisphere winter, *Monthly Weather Review.* Volume 109.

Wallace, J. M., 2000: North atlantic oscillation/annular mode: Two paradigms – one phenomenon*, Q.J.R. Meteorol. Soc*., 126: 791-805.

Wallace, J. M., and V. E. Kousky, 1968a: Observational evidence of Kelvin waves in the tropical stratosphere, *Journal of Atmospheric Sciences*, 25, 900-907.

Waugh D. W. and L. M. Polvani, 2000: Climatology of Intrusions into the Tropical Upper troposphere, *Geophysical research Letters*, Vol. 27, No. 23, Pages 3857-3860.

Waugh D. W. and L. M. Polvani, 2010: Stratospheric Polar Vortices, The Stratosphere: Dynamics, Transport, and Chemistry, *Geophysical Monograph*, series 190, 43-57.

Wilks D. S., 2011: Statistical Methods in Atmospheric Sciences, Second edition, *Elsevier*.

Witman M. A. H., A. J. Charlton and L. M. Polvani, 2004: On the meridional structure of annular modes, Notes and Correspondence, *American Meteorological Society*.

7 APPENDIX

7.1 Definition of the NAM indices at, 1000, 975, 750, 600, 500, 350, 250, 200, 150, 100, 50, 30, 20 and 10 hPa:

1) NAMI at 1000 hPa: NAMI = SLP (26.25°N) – SLP (63.75°N)

2) NAMI at 975 hPa: NAMI_975 = gph (27°N) – gph (63.75°N)

3) NAMI at 750 hPa: NAMI_750 = gph (37.5°N) – gph (64.5°N)

4) NAMI at 600 hPa: NAMI_600 = gph (41.25°N) – gph (66°N)

5) NAMI at 500 hPa: NAMI_500 = gph (41.25°N) – gph (65.25°N)

6) NAMI at 350 hPa: NAMI_350 = gph (42.75°N) – gph (66.75°N)

7) NAMI at 250 hPa: NAMI_250 = gph (47.75°N) – gph (70.5°N)

8) NAMI at 200 hPa: NAMI_200 = gph (46.5°N) – gph (73.5°N)

9) NAMI at 150 hPa: NAMI_150 = gph (46.5°N) – gph (76.5°N)

10) NAMI at 100 hPa: NAMI_100 = gph (46.5°N) – gph (83.25°N)

11) NAMI at 50 hPa: NAMI_50= gph (43.5°N) – gph (90°N)

12) NAMI at 30 hPa: NAMI_30 = gph (42°N) – gph (90°N)

13) NAMI at 20 hPa: NAMI_20 = gph (40.5°N) – gph (90°N)

14) NAMI at 10 hPa: NAMI_10 = gph (°N) – gph (°N)

where gph stands for geopotential height. The data used for the calculation of these indices is normalized with respect to the monthly means for the period 1979 to 2013. All the indices were calculated using the method of Li and Wang (2003, see section 4.3) using geopotential height with exception for the NAM index defined at the surface in which mean sea level pressure was used.

7.2 Maximum in anticorrelation for the NH (black line) and for the SH (red line) respectively from 10.5°N to 90°N and from 10.5°S to 90°S for each of the isentropic surfaces at 265 K, 275 K, 285 K, 300 K, 315 K, 330 K, 350 K, 370 K, 395 K, 430 K, 475 K, 530 K, 600 K, 700K and 850 K. Note that the correlation coefficients are in absolute value (|r|). The latitudes associated with the maximum in anticorrelation on the 330 K isentropic surface are 15°S and 30°S. For the 850 K isentrope the latitudes are 26.25°S and 49.5°S.

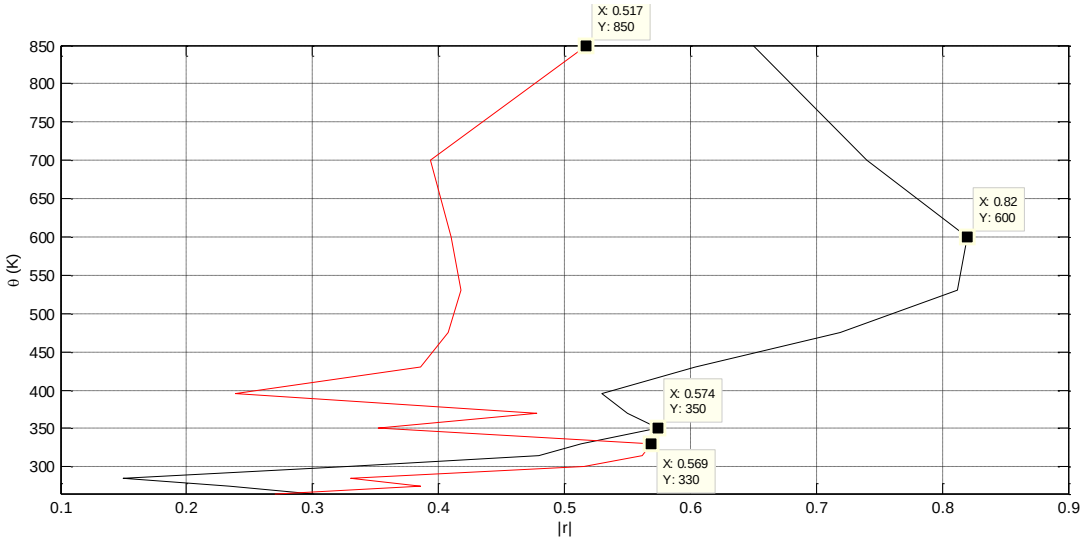
X: 0.517
Y: 850
X: 0.82
Y: 600
X: 0.574
Y: 350
X: 0.569
Y: 330
θ (K)
|r|
850
800
750
700
650
600
550
500
450
400
350
300
0.1
0.2
0.3
0.4
0.5
0.6
0.7
0.8
0.9